3.2.3. Geophysical Survey in Selected Fields

(1) Reanalysis of MT data acquired in the north-western portion of Rwanda

EWSA provided MT data acquired in the Karisimbi, Gisenyi and Kinigi fields and the total number of MT data sets provided was greater than 200. After eliminating several inadequate MT data sets containing a large amount of electromagnetic noise, three-dimensional resistivity inversion with smoothness constraints was conducted using 212 MT data sets. The impedance data used for the 3D inversion were real and imaginary components of Zxy and Zyx, which are rotated to a N35^{o}W direction, in a frequency range between 100 Hz and 0.01778 Hz. The 3D inversion scheme used in this work was based on the iterative linearized least-squares method (Gauss-Newton) using smoothness regularization. Forward modeling for a given, arbitrary 3D earth was done using the staggered-grid finite-difference method.

The location map for the MT stations is shown in Fig.3-2.63 and the location of the MT stations (UTM coordinates) used for the data analysis on this project is listed in Table 3-2.18.

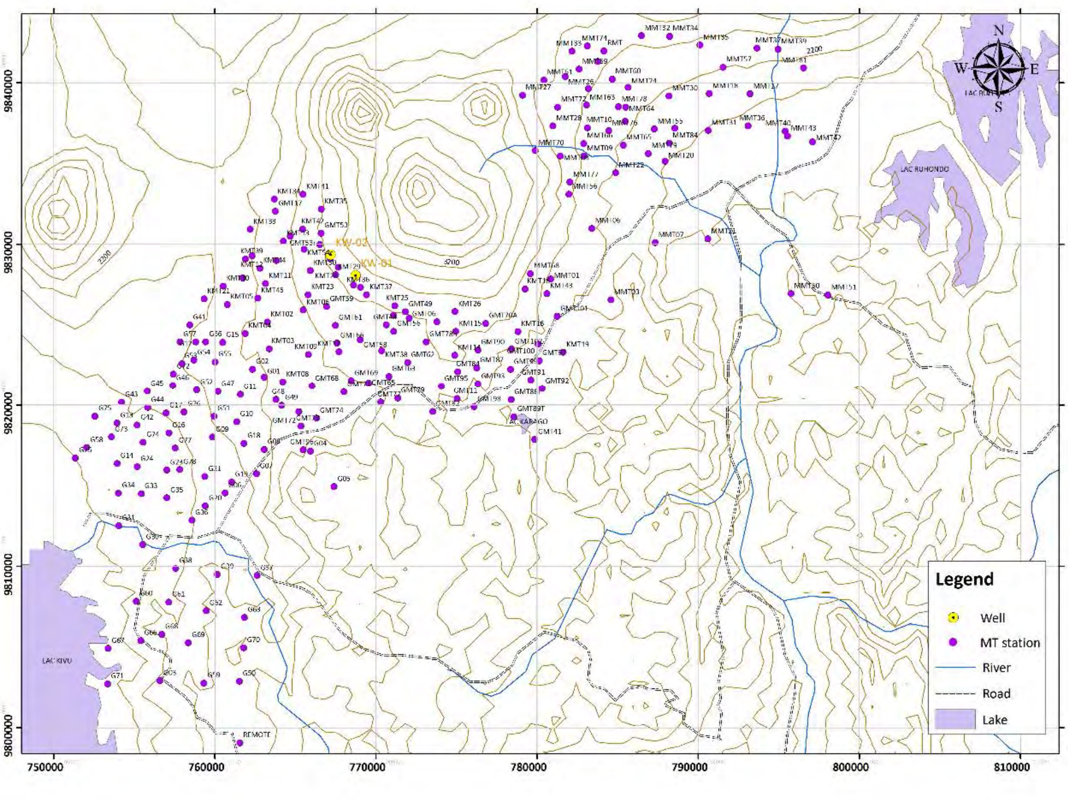

Source: JICA study team

Fig. 3-2.63 Location map for MT stations

Table 3-2.18 Locations of MT stations (1/2)

Station	Easting (UTM)	Northing (UTM)	Elevation (m)	Station	Easting (UTM)	Northing (UTM)	Elevation (m)
G01	763050	9821752	2187	G62	759465	9807252	1993
G02	762337	9822242	2163	G63	761833	9806835	2096
G03	756596	9802914	1809	G66	755405	9805398	1726
G04	765936	9817136	2395	G67	753380	9804918	1505
G05	767400	9814946	2744	G68	756705	9805781	1781
G06	760633	9814549	1885	G69	758361	9805263	1869
G07	762592	9815736	2057	G70	761787	9804951	2130
G08	763067	9817253	2139	G71	753343	9802718	1517
G09	759845	9818016	1967	G72	757426	9821949	1905
G10	761356	9818967	2101	G73	753584	9818027	1658
G11	761583	9820675	2113	G74	755544	9817692	1691
G12	758810	9823939	2050	G75	752568	9819312	1669
G13	753919	9818887	1693	G76	758094	9819579	1872
G14	753934	9816376	1626	G77	757541	9817331	1707
G15	760483	9823912	2102	G78	757827	9816003	1739
G16	757152	9818271	1718	KMT02	763258	9825178	2245
G17	756978	9819507	1821	KMT03	763383	9823519	2243
G18	761812	9817621	2025	KMT04	761885	9824467	2220
G19	761051	9815222	1910	KMT05	760767	9826260	2100
G20	759411	9813745	1861	KMT06	765486	9825929	2398
G21	759379	9815568	1862	KMT08	764222	9821462	2239
G23	757020	9815967	1715	KMT09	765811	9823159	2337
G24	755177	9816184	1651	KMT11	763147	9827566	2225
G25	751353	9816720	1601	KMT12	762317	9829285	2186
G30	755524	9811347	1788	KMT13	764254	9830186	2322
G31	754029	9812523	1642	KMT14	774887	9823118	2814
G33	755432	9814503	1652	KMT15	774945	9824596	2636
G34	754016	9814538	1656	KMT16	778814	9824588	2491
G35	757027	9814249	1704	KMT17	767697	9823342	2408
G36	758575	9812858	1799	KMT18	779265	9827225	2519
G37	762615	9809436	1916	KMT19	781611	9823303	2260
G38	757572	9809873	1690	KMT21	759327	9826615	1970
G39	760151	9809501	2074	KMT22	761731	9827903	2160
G41	758437	9824990	1964	KMT23	765775	9826866	2443
G42	755171	9818765	1719	KMT24	768602	9827468	2635
G43	754208	9820177	1747	KMT25	771164	9826177	2636
G44	755834	9819852	1785	KMT26	774909	9825822	2707
G45	755804	9820872	1869	KMT28	767660	9828563	2640
G46	757388	9821230	1899	KMT29	767502	9828111	2602
G47	760198	9820855	2052	KMT30	765928	9828365	2498
G48	763791	9820353	2235	KMT32	763826	9828985	2312
G49	764146	9819990	2247	KMT33	762189	9830917	2155
G50	761521	9802880	2100	KMT34	763691	9832783	2271
G51	759955	9819313	2015	KMT35	766603	9832162	2578
G52	758875	9820952	1960	KMT36	769038	9827317	2656
G53	757958	9822603	2013	KMT37	769408	9826861	2619
G54	758698	9822814	2039	KMT38	770354	9823403	2522
G55	760015	9822705	2099	KMT39	761890	9829079	2154
G56	759422	9823947	2064	KMT40	760512	9827403	2045
G57	757836	9823940	1957	KMT41	765466	9833089	2457
G58	752046	9817358	1612	KMT42	765454	9830925	2471
G59	759323	9802757	1939	KMT43	780607	9826940	2352
G60	755127	9807838	1675	KMT44	762798	9828510	2221
G61	757140	9807781	1701	KMT45	762663	9826657	2215

Source: JICA study team

Table 3-2.18 Locations of MT stations (2/2)

Station	Easting (UTM)	Northing (UTM)	Elevation (m)	Station	Easting (UTM)	Northing (UTM)	Elevation (m)
KMT52r	767156	9829092	2638	MMT81	796541	9840903	2147
KMT54r	765537	9829678	2492	MMT84	788208	9836250	2024
MMT01	780853	9827834	2374	RMT	784154	9841962	2443
MMT03	784578	9826545	2168	REMOTE	761557	9799054	2201
MMT06	783396	9830969	2209	GMT06	772054	9825408	2579
MMT07	787335	9830092	1806	GMT11	775042	9820404	2359
MMT08	781446	9835462	2549	GMT17	763752	9832037	2350
MMT09	782906	9835457	2337	GMT41	779851	9817866	2281
MMT10	783124	9837208	2347	GMT44	770634	9824995	2537
MMT17	793226	9839308	2041	GMT48b	771089	9825584	2587
MMT18	790693	9839324	2112	GMT49	771819	9825804	2614
MMT20	787950	9835138	2006	GMT50Y	764681	9830496	2392
MMT21	790595	9830327	1734	GMT51R	773779	9825188	2632
MMT22	784875	9834416	2172	GMT53	766589	9830672	2601
MMT23	785469	9837602	2229	GMT53r	766502	9829972	2574
MMT24	785651	9839710	2297	GMT56	771104	9824598	2540
MMT25	783195	9839633	2411	GMT58	769025	9824081	2450
MMT26	781745	9840376	2484	GMT59	766933	9826136	2493
MMT27	779093	9839223	2643	GMT61	767479	9824968	2464
MMT28	780984	9837318	2513	GMT62	771976	9822670	2561
MMT29	788559	9837181	2078	GMT63	770794	9821798	2449
MMT30	788187	9839173	2180	GMT65	769535	9821382	2395
MMT31	790628	9837040	1984	GMT66	767583	9823867	2421
MMT32	786481	9842909	2458	GMT68	766025	9821202	2310
MMT33	782159	9841952	2512	GMT69	768462	9821531	2380
MMT34	788225	9842870	2435	GMT70A	776804	9825092	2602
MMT35	790108	9842327	2363	GMT71	768016	9820828	2357
MMT36	793094	9837323	1961	GMT72	765216	9819589	2290
MMT37	793656	9842139	2294	GMT73	765341	9818704	2324
MMT39	794952	9842066	2275	GMT74	766310	9819182	2323
MMT40	795401	9836991	1907	GMT77	770297	9820195	2378
MMT42	797105	9836331	1890	GMT78R	773110	9823941	2590
MMT43	795546	9836693	1899	GMT79	771358	9820439	2405
MMT50	795766	9826931	1884	GMT82	773528	9819604	2371
MMT51	798055	9826842	1676	GMT84	775075	9822097	2437
MMT54	783766	9841308	2428	GMT87	776253	9822333	2398
MMT55	787285	9837130	2122	GMT88r	778400	9820339	2325
MMT56	781972	9833088	2430	GMT89T	778569	9819278	2300
MMT57	791542	9840961	2201	GMT90	776323	9823442	2486
MMT59	782609	9840829	2463	GMT91	779611	9821566	2306
MMT60	784665	9840216	2357	GMT92	780309	9821034	2291
MMT61	780425	9840159	2633	GMT93	776329	9821325	2350
MMT63	783064	9838610	2375	GMT95	774056	9821186	2415
MMT64	785501	9838478	2242	GMT96	765479	9817226	2322
MMT65	785356	9836124	2180	GMT97	780129	9822777	2313
MMT66	782894	9836234	2330	GMT98	776096	9819893	2358
MMT68	779594	9828168	2522	GMT99	778362	9822238	2348
MMT70	779888	9835792	2802	GMT100	780065	9823806	2301
MMT72	781282	9838480	2494	GMT101	781240	9825526	2222
MMT74	783112	9842267	2473	GMT102	778416	9823495	2332
MMT76	784451	9837023	2267				
MMT77	782035	9833835	2466				
MMT78	785053	9838503	2274				
MMT79	786912	9835609	2078				

Source: JICA study team

The data analysis procedure including the static shift correction and the three dimensional resistivity inversion scheme utilized in this study is as follows:

1) Data analysis

i) Static Shift Correction for MT data

Very shallow, small-scale inhomogeneities with dimensions much less than the skin depth at the highest recorded frequency can produce a shift in the log-log plot of the apparent resistivity versus frequency, moving it parallel to the undistorted curve. This parallel shift is commonly referred to as a static shift. Removing this effect from the data is important in interpreting the subsurface resistivity structure.

The estimation of the static shift values at each MT station has been primarily made by using static shift values previously determined by TDEM data described in Appendix D4 of the final report "Geoscientific Surveys of the Rwandan Karisimbi, Gisenyi and Kinigi Geothermal Prospectss" by Uniservices. The static shift values at MT stations without TDEM data were determined by spacial filtering using smoothing processing. The static shift correction values (listed in Table 3-2.19) were applied to the apparent resistivity values, rotated to a N35^{o}W direction.

For the 3D MT inversion in this data analysis, the impedance values (Zxy and Zyx) after static shift correction have been utilized.

Table 3-2.19 Static shift correction values (1/2)

Station	Static shift xy	Static shift yx	Station	Static shift xy	Static shift yx
G01	1.309	1.068	G62	2.318	1.848
G02	0.886	0.589	G63	1.661	0.642
G03	2.283	2.621	G66	1.095	1.327
G04	0.987	0.478	G67	1.535	0.658
G05	1.198	0.842	G68	1.419	1.513
G06	0.709	0.539	G69	0.735	1.315
G07	1.513	1.514	G70	0.848	0.532
G08	1.983	0.826	G71	1.330	0.891
G09	1.681	1.501	G72	1.356	2.064
G10	3.714	1.440	G73	0.905	0.639
G11	1.075	0.983	G74	1.698	1.249
G12	1.128	1.056	G75	1.142	1.271
G13	0.201	0.342	G76	0.293	0.970
G14	1.869	0.447	G77	0.574	0.576
G15	0.998	1.163	G78	0.719	0.644
G16	2.755	2.202	KMT02	0.590	1.090
G17	1.229	1.159	KMT03	1.724	1.188
G18	0.575	0.453	KMT04	1.656	2.179
G19	1.459	1.361	KMT05	1.631	0.937
G20	0.911	0.799	KMT06	1.202	0.504
G21	1.065	0.954	KMT08	1.285	0.596
G23	1.277	0.504	KMT09	0.985	1.098
G24	0.689	0.468	KMT11	2.363	1.284
G25	0.834	0.854	KMT12	0.914	1.011
G30	0.961	0.906	KMT13	1.027	0.852
G31	2.414	3.068	KMT14	0.862	0.876
G33	1.433	1.122	KMT15	0.548	0.498
G34	1.046	3.653	KMT16	1.748	0.989
G35	1.154	1.236	KMT17	1.200	1.114
G36	1.444	1.821	KMT18	0.497	0.963
G37	0.727	0.710	KMT19	1.597	0.881
G38	2.143	0.961	KMT21	0.798	0.843
G39	2.091	3.853	KMT22	1.022	1.233
G41	0.895	0.725	KMT23	1.603	1.262
G42	0.923	0.796	KMT24	2.497	2.550
G43	0.906	1.079	KMT25	1.380	1.368
G44	1.781	1.412	KMT26	0.927	0.782
G45	0.926	0.628	KMT28	0.667	0.687
G46	1.220	1.098	KMT29	1.178	1.092
G47	1.600	0.529	KMT30	0.801	0.696
G48	1.323	0.947	KMT32	1.110	0.926
G49	1.327	1.200	KMT33	1.181	0.827
G50	1.067	1.644	KMT34	0.955	0.946
G51	0.847	0.578	KMT35	0.460	0.544
G52	1.895	1.058	KMT36	0.758	0.712
G53	1.365	1.244	KMT37	0.377	0.392
G54	1.221	0.583	KMT38	1.322	1.150
G55	0.892	0.878	KMT39	1.260	1.802
G56	0.594	0.959	KMT40	1.340	1.358
G57	1.260	1.295	KMT41	0.897	0.882
G58	1.215	1.348	KMT42	1.046	0.930
G59	1.405	1.805	KMT43	0.943	0.711
G60	0.629	0.779	KMT44	1.666	0.890
G61	0.307	3.210	KMT45	1.074	0.851

Source: JICA study team

Table 3-2.19 Static shift correction values (2/2)

Station	Static shift xy	Static shift yx	Station	Static shift xy	Static shift yx
KMT52r	1.225	1.137	MMT81	0.950	0.956
KMT54r	0.440	0.446	MMT84	1.901	1.567
MMT01	0.653	0.803	RMT	0.923	1.455
MMT03	0.657	0.969	REMOTE	0.613	1.315
MMT06	1.273	1.364	GMT06	1.260	1.288
MMT07	1.325	1.949	GMT11	1.087	1.224
MMT08	1.867	1.161	GMT17	0.974	0.960
MMT09	0.813	1.465	GMT41	1.237	1.584
MMT10	0.968	1.033	GMT44	0.437	0.593
MMT17	1.625	1.015	GMT48b	1.015	0.816
MMT18	0.712	1.241	GMT49	1.000	0.899
MMT20	2.786	2.946	GMT50Y	0.875	0.910
MMT21	8.428	2.923	GMT51R	0.936	0.612
MMT22	1.294	1.080	GMT53	34.424	33.817
MMT23	1.403	1.309	GMT53r	0.719	0.775
MMT24	0.684	0.671	GMT56	0.672	0.482
MMT25	1.563	1.076	GMT58	0.870	0.909
MMT26	0.948	0.593	GMT59	1.229	0.803
MMT27	1.138	1.667	GMT61	6.391	26.451
MMT28	1.342	1.143	GMT62	0.734	0.934
MMT29	0.691	0.641	GMT63	0.565	0.317
MMT30	0.819	1.024	GMT65	0.495	1.012
MMT31	1.475	0.816	GMT66	0.828	1.133
MMT32	0.759	0.895	GMT68	0.984	1.286
MMT33	1.449	0.684	GMT69	1.162	1.188
MMT34	0.971	0.901	GMT70A	0.891	1.977
MMT35	1.022	1.088	GMT71	0.915	1.461
MMT36	0.850	1.124	GMT72	1.515	0.854
MMT37	0.995	0.848	GMT73	1.008	1.551
MMT39	1.594	0.932	GMT74	0.804	1.272
MMT40	1.490	3.197	GMT77	1.891	0.858
MMT42	2.320	2.314	GMT78R	0.638	0.598
MMT43	0.980	2.504	GMT79	1.227	0.877
MMT50	1.639	1.947	GMT82	1.420	1.317
MMT51	0.972	0.293	GMT84	0.905	0.903
MMT54	0.649	0.805	GMT87	0.914	0.873
MMT55	1.562	1.578	GMT88r	0.761	0.746
MMT56	1.213	1.102	GMT89T	0.495	0.570
MMT57	1.929	1.662	GMT90	0.789	0.767
MMT59	1.046	1.127	GMT91	0.972	0.608
MMT60	1.488	1.281	GMT92	1.028	0.791
MMT61	0.690	0.587	GMT93	0.550	0.670
MMT63	1.077	0.963	GMT95	1.477	1.182
MMT64	1.593	1.438	GMT96	0.798	0.476
MMT65	0.802	0.658	GMT97	0.809	1.081
MMT66	1.783	1.848	GMT98	1.028	0.835
MMT68	1.342	0.777	GMT99	1.213	1.331
MMT70	0.988	1.056	GMT100	1.106	0.728
MMT72	0.938	0.916	GMT101	2.036	4.712
MMT74	1.465	1.149	GMT102	2.872	0.769
MMT76	0.820	0.631			
MMT77	1.011	0.801			
MMT78	2.122	1.286			
MMT79	2.109	1.879			

Source: JICA study team

ii) Three dimensional resistivity inversion scheme

a) Concept of 3D resistivity modeling

In three-dimensional modeling, a three-dimensional resistivity structure whose resistivity distribution varies in the x and y (horizontal) directions and the z (vertical) direction, as shown in Fig.3-2.64, is assumed. Resistivity values of each element of the 3D resistivity model are determined by iterating the calculation to minimize the value of Σ((observed impedance values) – (calculated impedance values))^2. This analysis is expected to lead to a more accurate subsurface resistivity model than that derived from 1D and 2D resistivity analysis.

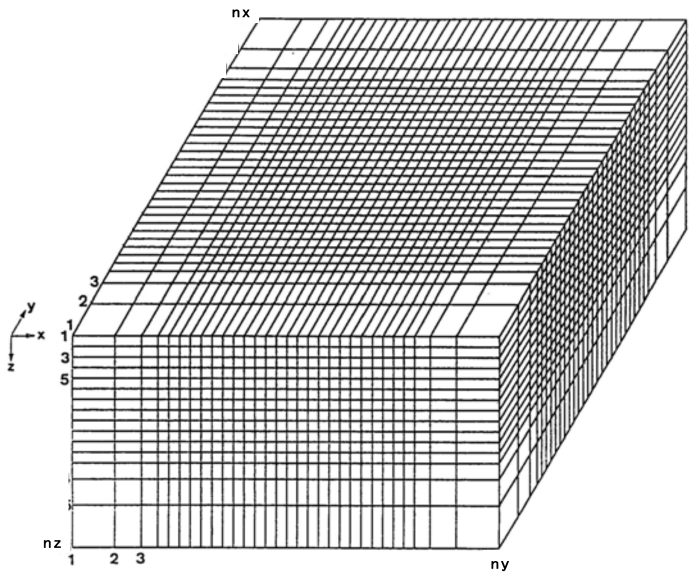

Source: JICA study team

Fig. 3-2.64 Conceptual illustration of mesh for 3D Resistivity Modeling using the finite-difference method

b) Basic theory of 3D resistivity modeling

In the forward modeling of the electromagnetic field, the earth is divided into a number of blocks of constant conductivity and so the forward modeling method needs to have the ability to handle a variety of conductivity distribution. The 3-D electromagnetic field can be explained by Maxwell's equations shown below.

$$\nabla \times E = i\omega\mu H \qquad (1)$$

$$\nabla \times H = \sigma E \qquad (2)$$

where

ωh: angular frequency

μ : magnetic permeability

σ : electric conductivity

The displacement current is ignored because it is very small. From equations (1) and (2), the following equations are derived.

$$\nabla \times (\nabla \times H) = \nabla \times \sigma E = \sigma \times \nabla \times E = k^2 H \qquad (3)$$

$$\nabla \times (\nabla \times E) = \nabla \times i\omega\mu H = i\omega\mu \times \nabla \times H = k^2 E \qquad (4)$$

where

$$k^2 = i\omega\mu\sigma$$

After introducing the orthogonal coordinate system, (3) and (4) lead to equations (5) and (6) respectively.

$$\left.\begin{aligned}
&\partial^2 Hx/\partial y^2 + \partial^2 Hx/\partial z^2 - \partial^2 Hy/\partial x\partial y - \partial^2 Hz/\partial x\partial z - k^2 Hx = 0\\
&\partial^2 Hy/\partial x^2 + \partial^2 Hy/\partial z^2 - \partial^2 Hx/\partial y\partial x - \partial^2 Hz/\partial y\partial z - k^2 Hy = 0\\
&\partial^2 Hz/\partial x^2 + \partial^2 Hz/\partial y^2 - \partial^2 Hx/\partial z\partial x - \partial^2 Hz/\partial z\partial y - k^2 Hz = 0
\end{aligned}\right\} \quad (5)$$

$$\left.\begin{aligned}
&\partial^2 Ex/\partial y^2 + \partial^2 Ex/\partial z^2 - \partial^2 Ey/\partial x\partial y - \partial^2 Ez/\partial x\partial z - k^2 Ex = 0\\
&\partial^2 Ey/\partial x^2 + \partial^2 Ey/\partial z^2 - \partial^2 Ex/\partial y\partial x - \partial^2 Ez/\partial y\partial z - k^2 Ey = 0\\
&\partial^2 Ez/\partial x^2 + \partial^2 Ez/\partial y^2 - \partial^2 Ex/\partial z\partial x - \partial^2 Ez/\partial z\partial y - k^2 Ez = 0
\end{aligned}\right\} \quad (6)$$

In a finite-difference scheme on a staggered-grid (Fig.3-2.65), the solution region (including air) is discretized into rectangular cells (Fig.3-2.64). To calculate the electric fields (Ex, Ey and Ez), the three equations in (6) should be solved simultaneously.

In solving the equations in (6) simultaneously, the tangential electric fields on the boundaries of the model for the appropriate source polarization will be assigned. These boundary values come from a one-dimensional (horizontally layered) calculation. The values obtained at the positions corresponding to the boundaries of the 3-D model are then used as boundary values for the 3-D electromagnetic forward modeling of MT response. In addition, several air layers were added on the top of the Earth model with an approximately logarithmically increasing thickness for each air layer. The layer should be extended far enough above Earth to allow the longest wavelength perturbations to be damped out (usually three times the largest wavelength of the horizontal conductivity variations in the Earth model is used). These air layers are given a finite, but high, resistivity value of 10^8 ohm-m. At the top of the air layers, a one-dimensional plane-wave impedance for outgoing fields is used.

Although the topography was not incorporated in the forward modeling, we could assume that topographic effects were accounted for as part of the static shift. In addition, considering the apparent resistivity distributions at different frequencies which are not presented in this report, topography effect is not severe in the study area.

The electric field (Ex, Ey and Ez) is first solved as a total field, in the frequency domain by the finite difference method with the equation (6). Then, the magnetic field (Hx, Hy and Hz) is computed from the electric field obtained. After obtaining the electric fields and magnetic fields for two polarizations (Ex1, Ey1, Hx1, Hy1 and Ex2, Ey2, Hx2, Hy2), impedance values (Zxy and Zyx) can be calculated by using the equation (7).

$$\left.\begin{aligned} Zxy &= (Ex2 \times Hx1 - Ex1 \times Hx2) / (Hx1 \times Hy2 - Hx2 \times Hy1) \\ Zyx &= (Ey1 \times Hy2 - Ey2 \times Hy1) / (Hx1 \times Hy2 - Hx2 \times Hy1) \end{aligned}\right\} \quad (7)$$

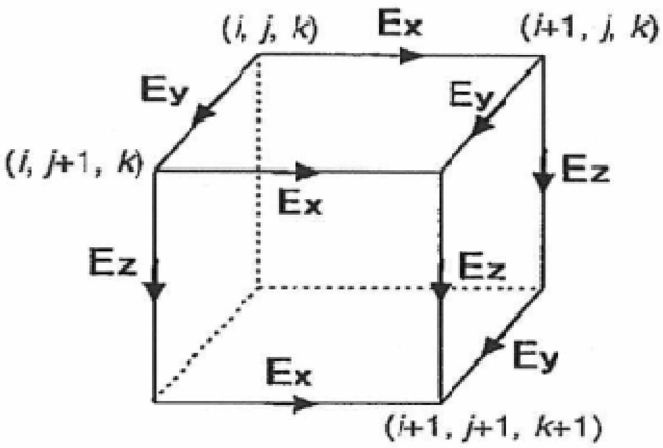

Fig. 3-2.65 Conceptual illustration for Staggered Grid configuration (After Sasaki, Y., 1999)

c) Basic theory in 3D inversion scheme

The 3D inversion algorithms use the principle of finite differences to discretize the model space with rectangular cells and follow Occam's inversion scheme to find a smooth resistivity model. Their advantage is the approach of performing the inversion in the data space, which can downsize the problem to a computational load that is manageable on a desktop computer. The resistivity of each block is treated as an unknown parameter in the inversion. The Jacobian matrix, consisting of partial derivatives (sensitivities) of MT responses with respect to block resistivities in the 3D model, should be evaluated from an estimated model at each iteration step.

To stabilize the model correction at each iteration step, smoothness regularization is adopted. The objective function W (m) to be minimized in the inversion is defined as

$$W(m) = (m-m_0)^T C_m^{-1}(m-m_0) + \lambda^{-1}((d-F(m))^T C_d^{-1}(d-F(m))) \qquad (8)$$

where m is the resistivity model parameter, m0 is the prior model parameter, Cm is the model covariance matrix which defines the model norm, d is the observed data (impedance elements, Zxy, Zyx, Zxx and Zyy), Cd is the data covariance matrix, and F(m) is a non-linear function that works on the model m to produce MT responses. The second term of the right-hand side is for the misfit minimization, and the first term is for equality minimization. The parameters λ minimization. The parameters for a trade-off parameter controlling whether to heavily minimize the data misfit or the model norm. For large whether to heavily minimize the data misfit or the model ponses. ed data adopted. The objective function mod small l l or the model ponses. ed data adopted. The objectivproduce a rougher model. The model covariance matrix characterizes the smoothness of resistive variation relative to the base model.

Because of nonlinearity of the magnetotelluric inversion problem, an iterative approach is required, based on linealizing F(m) such that:

$$F(m_{i+1}) = F(m_i + \delta m) = F(m_i) + J_i \cdot (m_{i+1} - m_i) \qquad (9)$$

Where I denotes iteration number, and Ji is the N(number of data) x M(number of model parameters) Jacobian matrix calculated at each iteration i. Substituting (9) into (8), and applying the data space method, we obtain a series of iterative approximate solutions:

$$m_{i+1} - m_0 = C_m J_i^T C_d^{-1/2} [\lambda I + C d_d^{-1/2} J_i C_m J_i^T C_d^{-1/2}]^{-1}$$

$$\times [d - F(m) + J_k (m_{i+1} - m_0)] \qquad (10)$$

The final 3-D model parameters (resistivity values in the 3-D resistivity model blocks) can be obtained to solve equation (10) repeatedly until the misfit value between the observed data (impedance elements) and calculated data obtained from the 3-D resistivity model becomes small. The approach in data space by Siripunvaraporn et al. (2005) is computationally advantageous, since in most practical applications, there are far fewer data points than model parameters.

On the basis of the results obtained from the three-dimensional resistivity inversion with the MT data acquired in the Gisenyi, Karisimbi and Kinigi fields, resistivity maps at different depths, namely 100 m, 300 m, 500 m, 750 m, 1,000 m, 1,500 m, 2,000 m, 2,500 m, 3,000 m, 4,000 m and 5,000 m were drawn. These maps are shown in Fig.3-2.67 to Fig.3-2.77. In addition, resistivity sections along lines A, B, C, D, E and F (refer to Fig.3-2.78 for the locations of the sections) were prepared and these resistivity sections are shown in Fig.3-2.79.

Furthermore, because a widely distributed remarkably low resistivity zone has been detected in the Kinigi field, another more precise 3D MT inversion only in and around the Kinigi field (smaller resistivity cells were used for the inversion) has been conducted with the MT data acquired in the Kinigi field. The objective of this second three-dimensional resistivity inversion is to delineate precise shape and location of the remarkably low resistivity zone. Based on the results obtained from the three-dimensional resistivity inversion in and around the Kinigi field, resistivity maps at different depths, namely 100 m, 300 m, 500 m, 750 m, 1,000 m, 1,500 m, 2,000 m, 2,500 m, 3,000 m, 4,000 m and 5,000 m were also drawn. These maps are shown in Fig.3-2.80 to Fig.3-2.90.

2) General resistivity structure of geothermal fields in volcanic areas

The geoelectrical features of a low resistivity zone and a resistive zone at depth in and around a geothermal reservoir are as follows.

- A remarkable resistivity discontinuity can be continuously mapped from station to neighboring station. An uplifted structure is clearly identified along the resistivity discontinuity (An uplifted high resistivity zone sometimes indicates deep-seated intrusive rock. However, in cases where a remarkably low resistivity zone is distributed above the high resistivity uplifted zone, the uplifted high resistivity zone usually reflects a hydrothermally altered zone formed under high temperature conditions in a geothermal field). The resistivity discontinuity usually reflects fractured zones along a fault.

- Resistivity values for the low resistivity zone along the resistivity discontinuity are smaller than those in the surrounding area and the low resistivity zone usually is an indication of the cap rock of the reservoir in geothermal fields. Such a zone is marked in Fig.3-2.66.

- The hotter parts of geothermal systems are characterized by higher resistivity than is seen in the overlying conductive zone. The higher resistivity is due to the fact that the rock matrix is much less conductive than the saturating fluids, because low conductivity alteration products dominate the mineralization in this zone. High temperature alteration processes may increase the resistivity of some rocks by changing the resulting secondary minerals, for instance from smectite to illite or chlorite.

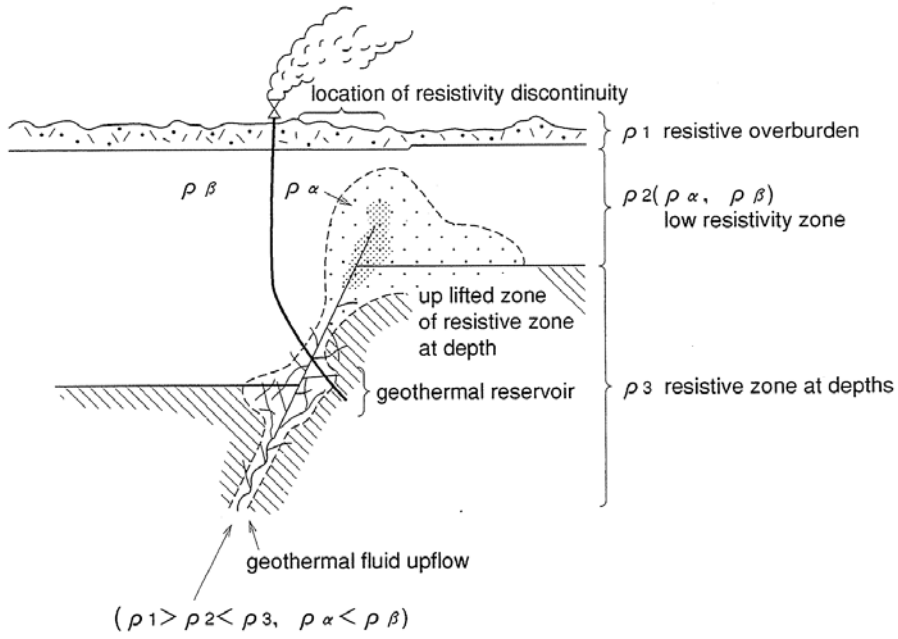

Source: JICA study team

Fig. 3-2.66 Representative Model of Resistivity Structure in and around Geothermal Reservoir

Considering that most geothermal reservoirs in volcanic areas are of the fracture-type and are controlled by faults, the low resistivity zone located around the faults obtained from resistivity surveys can be regarded as reflecting an impermeable zone, as a result of argillization, formed over the geothermal reservoir under temperatures ranging between approximately 70^{o}C and 200^{o}C. This impermeable zone functions as the cap rock of the reservoir in many geothermal fields. A geothermal reservoir will be expected along a fault in a resistive zone at depth below a low resistivity zone. Therefore, when the drilling target is considered on the basis of the resistivity structure, the target must be decided not only on the basis of information concerning the low resistivity zones, but also after considering the geothermal structure, such as faults, and other geological and hydrological information.

3) 3D MT inversion results in the Karisimbi, Gisenyi and Kinigi fields

Based on the 3D MT inversion results, the following interpretations were reached concerning the resistivity structure in and around the Karisimbi, Gisenyi and Kinigi fields

i) Resistivity discontinuity

The resistivity discontinuity is a structure exhibiting a significant lateral change in resistivity. If such structures are distributed continuously along a line, a fault and/or fractured zone will be expected along the resistivity discontinuities. In general, geothermal fluid is often reserved in and around the fault/fractured zone, so detecting the resistivity discontinuities is important in studying the geothermal structure in the study area. In the Karisimbi, Gisenyi and Kinigi geothermal fields, the following resistivity discontinuities R1, R2 and R3 are recognized based on the 3D inversion results.

Resistivity discontinuity R1

Resistivity discontinuity R1 runs from the southern portion of the Gisenyi field to the central portion of the Karisimbi field, and is roughly aligned in a NE-SW direction. Resistivity discontinuity R1 can be defined in the resistivity distribution at depths between 500 m and 2,000 m (Fig.3-2.69 and Fig.3-2.73) obtained from 3D inversion results.

Resistivity discontinuity R2 and R3

Resistivity discontinuities R2 and R3 run in the Kinigi field, and are roughly aligned in a NNW-SSE direction. The resistivity discontinuities R2 and R3 can be defined in the resistivity distribution at a depth of 1,500 m and deeper (Fig.3-2.85 through Fig.3-2.90) obtained from 3D inversion results.

The resistivity discontinuity R1 is likely to reflect a fault, since the indication of R1 is very clear and a large-scale lineament identified by the geological study is present at a similar location and direction as those of the resistivity discontinuity R1. The resistivity discontinuities R2 and R3 located in the Kinigi field are situated in and around the low resistivity zone and are probably the result of hydrothermal alteration products, which will be described later, thereby these resistivity discontinuities R2 and R3 possibly indicate faults controlling geothermal fluid migration.

ii) Low resistivity (conductive) zones

No low resistivity zones of less than 25 ohm-m are detected in the Gisenyi and Karisimbi fields based on the 3D MT inversion. This fact suggests that geothermal activity in the Gisenyi and Karisimbi fields is relatively weak and the hydrothermal alteration zone working as a cap rock of the geothermal reservoir is not well developed. Some hot springs are located in the southern portion of the Gisenyi field, but no low resistivity zone can be found in the area around the hot springs, suggesting large-scale geothermal activities have not developed around the hot springs located in the Gisenyi field.

Meanwhile remarkably low resistivity zone of less than 10 ohm-m is recognized in the northern portion of the Kinigi field at a depth of 1,500 m and deeper. Since the low resistivity zone is situated around and in between the discontinuities R2 and R3, which probably indicate fracture zones, the low resistivity zone in the northern portion of the Kinigi field is possibly resulted from an argillized rock affected by geothermal activity and containing considerable amounts of smectite and/or interstratified clay minerals.

iii) High resistivity (resistive) zone in relatively deep areas

A large-scale high resistivity zone is distributed in the southern portion of the Karisimbi field at depths between 1,000 m and 2,500 m (Fig.3-2.71 through Fig.3-2.74). Since this high resistivity zone shows extremely high resistivity values of greater than 640 ohm-m and a low resistivity zone cannot be found above this high resistivity zone, this high resistivity zone is not likely to be the result of high temperature alteration minerals such as illite and/or chlorite, but instead the result of a less permeable rock body where fractures are not well developed.

4) Resistivity structure in the Karisimbi, Gisenyi and Kinigi fields

The previously described 3D MT inversion results for the Karisimbi, Gisenyi and Kinigi fields suggest the following.

A broadly distributed high resistivity zone of greater than 630 ohm-m has been detected in the southern portion of the Karisimbi and Gisenyi fields at depths from approximately 1,000 m to 3,000 m (Fig.3-2.71 through Fig.3-2.75). At the same time, many areas of the central and northern portion of the Karisimbi and Gisenyi fields indicate relatively low resistivity values compared with that of the above-mentioned high resistivity zone. In between the above mentioned high resistivity zone situated in the southern portion of the Karisimbi and Gisenyi fields, and the relatively low resistivity zone situated in the central and northern portions of the Karisimbi and Gisenyi fields, a resistivity discontinuity R1 can be clearly recognized.

A large-scale lineament has been identified in the area in between the central portion of Gisenyi field and the southern portion of the Karisimbi field and is roughly aligned in a NE-SW direction. Since the lineament identified by the geological study runs close to the resistivity discontinuity R1 and the indication of R1 is very clear, the resistivity discontinuity R1 is likely to reflect a fault, and fracture zones may be developed along the fault. But unfortunately, there is no low resistivity zone around the resistivity discontinuity R1, suggesting that high temperature geothermal fluid is not likely to migrate along the resistivity discontinuity R1. In addition, since the area located to the south of the resistivity discontinuity R1 shows remarkably high resistivity, the area at depth is considered to be composed of low permeable rock where fractures are not well developed.

As described previously, low resistivity zones of less than 10 ohm-m which are the results of argillized rock affected by geothermal activity which contain considerable amounts of smectite and/or interstratified clay minerals are detected in many geothermal fields. These kinds of low resistivity zones resulting from hydrothermal alteration minerals are usually impermeable. Hence the low resistivity zone distributed at relatively shallow depths often work as cap rocks for geothermal reservoirs so that high temperature geothermal fluid ascending along fracture zones from the deep portion is accumulated and stored below the impermeable zone. Therefore these kinds of low resistivity zones are good indicators of geothermal structure and are of importance for detecting geothermal reservoirs.

However, no low resistivity zone of less than 40 ohm-m has been detected from the ground surface level down to a depth of 5,000 m in the whole area of the Gisenyi and Karisimbi fields, even around the resistivity discontinuity R1. This fact suggests that hydrothermal alteration minerals, such as smectite and/or zeolite have not been well developed, therefore geothermal activities in the Gisenyi and Karisimbi fields are likely to be relatively weak compared with other geothermal fields where geothermal power stations were installed and are being operated. It should be noted that the structure just beneath the area around the peak of Mt. Karisimbi cannot be inferred because no MT stations are located around the peak of Mt. Karisimbi.

A high temperature hot spring is located in the Karago field, and the area south of Karago shows relatively low resistivity at depth compared with the high resistivity zone widely distributed in the area north of Karago. However only a few MT stations are located in and around the Karago field and no MT stations are available in the east, west or south part of the Karago field, thus subsurface resistivity structure around the Karago field could not be defined properly.

Meanwhile, a widely distributed low resistivity zone is clearly detected at a depth of 2,000 m and deeper in the northern portion of the Kinigi field (Fig.3-2.86 through Fig.3-2.90). In addition, two remarkable resistivity discontinuities, R2 and R3 can be identified at a depth of 1,500 m and deeper in and around the areas of the eastern edge and the western edge of the remarkable low resistivity zone respectively. Because of this fact, the resistivity discontinuities R2 and R3 probably reflect fracture zones at depth with relatively high temperature geothermal fluids possibly ascending in the fracture zones around the resistivity discontinuities R2 and R3, and these geothermal fluids possibly migrate in and around the low resistivity zone.

In many productive geothermal fields, high temperature geothermal fluids with temperature over 200^{o}C are reserved at depth. This usually occurs as a result of an uplifted relatively high resistivity zone consisting of high temperature alteration products such as illite and chlorite which are usually located below a widely distributed shallow low resistivity zone. However, in the northern portion of the Kinigi field, such an up-lifted relatively high resistivity zone cannot be detected below the remarkable low resistivity zone. This may suggest that if geothermal fluids are reserved in and around the low resistivity zone in the northern portion of the Kinigi field, the temperature of the geothermal fluids are considered not to be sufficiently high for conventional type geothermal power generation.

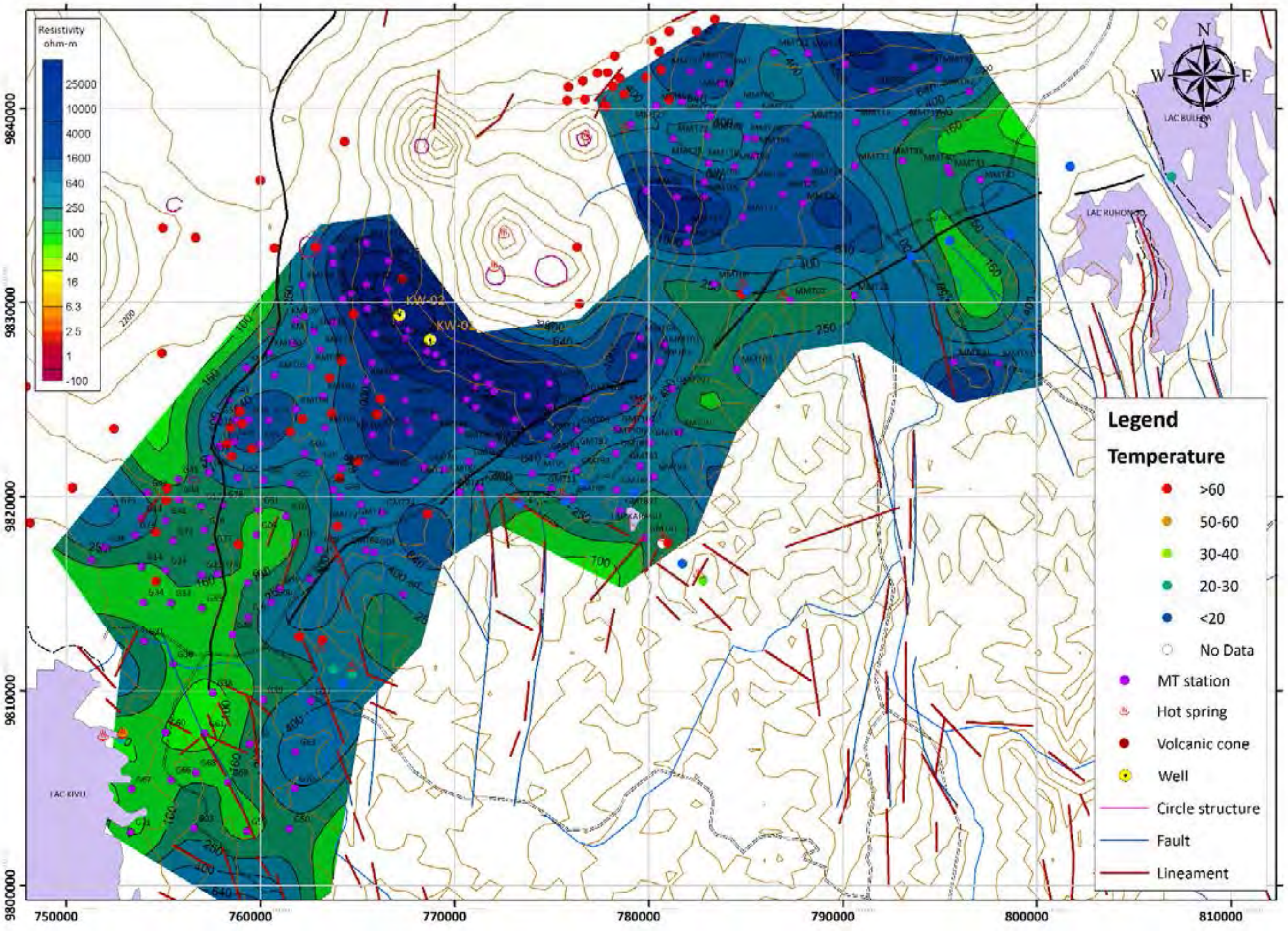

Source: JICA study team

Fig. 3-2.67 Resistivity map at a depth of 100m

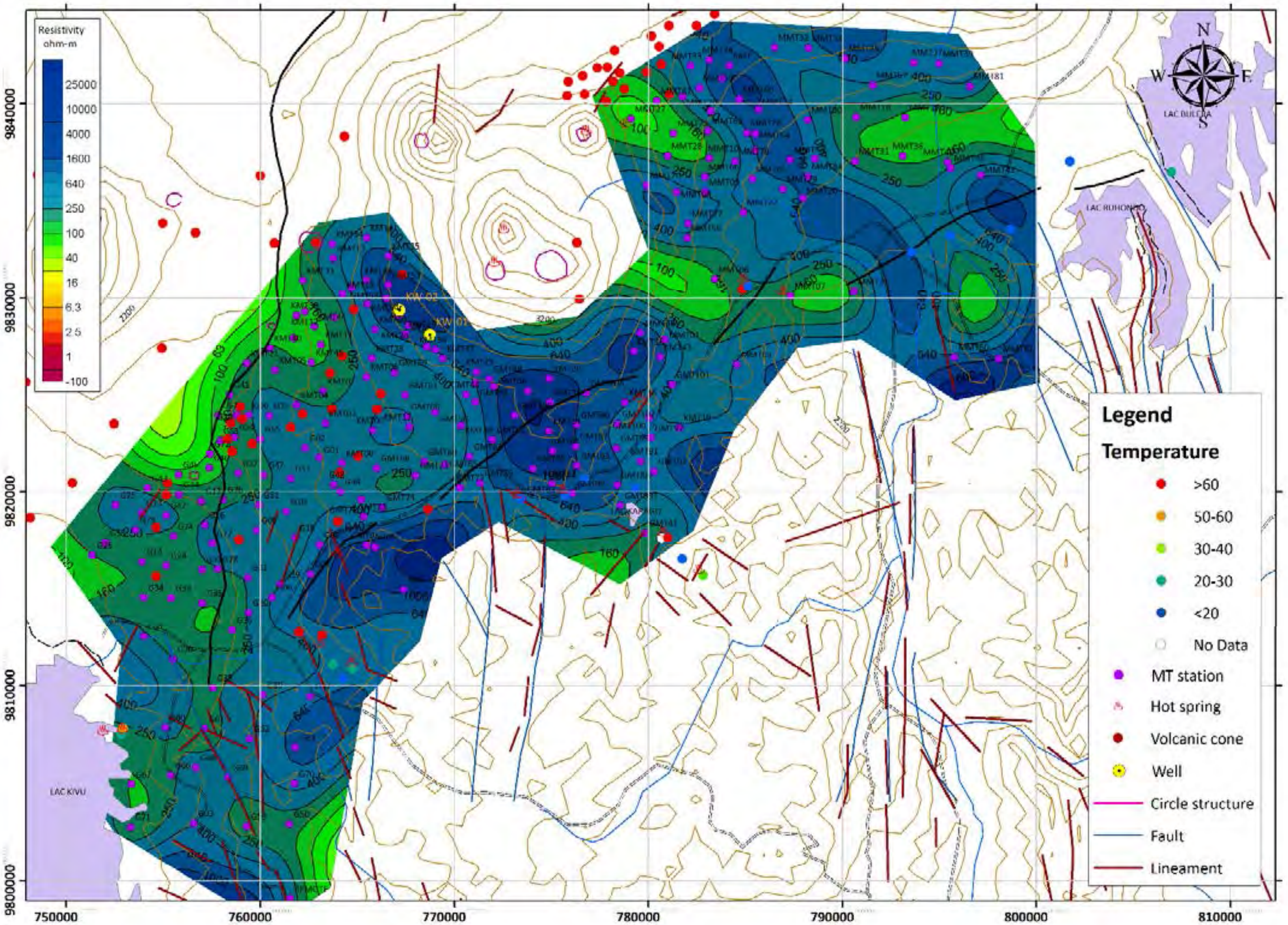

Source: JICA study team

Fig. 3-2.68 Resistivity map at a depth of 300m

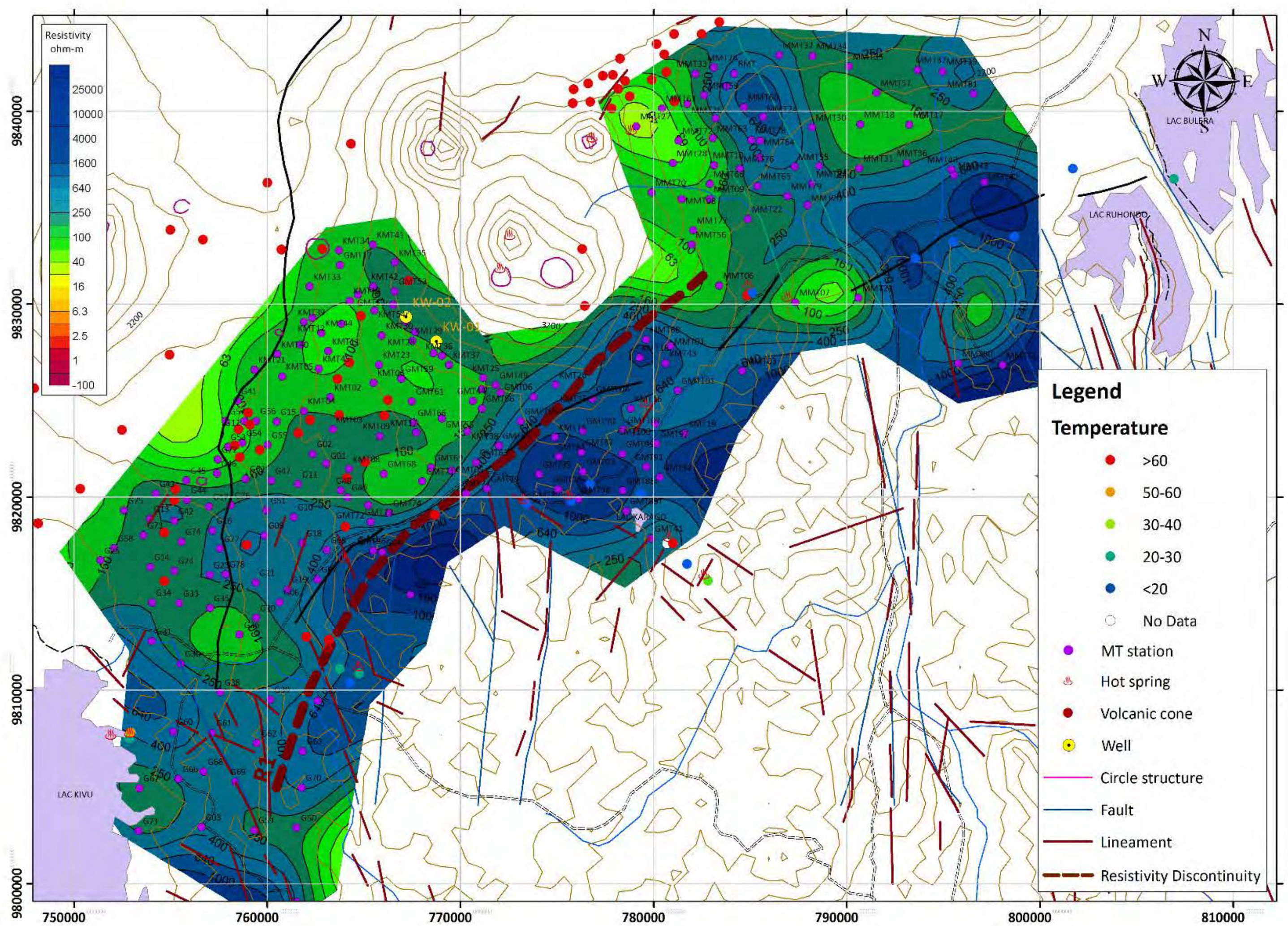

Source: JICA study team

Fig. 3-2.69 Resistivity map at a depth of 500m

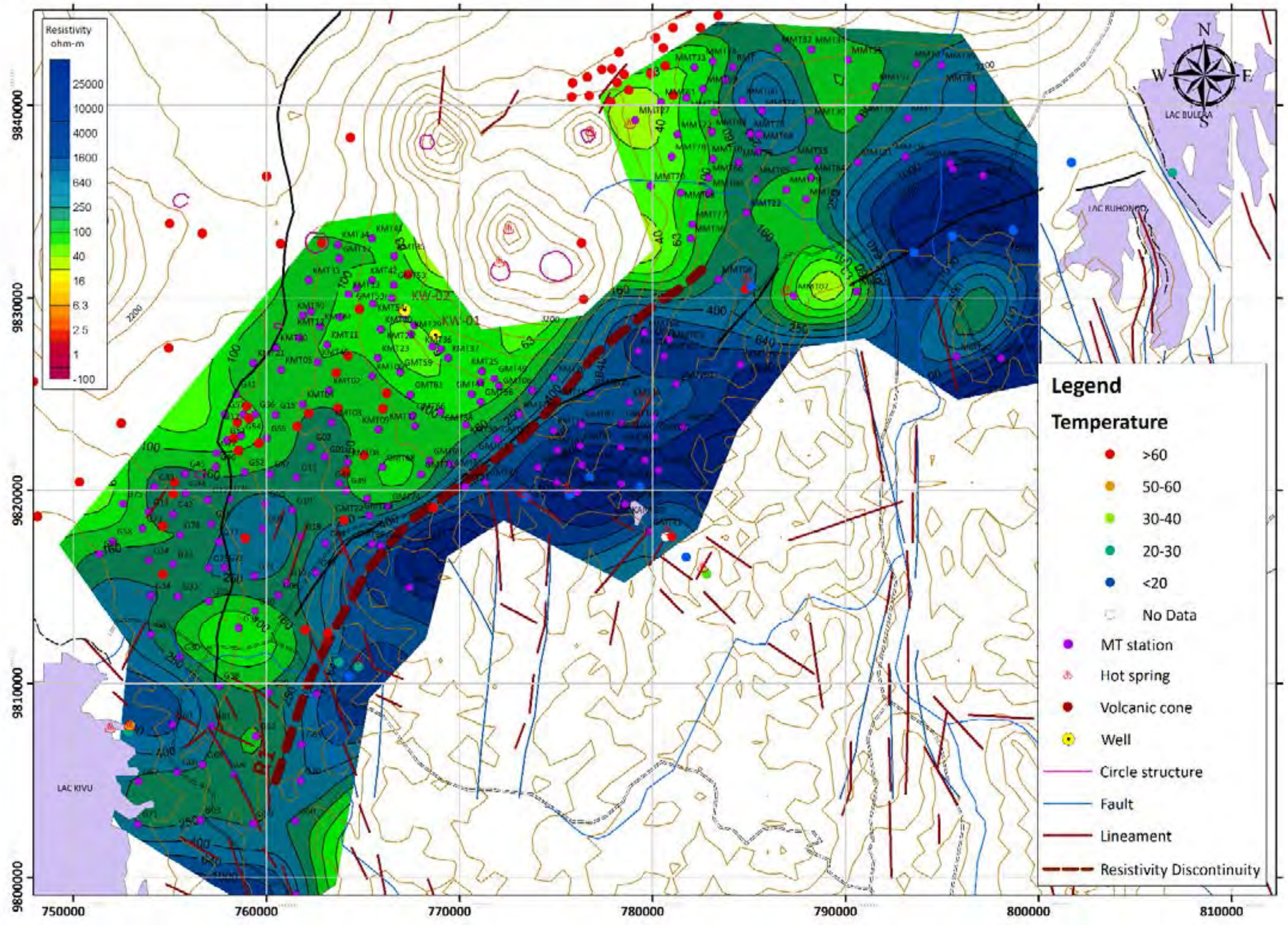

Source: JICA study team

Fig. 3-2.70 Resistivity map at a depth of 750m

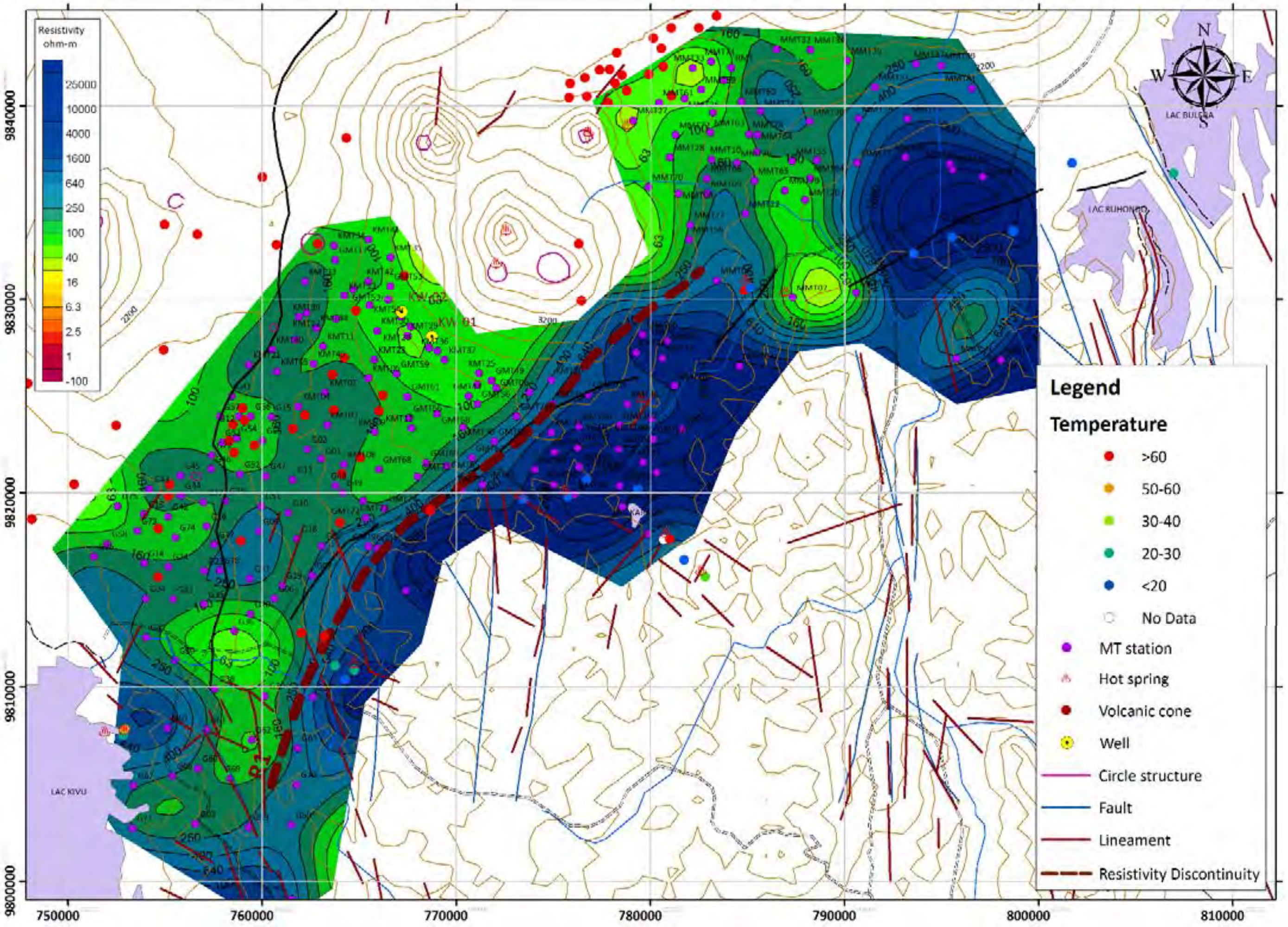

Source: JICA study team

Fig. 3-2.71 Resistivity map at a depth of 1,000m

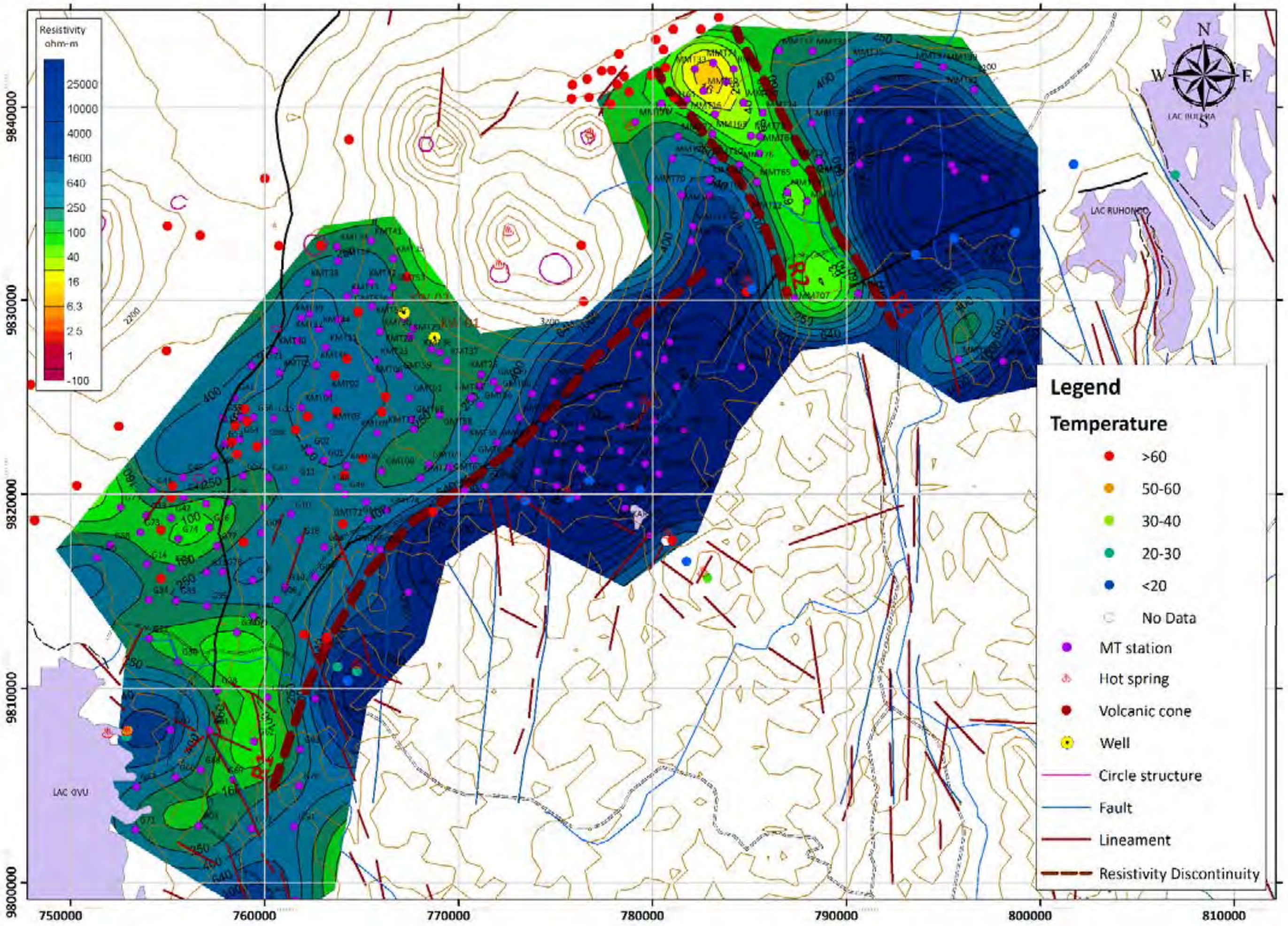

Source: JICA study team

Fig. 3-2.72 Resistivity map at a depth of 1,500m

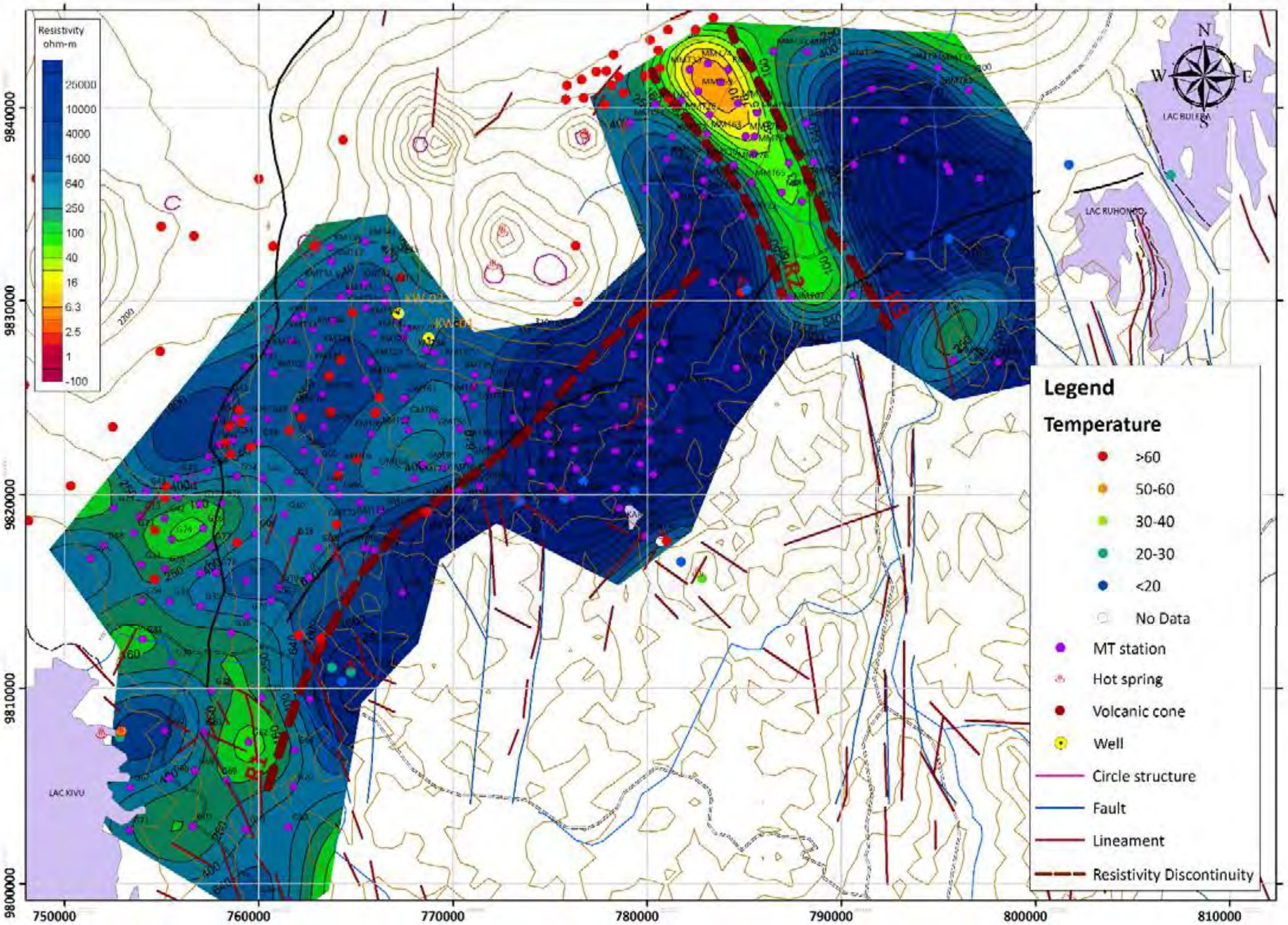

Source: JICA study team

Fig. 3-2.73 Resistivity map at a depth of 2,000m

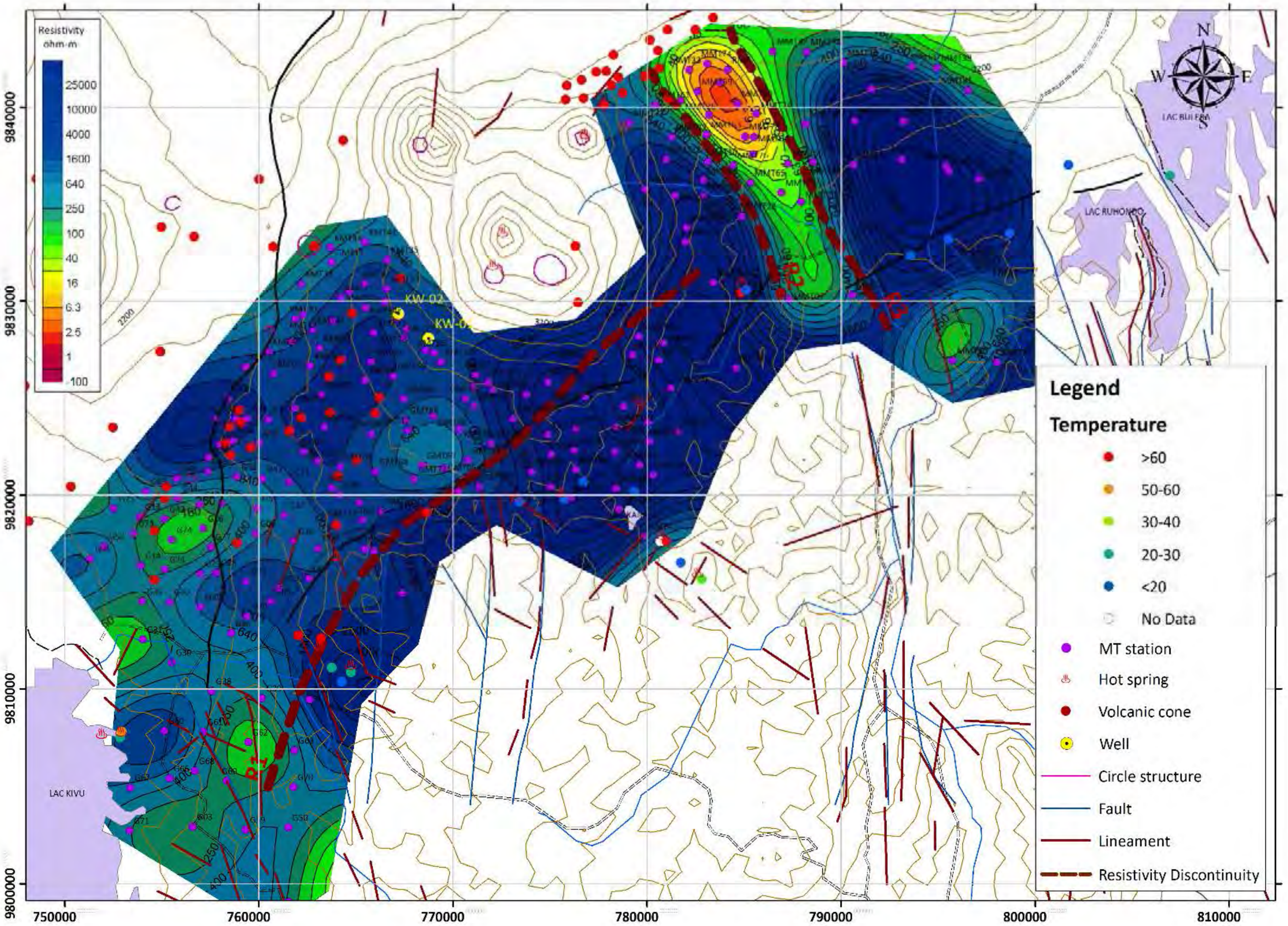

Source: JICA study team

Fig. 3-2.74 Resistivity map at a depth of 2,500m

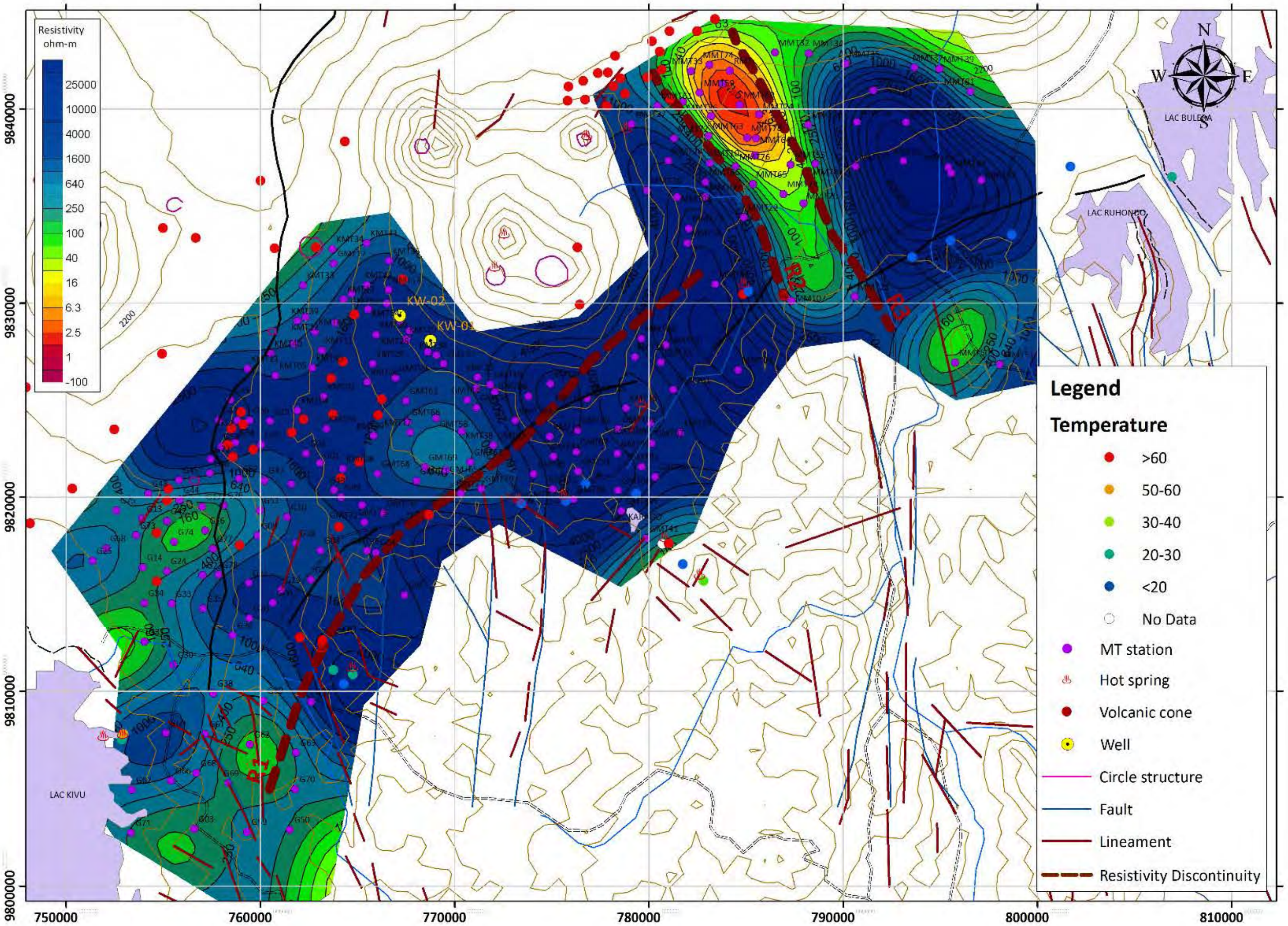

Source: JICA study team

Fig. 3-2.75 Resistivity map at a depth of 3,000m

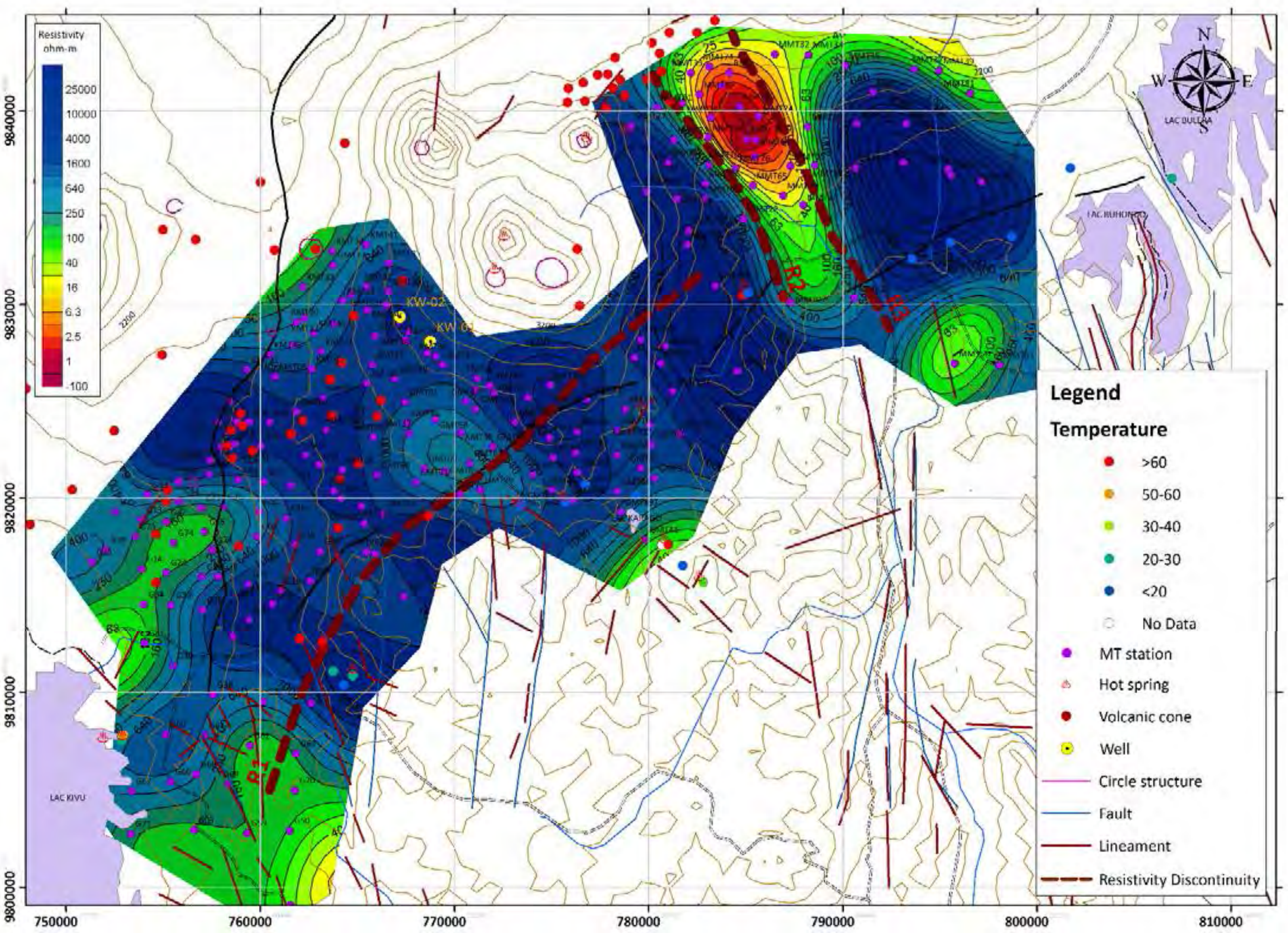

Source: JICA study team

Fig. 3-2.76 Resistivity map at a depth of 4,000m

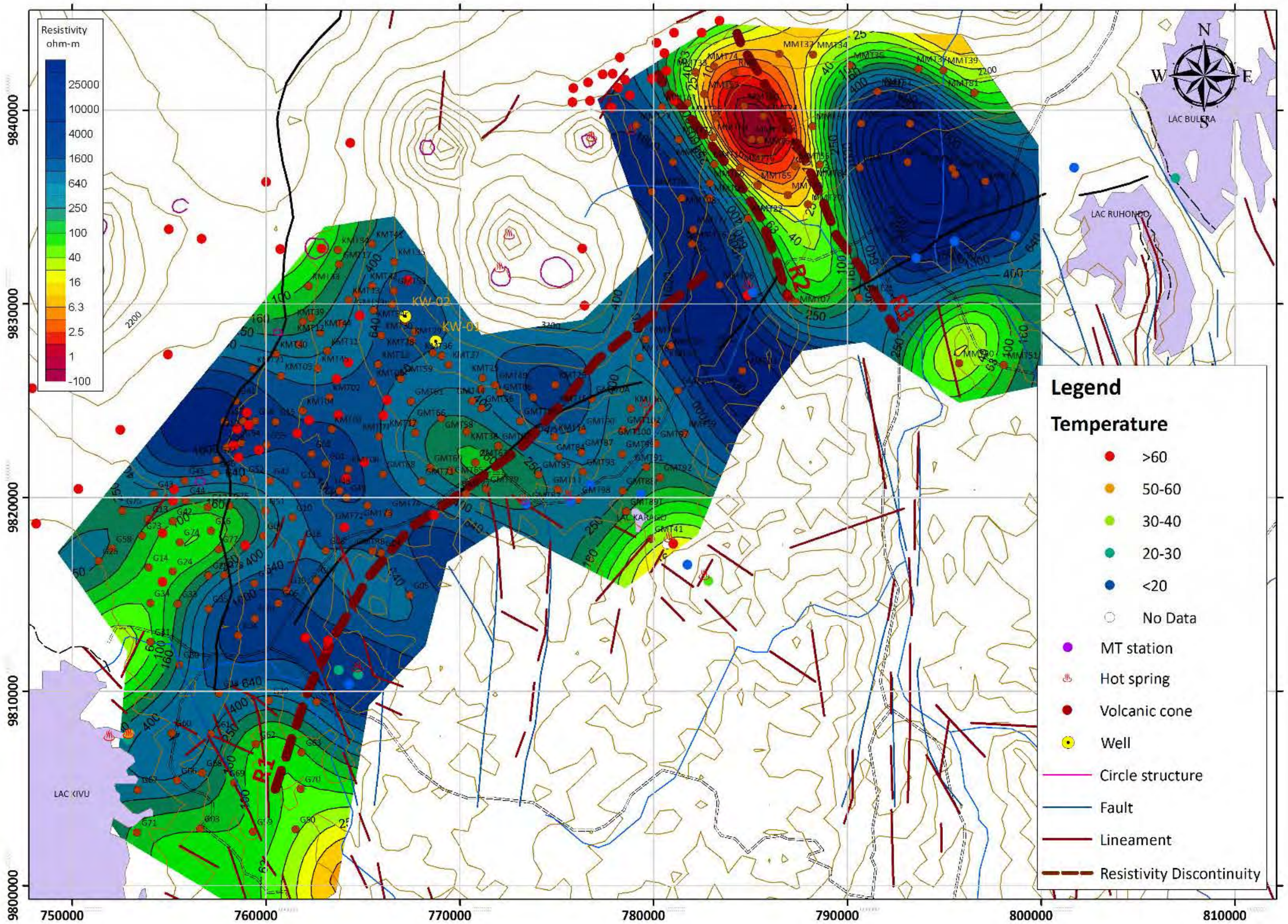

Source: JICA study team

Fig. 3-2.77 Resistivity map at a depth of 5,000m

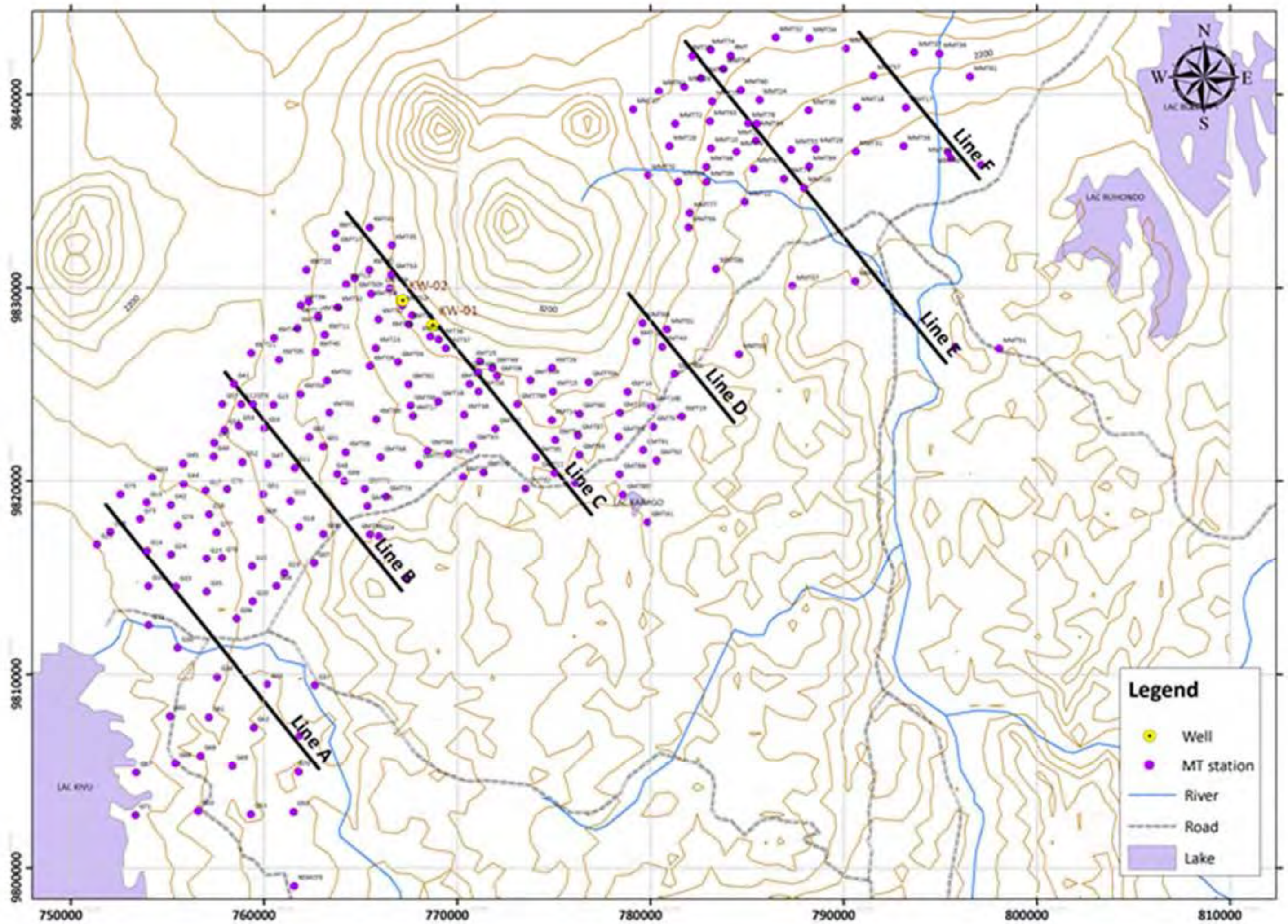

Source: JICA study team

Fig. 3-2.78 Locations of Resistivity Sections

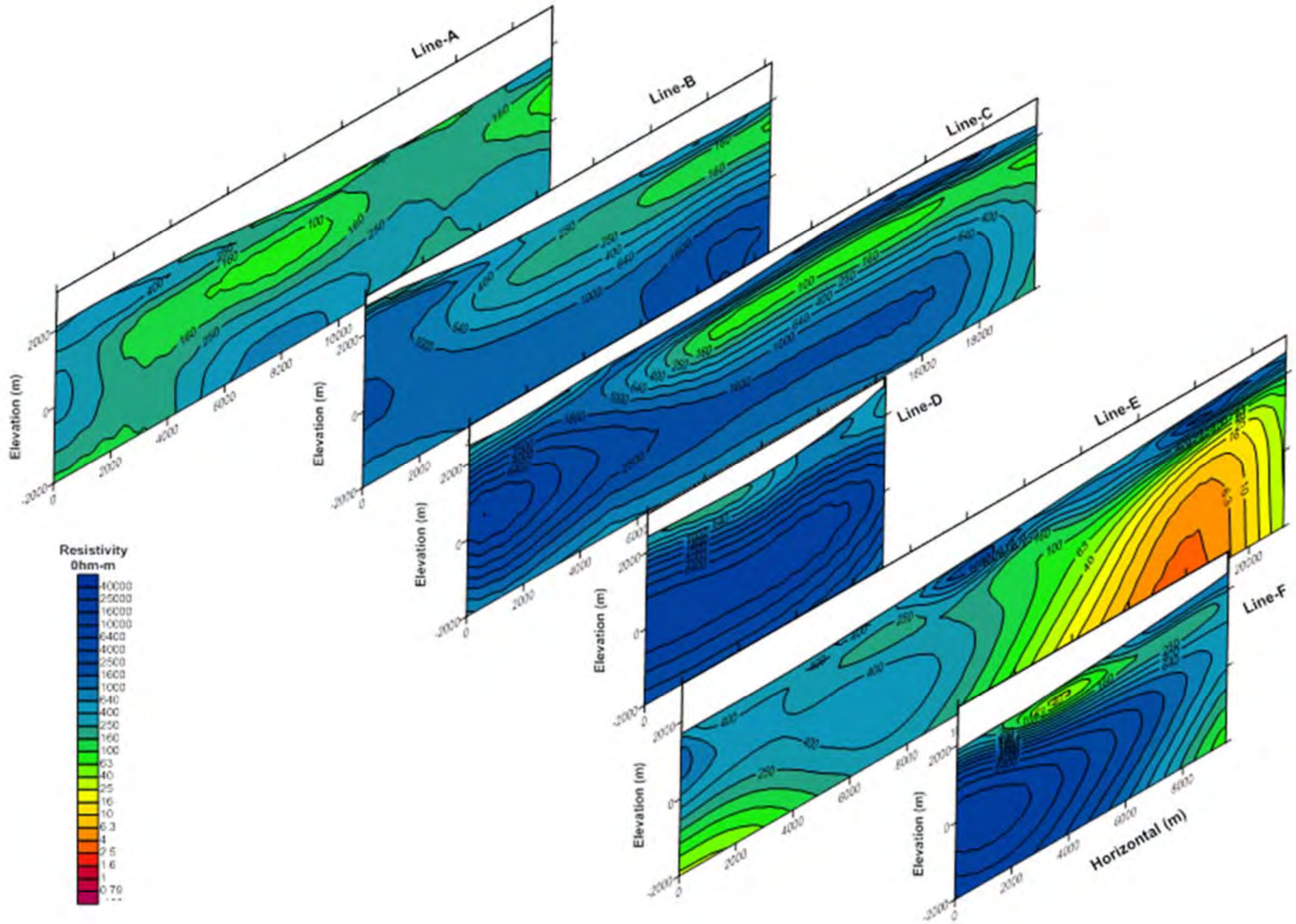

Source: JICA study team

Fig. 3-2.79 Resistivity Section (Line-A, B, C, D, E and F)

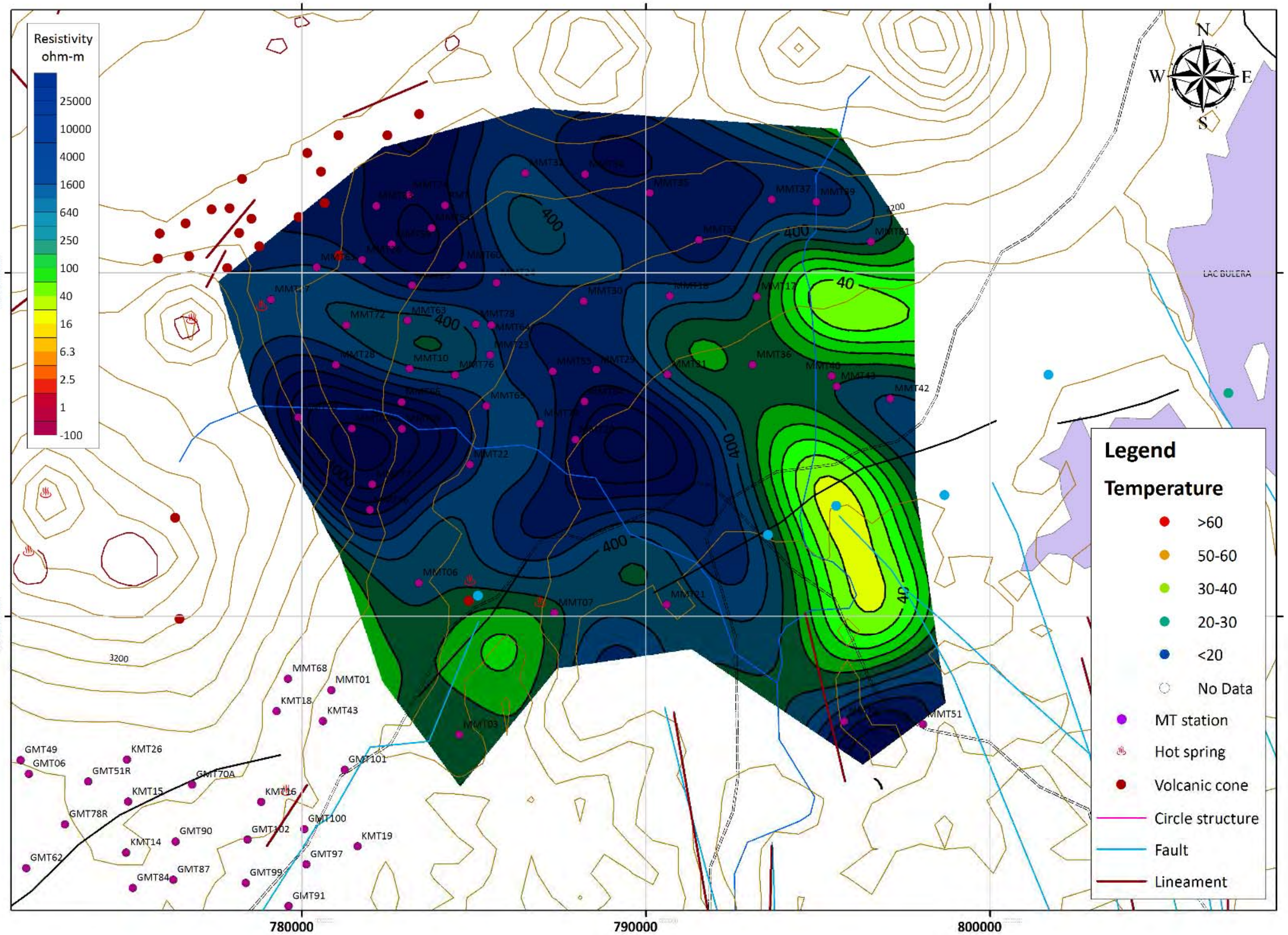

Source: JICA study team

Fig. 3-2.80 Resistivity map at a depth of 100m (Kinigi field)

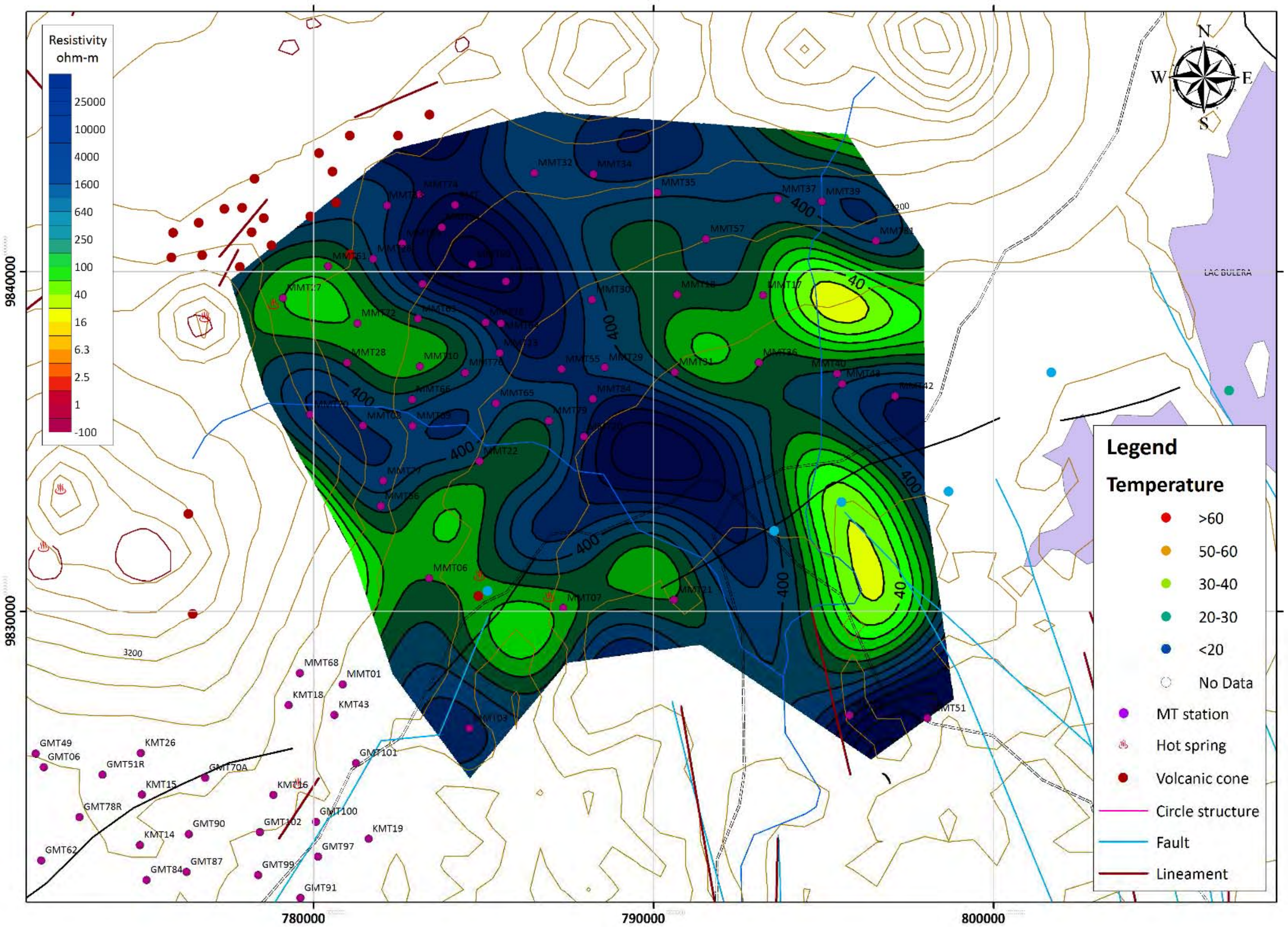

Source: JICA study team

Fig. 3-2.81 Resistivity map at a depth of 300m (Kinigi field)

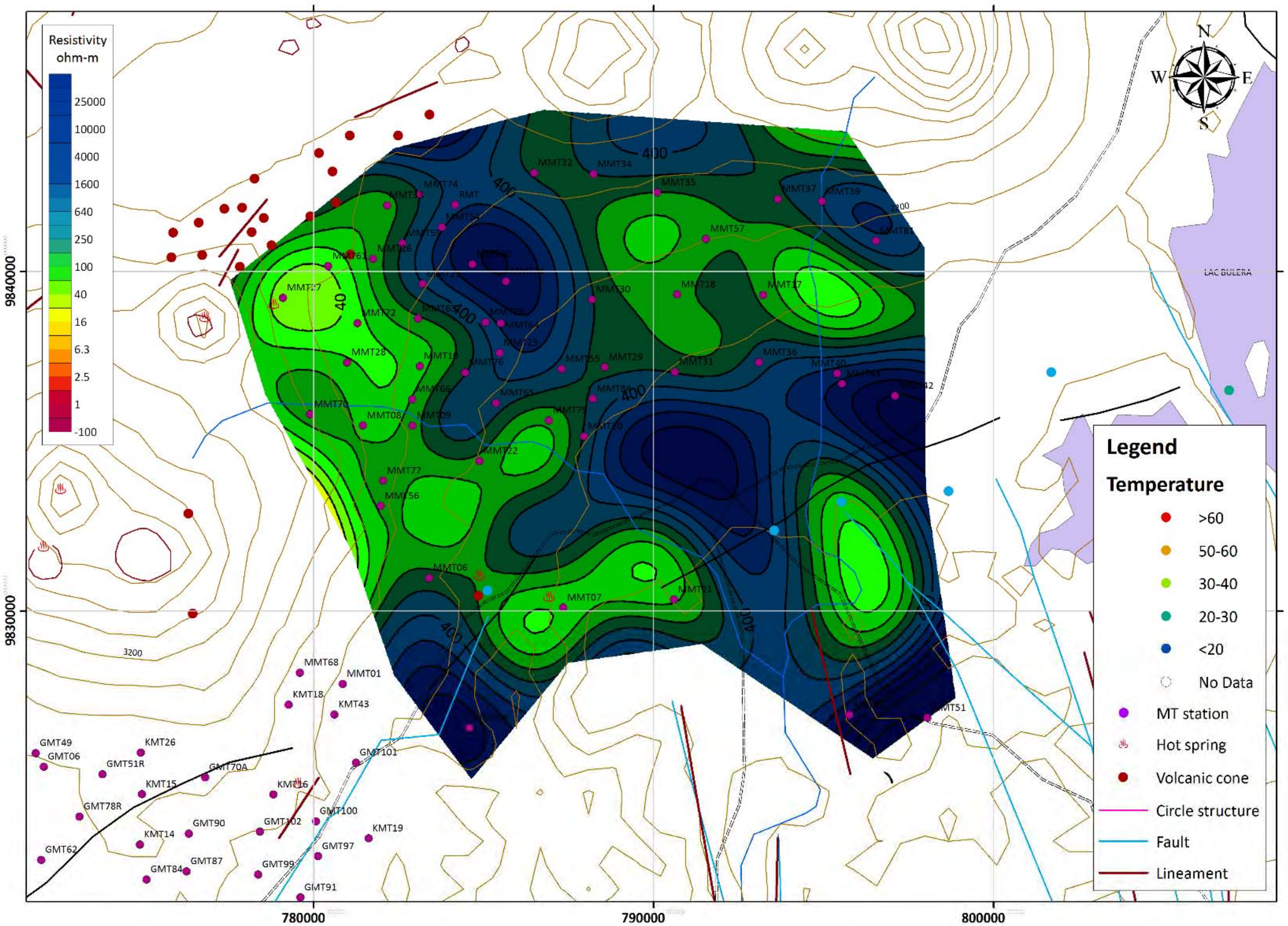

Source: JICA study team

Fig. 3-2.82 Resistivity map at a depth of 500m (Kinigi field)

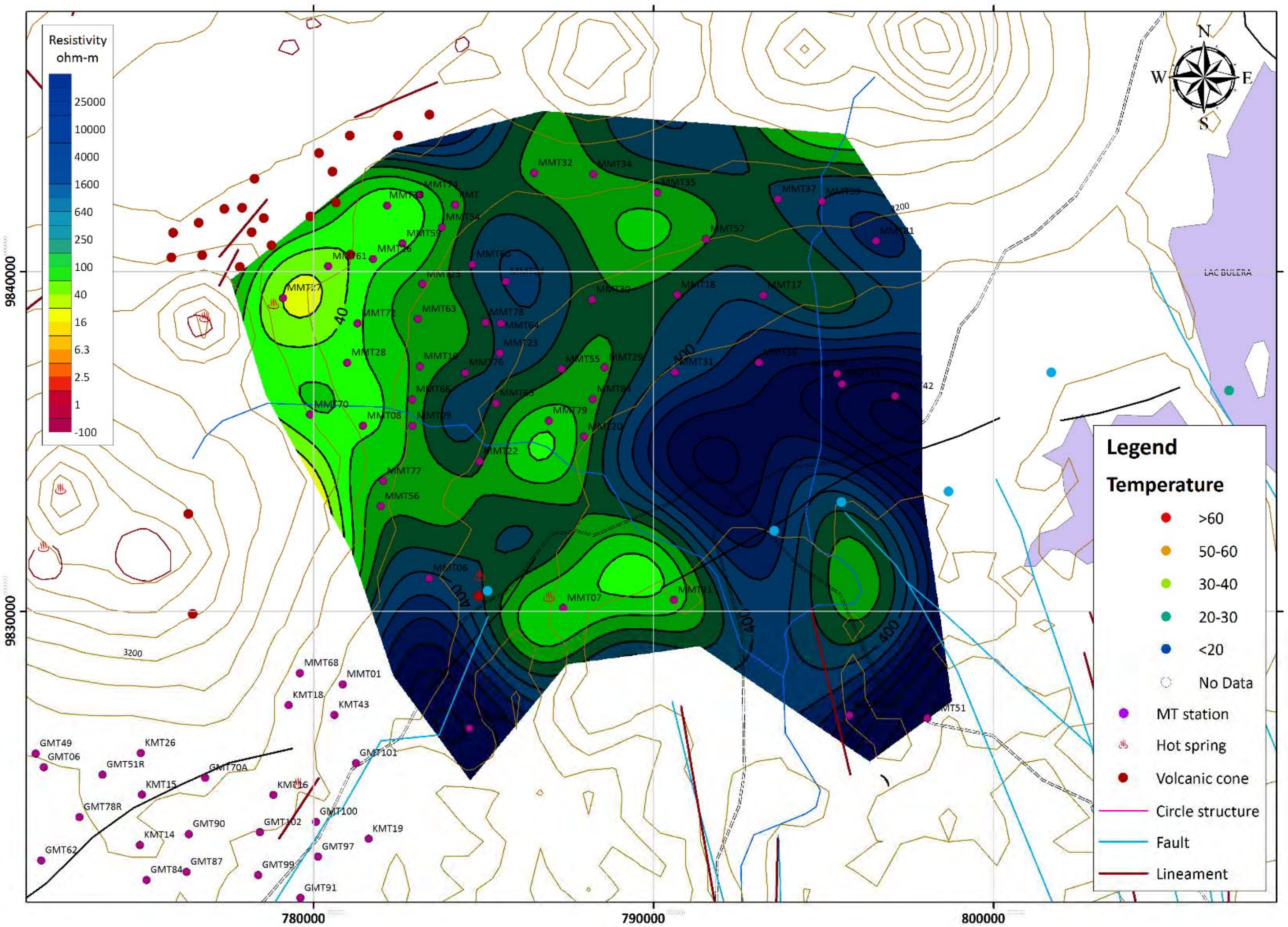

Source: JICA study team

Fig. 3-2.83 Resistivity map at a depth of 750m (Kinigi field)

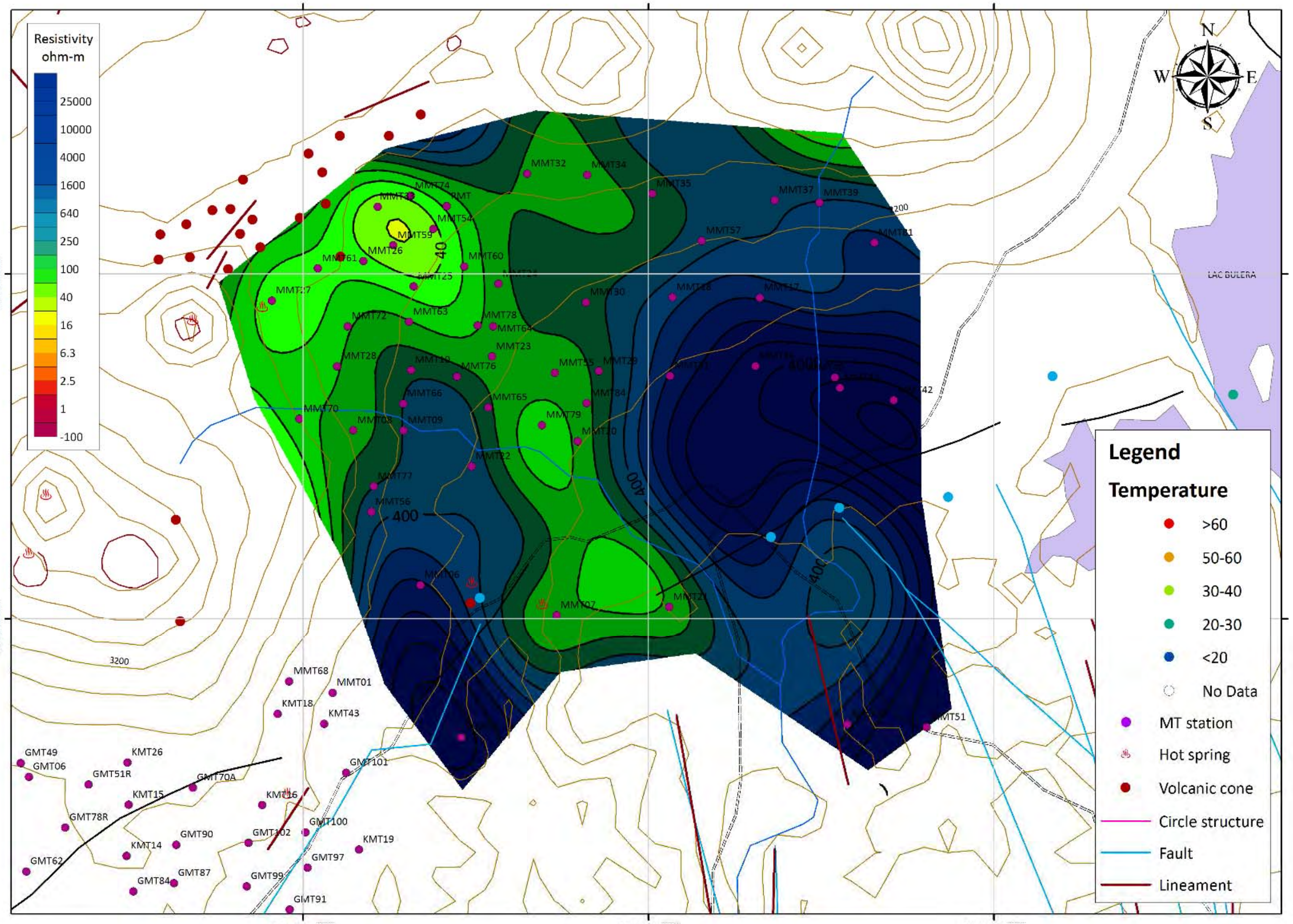

Source: JICA study team

Fig. 3-2.84 Resistivity map at a depth of 1,000m (Kinigi field)

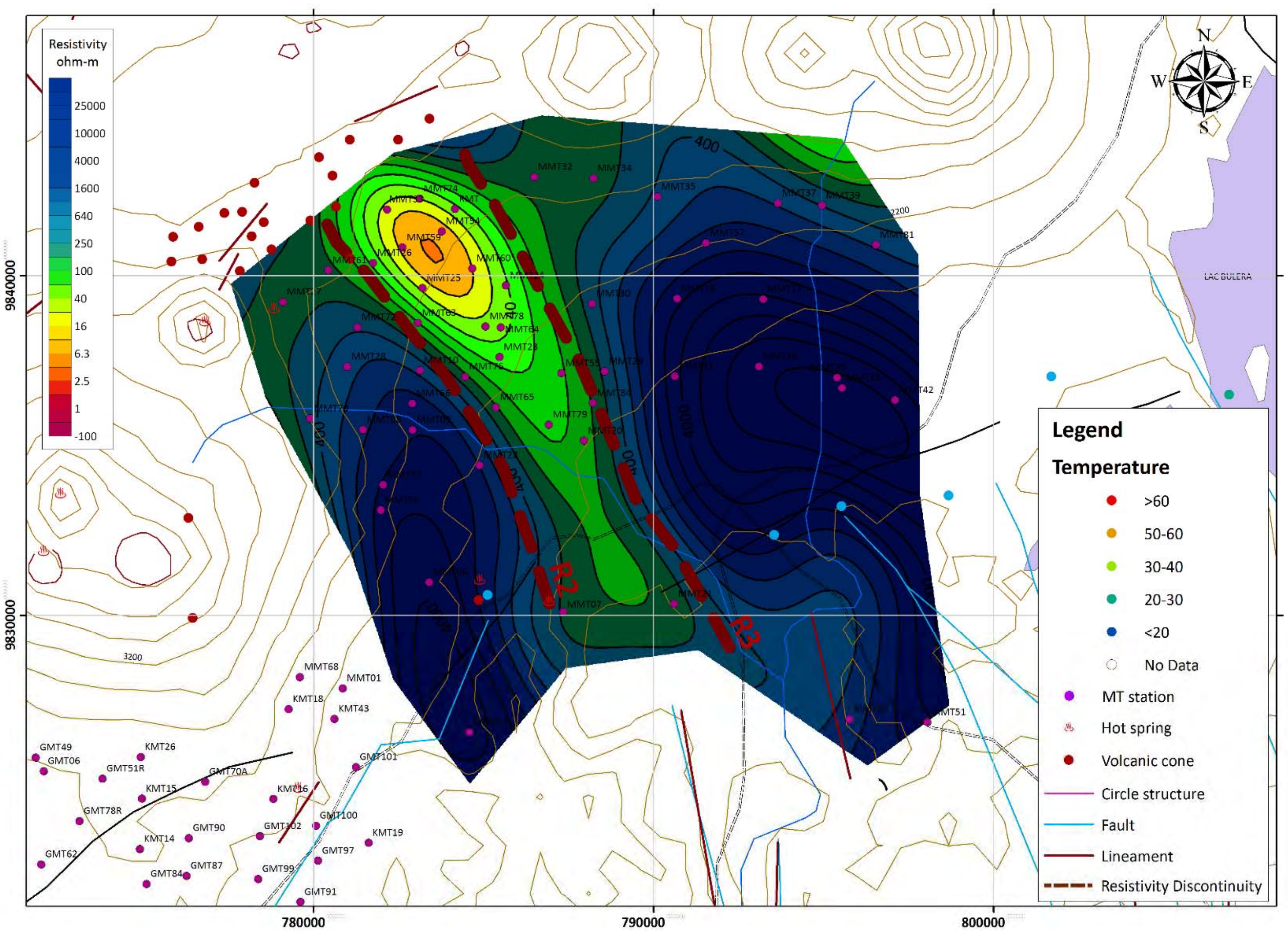

Source: JICA study team

Fig. 3-2.85 Resistivity map at a depth of 1,500m (Kinigi field)

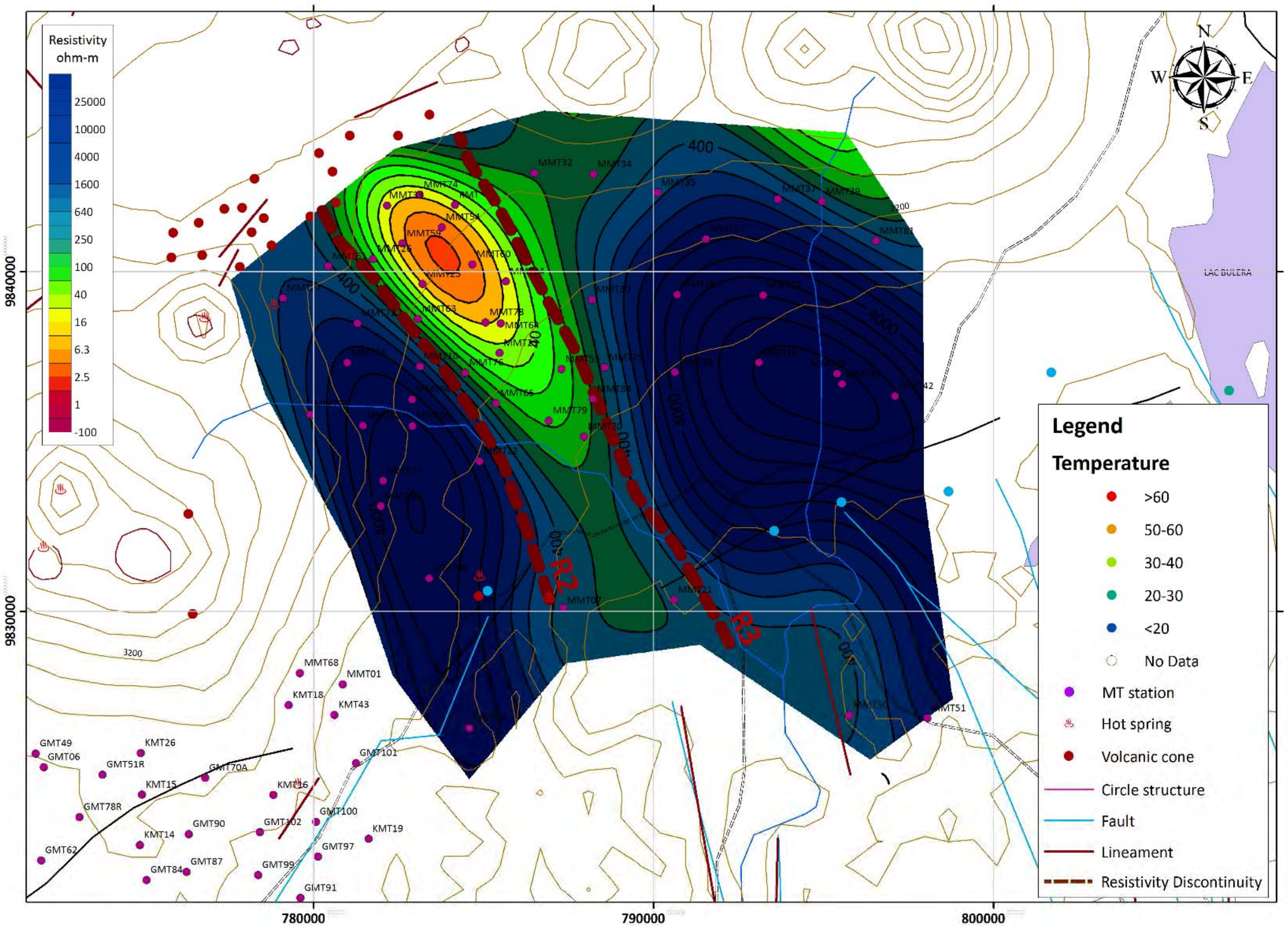

Source: JICA study team

Fig. 3-2.86 Resistivity map at a depth of 2,000m (Kinigi field)

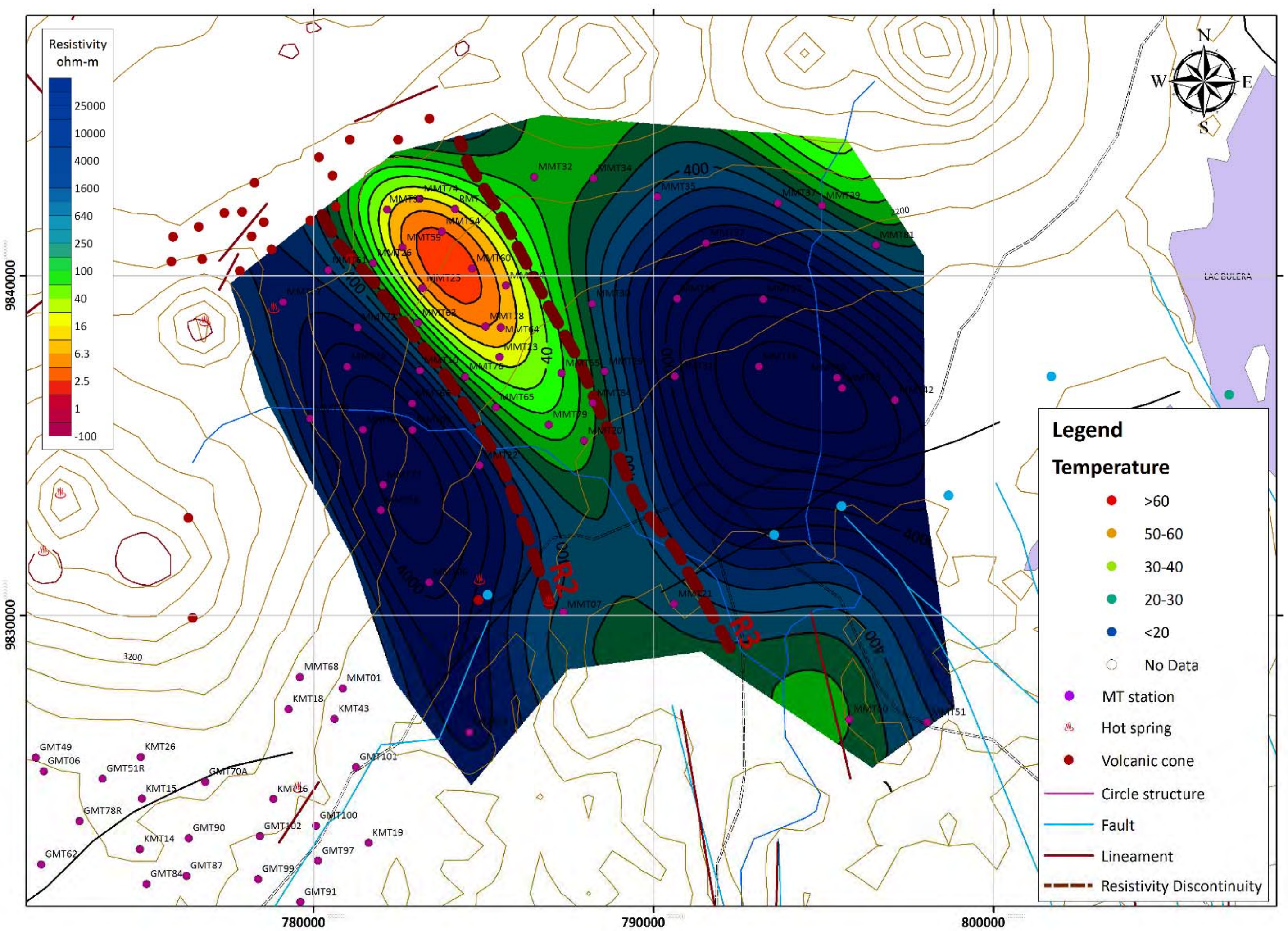

Source: JICA study team

Fig. 3-2.87 Resistivity map at a depth of 2,500m (Kinigi field)

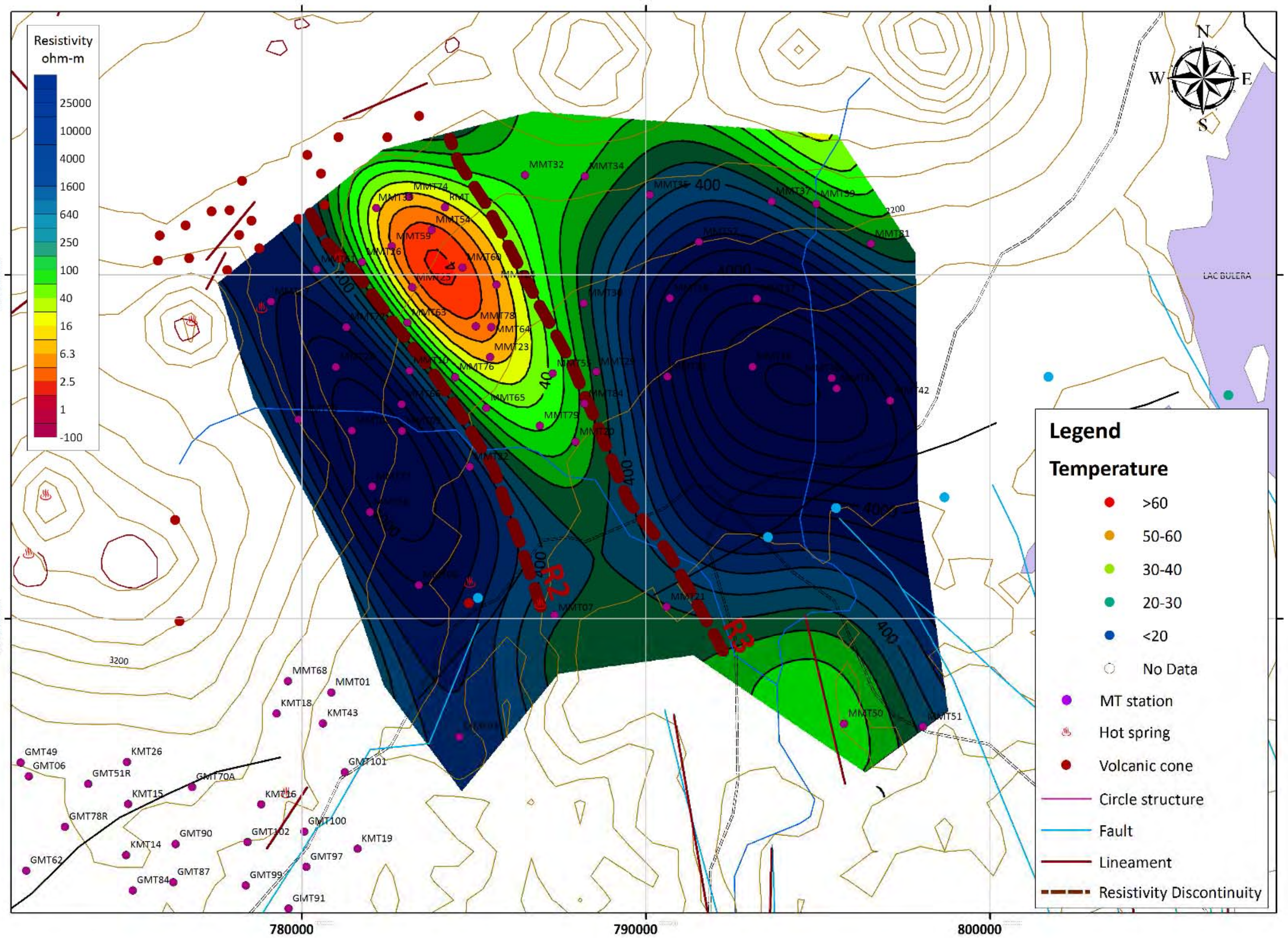

Source: JICA study team

Fig. 3-2.88 Resistivity map at a depth of 3,000m (Kinigi field)

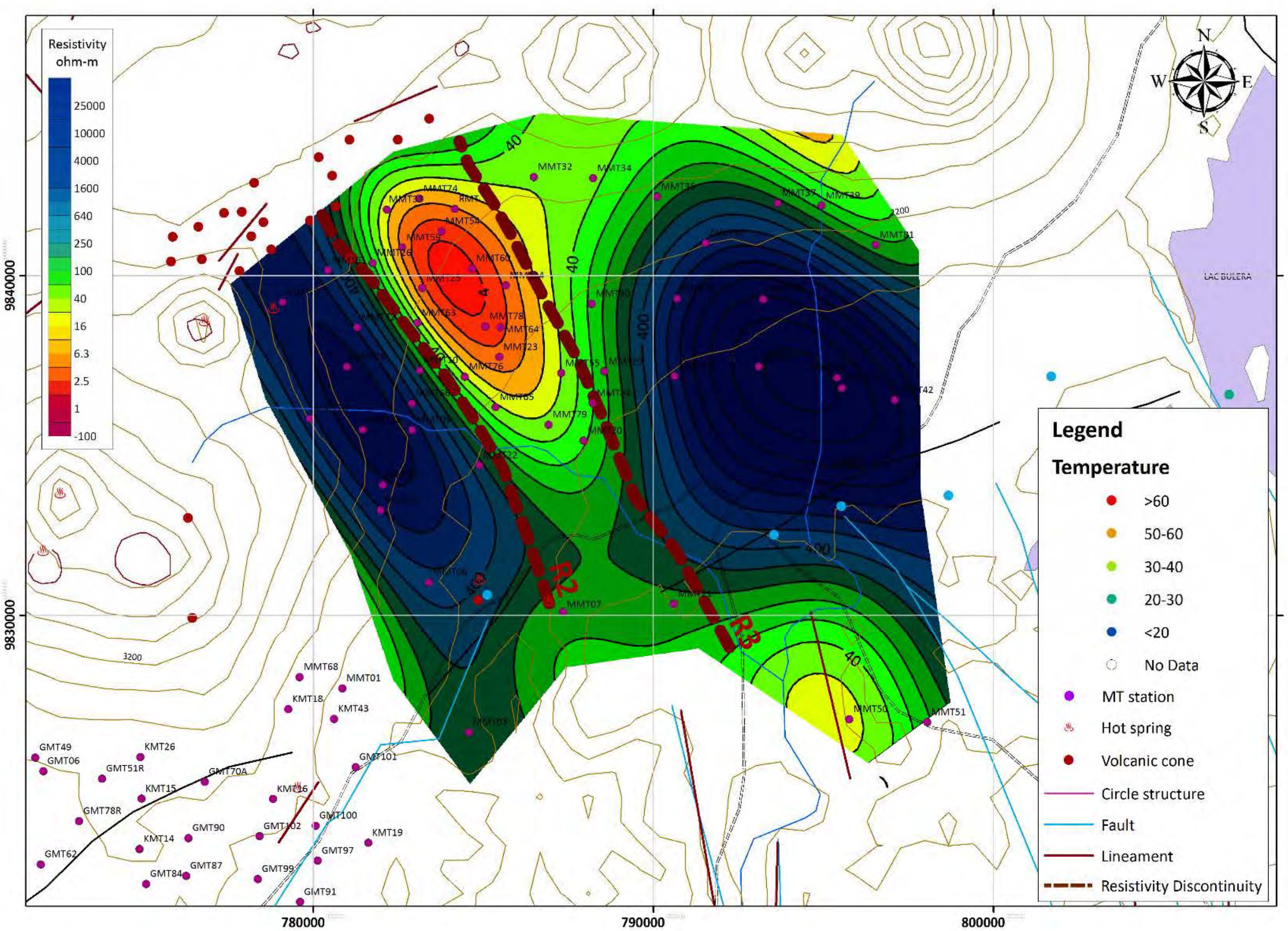

Source: JICA study team

Fig. 3-2.89 Resistivity map at a depth of 4,000m (Kinigi field)

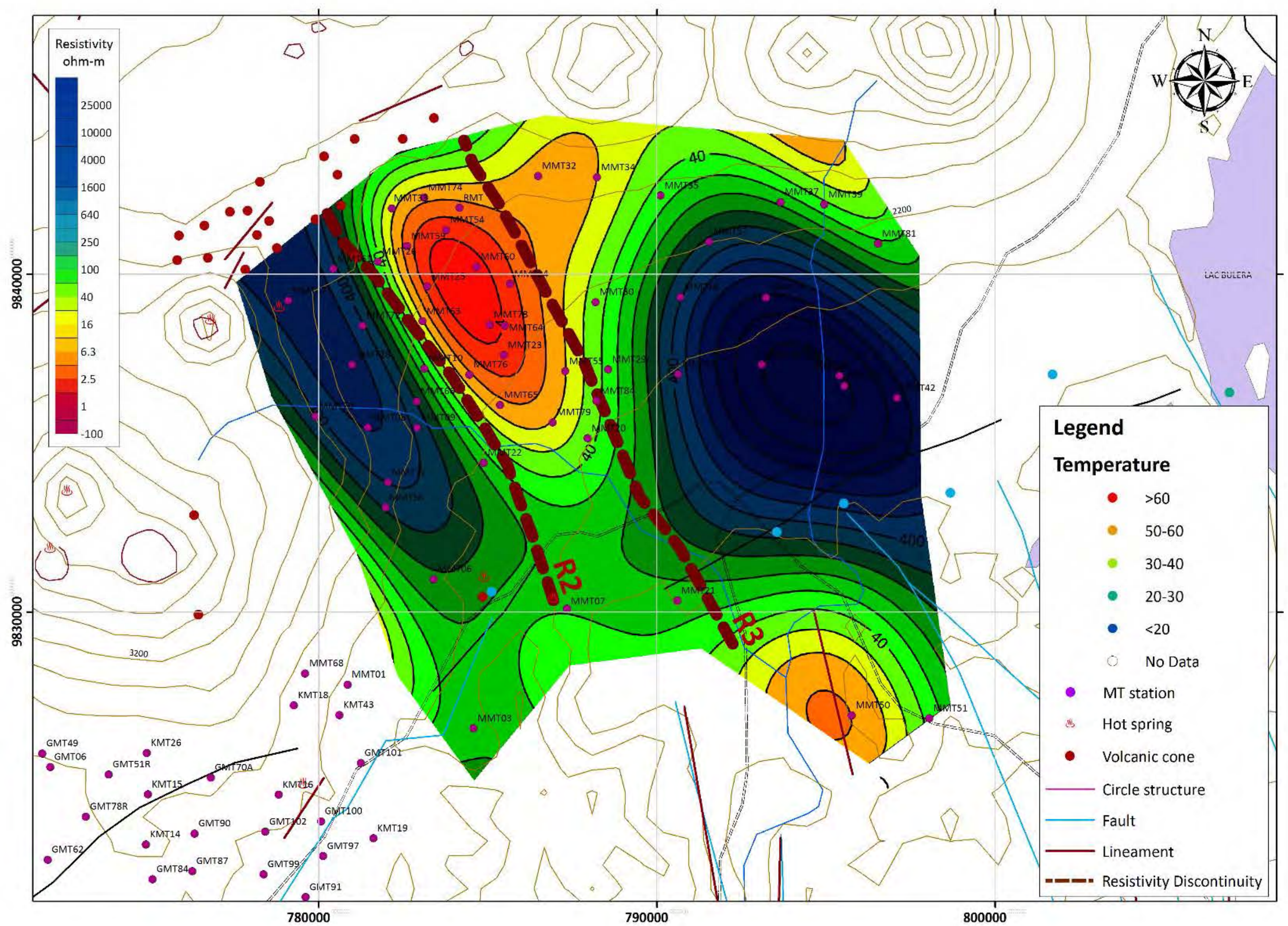

Source: JICA study team

Fig. 3-2.90 Resistivity map at a depth of 5,000m (Kinigi field)

(2) **Gravity survey in Bugarama**

1) Field work for data acquisition

i) Time schedule of the field survey

The time schedule of the field survey for acquiring gravity data in the Bugarama field is shown in Table 3-2.20. The detailed daily activities for the field work are presented in Table 3-2.20.

Table 3-2.20 Time schedule of field survey

Activity \ Date	June																July																	
	15	16	17	18	19	20	21	22	23	24	25	26	27	28	29	30	1	2	3	4	5	6	7	8	9	10	11	12	13	14	15	16	17	18
1. Transfer（Fukuoka→Kigali）	—	—	—	—	—																													
2. Preparation of measurement						—																												
3. Transfer（Kigali→Bugarama）							—																											
4. Meeting, Preparation								—																										
5. Gravity measurement									—	—	—	—	—	—	—	—	—	—	—		—	—	—	—	—	—	—	—						
6. Data processing									—	—	—	—	—	—	—	—	—	—	—	—	—	—	—	—	—	—	—	—						
7. Transfer（Bugarama→Kigali）													—																—					
8. Procedure for machinery shipping																														—	—	—		
9. Transfer（Kigali→Fukuoka）														—	—																		—	—

Source: JICA study team

ii) Equipment utilized for the gravity data acquisition

a) Gravimeter

In this gravity survey, gravity differences between a reference station and actual survey stations were measured using a relative gravimeter.

Relative Gravimeter

The relative gravimeter used in the survey was the CG-5 gravimeter manufactured by CANADA SCINTREX as shown in Fig.3-2.91. During the measurements, statistical data processing using 720 data samples was performed to improve the measurement accuracy (120 seconds of measurement was done with 6 data samples measured per second). This gravimeter is capable of storing the acquired data in internal memory, and thus it is easy to transfer and manage the data using a personal computer with a USB port. The specifications of the CG-5 gravimeter are shown in Table 3-2.21.

Source: JICA study team

Fig. 3-2.91 CG-5 Gravimeter

Table 3-2.21 Table of specifications of CG-5

Sensor type	Fused Quartz using electrostatic nulling
Reading resolution	1 micro Gal
Standard Field Repeatability	<5 micro Gal
Automated Corrections	Tidal correction, terrain correction, temperature correction, drift correction
Data output	RS-232C, USB interface
Dimensions	21cm×22cm×31cm
Weight (including battery)	8kg

Source: JICA study team

b) GPS receiver

A GPS receiver is a device used for measuring position information (latitude, longitude, altitude) at a measurement point. It is necessary to perform various corrections of gravity value in order to calculate the Bouguer anomaly data. The corrections of gravity value require latitude, longitude and altitude information. Two types of GPS receivers, TOPCON’s GRS-1 and TRIMBLE’s 5700 L1 were used in this survey. The receivers are shown in Table 3-2.22. The GRS-1 uses two-frequencies, while the 5700 L1 uses one frequency in order to acquire position information. These devices are composed of an antenna, a controller and a receiver. The antenna is to receive a signal from GPS satellites which are located at an altitude of around 20,000 km. The receiver is composed of a CPU and an internal ROM program for calculating the location of the receiver. The controller consists of a small computer equipped with Windows Mobile, which is used for setting measurement parameters (station name, antenna height, measurement method, observation time, etc.) of the survey station. A GPS receiver is shown in Fig.3-2.92.

Table 3-2.22 The specification of GPS receiver

Name	GRS-1	5700 L1
Receiver wave	Code L1 L2 C/A P（2-frequency）	Code L1 C/A（1-frequency）
Accuracy（Static）	Horizontal：±（3mm+0.5ppm×baseline length km）	Horizontal：±（5mm+0.5ppm×baseline length km）
	Vertical：±（5mm+0.5ppm×baseline length km）	Vertical：±（5mm+1.0ppm×baseline length km）
Dimensions	215mm×93mm×53mm（Main body of receiver）	135mm×85mm×240mm（Main body of receiver）
Weight	0.77kg	1.4 kg
	（Including battery）	（Including battery）
Software for data analysis	GNSS Pro Ver.7.52 (TOPCON), Trimble Total Control™ (TRIMBLE)	
Interval sampling	30 second (short static)	
Data acquisition time	30 minutes/ 1 measurement station (short static)	
Ephemeris	Broadcast Ephemeris	

Source: JICA study team

Source: JICA study team

Fig. 3-2.92 GPS receiver

iii) Measurement method

a) Gravity measurement at each station

In this gravity survey, gravity value at each station was determined by the difference between the measured data at each station and the measured data at the reference station, using the relative gravimeter. During the measurement at each station, the 720 gravity data samples were acquired in 120 seconds (6 data samples were measured in a second). If the standard deviation of the acquired data was large, re-measurement was conducted until satisfactory data was obtained. It should be noted that the gravity measurement was conducted after confirming that the gravimeter tripod was steady.

b) Survey of each measurement point

In this survey, the electronic reference point was located far from the survey area and was not suitable as a reference station for the survey. As the result, we installed a GPS receiver at a station which is roughly 10km from the survey area, and this station was used as a reference point during the survey period. Since the coordinates of the reference station was unknown, we carried out a coordinate survey using a NURK reference point. After installing the 5700 L1 at the reference station, measurement at each of the other stations using the GRS-1 was performed. The duration for the observation at each measurement station was approximately 30 minutes. GPS (GNSS) data processing was done using data processing software developed by TOPCON Inc. The two types of software used were GNSS integrated data processing program (GNSS-Pro ver 7.52) and Trimble Total Control™ developed by TRIMBLE Company. After calculating the baseline between the 5700 L1 and the reference point (the 3D vector between the two points), the position of the reference point was precisely obtained. In addition, since the height of the GPS survey station was determined from the ellipsoid, and the height differs from altitude, a deduction of the ellipsoid height from the geoid height must be done to obtain an altitude conversion. In this survey, the heights of the measurement stations was calculated from the height data obtained by GPS, then integrated data processing was performed using Trimble Total Control™.

The latitude, longitude and altitude of each station was determined by performing the above-mentioned process. The result of the GPS measurements are shown in Table 3-2.23, while the location of each station is shown in Fig.3-2.93.

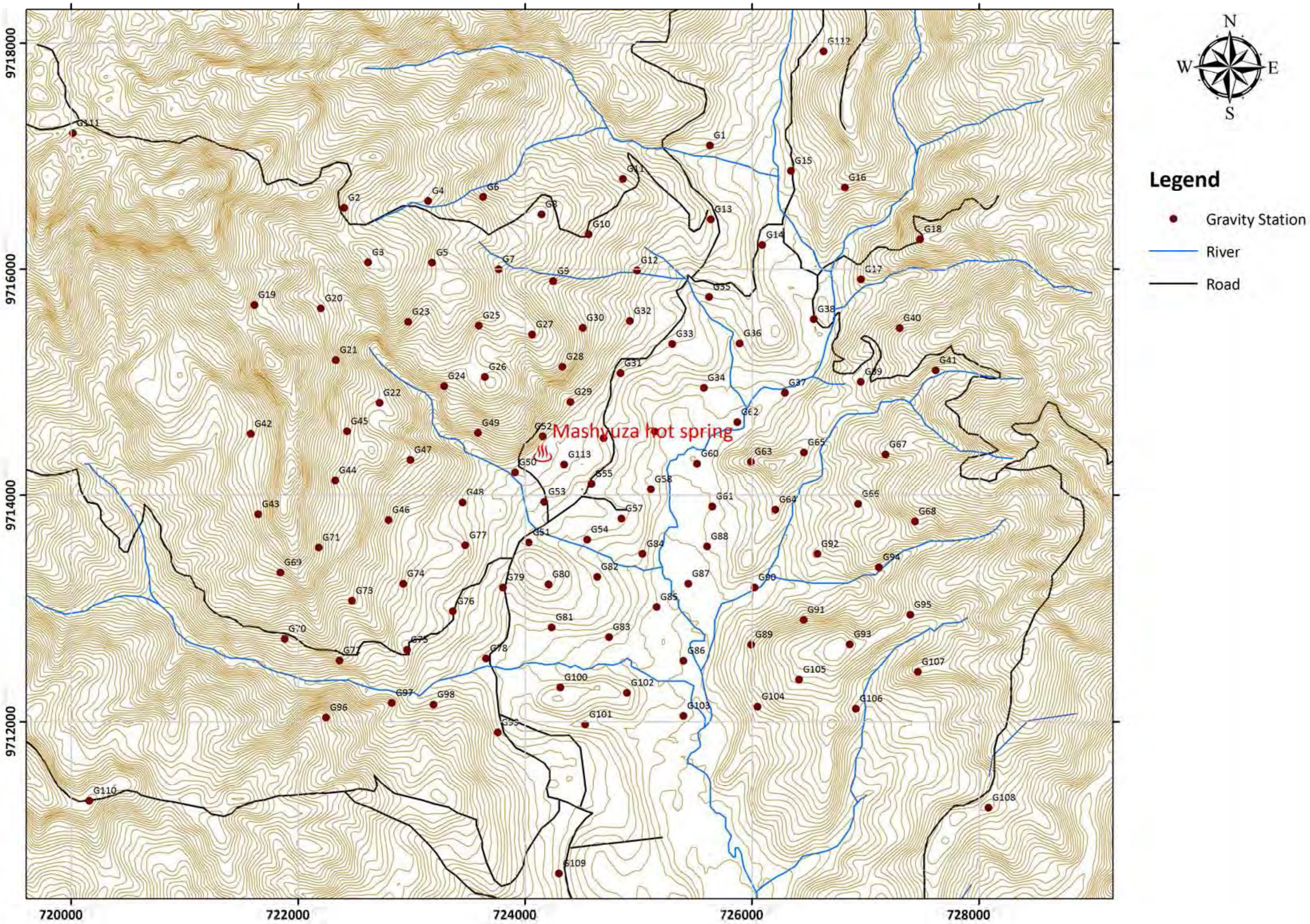

Source: JICA study team

Fig. 3-2.93 Location of each station

Table 3-2.23 Result of GPS measurement (1)

Station	WGS84						UTM		Elevation
	Latitude			Longitude			NS	EW	
	Deg	Min	Sec	Deg	Min	Sec	(m)	(m)	(m)
G1	-2	33	28.396	29	1	45.250	9717096.277	725627.013	1228.585
G2	-2	33	46.532	29	0	0.991	9716544.167	722404.707	1731.421
G3	-2	34	2.276	29	0	7.811	9716060.152	722614.659	1752.293
G4	-2	33	44.534	29	0	24.931	9716604.399	723144.500	1621.019
G5	-2	34	2.314	29	0	26.067	9716058.090	723178.728	1615.092
G6	-2	33	43.331	29	0	40.599	9716640.594	723628.674	1469.421
G7	-2	34	4.170	29	0	45.077	9716000.143	723766.029	1475.633
G8	-2	33	48.376	29	0	57.263	9716484.788	724143.300	1470.638
G9	-2	34	7.568	29	1	0.602	9715895.013	724245.551	1409.839
G10	-2	33	54.041	29	1	10.743	9716310.091	724559.539	1384.907
G11	-2	33	38.070	29	1	20.498	9716800.275	724861.746	1314.913
G12	-2	34	4.407	29	1	24.500	9715990.944	724984.096	1263.087
G13	-2	33	49.678	29	1	45.573	9716442.437	725635.929	1217.596
G14	-2	33	57.000	29	2	0.235	9716216.747	726088.611	1145.407
G15	-2	33	35.679	29	2	8.397	9716871.397	726341.854	1176.268
G16	-2	33	40.440	29	2	23.771	9716724.388	726816.647	1278.450
G17	-2	34	6.902	29	2	28.398	9715911.167	726958.333	1188.802
G18	-2	33	55.259	29	2	45.293	9716268.025	727480.948	1370.198
G19	-2	34	14.558	28	59	35.438	9715684.373	721613.831	1786.533
G20	-2	34	15.530	28	59	54.385	9715653.593	722199.195	1628.665
G21	-2	34	30.343	28	59	58.671	9715198.305	722330.911	1608.006
G22	-2	34	42.668	29	0	11.134	9714819.066	722715.385	1485.878
G23	-2	34	19.354	29	0	19.298	9715534.921	722968.777	1589.321
G24	-2	34	37.860	29	0	29.582	9714965.870	723285.640	1445.872
G25	-2	34	20.375	29	0	39.447	9715502.572	723591.292	1517.251
G26	-2	34	35.217	29	0	41.189	9715046.495	723644.378	1474.700
G27	-2	34	22.906	29	0	54.604	9715424.061	724059.490	1493.343
G28	-2	34	32.144	29	1	3.266	9715139.851	724326.665	1394.368
G29	-2	34	42.387	29	1	5.619	9714825.042	724398.873	1228.453
G30	-2	34	21.007	29	1	9.116	9715481.723	724507.953	1337.598

Source: JICA study team

Table 3-2.23 Result of GPS measurement (2)

Station	WGS84						UTM		Elevation
	Latitude			Longitude			NS	EW	
	Deg	Min	Sec	Deg	Min	Sec	(m)	(m)	(m)
G31	-2	34	34.017	29	1	19.868	9715081.487	724839.537	1158.389
G32	-2	34	19.026	29	1	22.533	9715541.915	724922.614	1223.654
G33	-2	34	25.591	29	1	34.611	9715339.623	725295.497	1157.619
G34	-2	34	38.270	29	1	43.632	9714949.653	725573.586	1109.812
G35	-2	34	12.038	29	1	45.139	9715755.482	725621.454	1159.592
G36	-2	34	25.409	29	1	53.870	9715344.269	725890.564	1136.931
G37	-2	34	39.630	29	2	6.755	9714906.711	726287.996	1103.806
G38	-2	34	18.423	29	2	14.933	9715557.875	726541.712	1128.579
G39	-2	34	36.393	29	2	28.424	9715005.112	726957.673	1215.935
G40	-2	34	20.961	29	2	39.464	9715478.684	727299.560	1297.277
G41	-2	34	33.109	29	2	49.759	9715104.939	727617.077	1295.461
G42	-2	34	51.665	28	59	34.431	9714544.417	721580.925	1574.858
G43	-2	35	14.853	28	59	36.582	9713831.934	721646.293	1585.410
G44	-2	35	5.023	28	59	58.511	9714132.878	722324.313	1531.108
G45	-2	34	50.871	29	0	1.894	9714567.501	722429.494	1538.519
G46	-2	35	16.445	29	0	13.781	9713781.233	722795.564	1348.637
G47	-2	34	59.083	29	0	19.985	9714314.316	722988.089	1410.594
G48	-2	35	11.323	29	0	34.890	9713937.564	723448.025	1221.349
G49	-2	34	51.356	29	0	39.238	9714550.781	723583.323	1298.285
G50	-2	35	2.592	29	0	49.820	9714205.064	723909.721	1186.285
G51	-2	35	22.798	29	0	53.775	9713584.085	724030.946	1139.319
G52	-2	34	52.310	29	0	57.748	9714520.568	724155.208	1213.968
G53	-2	35	11.113	29	0	58.201	9713942.864	724168.281	1155.004
G54	-2	35	21.967	29	1	10.421	9713608.789	724545.325	1115.162
G55	-2	35	5.931	29	1	11.646	9714101.404	724583.960	1134.405
G56	-2	34	52.710	29	1	15.104	9714507.410	724691.447	1142.143
G57	-2	35	15.864	29	1	20.247	9713795.821	724849.213	1128.705
G58	-2	35	7.480	29	1	28.594	9714052.981	725107.523	1091.411
G59	-2	34	50.807	29	1	29.693	9714565.166	725142.302	1086.473
G60	-2	35	0.043	29	1	41.768	9714280.805	725514.944	1078.010

Source: JICA study team

Table 3-2.23 Result of GPS measurement (3)

Station	WGS84						UTM		Elevation
	Latitude			Longitude			NS	EW	
	Deg	Min	Sec	Deg	Min	Sec	(m)	(m)	(m)
G61	-2	35	12.380	29	1	46.080	9713901.567	725647.565	1082.157
G62	-2	34	48.077	29	1	53.212	9714647.876	725869.107	1091.819
G63	-2	34	59.494	29	1	57.093	9714296.938	725988.467	1188.054
G64	-2	35	13.225	29	2	4.080	9713874.723	726203.685	1164.125
G65	-2	34	56.822	29	2	12.231	9714378.260	726456.349	1181.963
G66	-2	35	11.561	29	2	27.716	9713924.661	726934.066	1198.665
G67	-2	34	57.324	29	2	35.489	9714361.679	727174.954	1288.720
G68	-2	35	16.567	29	2	43.891	9713770.062	727433.603	1325.242
G69	-2	35	31.614	28	59	42.922	9713316.705	721841.369	1542.602
G70	-2	35	50.724	28	59	44.226	9712729.554	721880.730	1316.688
G71	-2	35	24.394	28	59	53.877	9713537.991	722180.189	1556.561
G72	-2	35	56.846	28	59	59.846	9712540.706	722363.046	1279.781
G73	-2	35	39.688	29	0	3.364	9713067.667	722472.569	1391.422
G74	-2	35	34.732	29	0	17.958	9713219.215	722923.727	1278.907
G75	-2	35	53.776	29	0	19.067	9712634.064	722957.048	1220.033
G76	-2	35	42.720	29	0	32.172	9712973.082	723362.487	1189.494
G77	-2	35	23.680	29	0	35.690	9713557.879	723472.122	1233.907
G78	-2	35	56.262	29	0	41.654	9712556.594	723654.819	1107.406
G79	-2	35	35.797	29	0	46.417	9713185.088	723802.958	1132.942
G80	-2	35	34.866	29	0	59.404	9713213.059	724204.270	1168.579
G81	-2	35	47.277	29	1	0.402	9712831.705	724234.522	1107.660
G82	-2	35	32.694	29	1	13.328	9713279.104	724634.601	1116.552
G83	-2	35	50.075	29	1	16.705	9712744.952	724738.090	1081.109
G84	-2	35	26.063	29	1	26.265	9713482.164	725034.638	1082.055
G85	-2	35	41.367	29	1	30.291	9713011.785	725158.294	1062.490
G86	-2	35	56.784	29	1	37.993	9712537.773	725395.521	1052.085
G87	-2	35	34.654	29	1	39.329	9713217.604	725437.873	1058.160
G88	-2	35	23.868	29	1	44.616	9713548.691	725601.766	1077.573
G89	-2	35	52.166	29	1	57.291	9712678.674	725991.988	1175.605
G90	-2	35	35.708	29	1	58.196	9713184.272	726020.759	1072.862

Source: JICA study team

Table 3-2.23 Result of GPS measurement (4)

Station	WGS84						UTM		Elevation
	Latitude			Longitude			NS	EW	
	deg	Min	Sec	Deg	Min	Sec	(m)	(m)	(m)
G91	-2	35	44.993	29	2	12.236	9712898.317	726454.125	1190.772
G92	-2	35	25.956	29	2	16.134	9713482.984	726575.489	1173.240
G93	-2	35	51.984	29	2	25.428	9712682.864	726861.390	1279.619
G94	-2	35	29.865	29	2	33.682	9713362.040	727117.496	1196.259
G95	-2	35	43.464	29	2	42.648	9712943.773	727393.851	1261.956
G96	-2	36	13.354	28	59	56.043	9712033.718	722244.743	1391.289
G97	-2	36	9.100	29	0	14.795	9712163.491	722824.301	1230.693
G98	-2	36	9.539	29	0	26.672	9712149.407	723191.269	1166.390
G99	-2	36	17.595	29	0	45.037	9711901.010	723758.294	1118.127
G100	-2	36	4.580	29	1	2.862	9712299.979	724309.661	1115.379
G101	-2	36	15.237	29	1	9.920	9711972.237	724527.233	1063.941
G102	-2	36	6.061	29	1	21.862	9712253.558	724896.634	1094.723
G103	-2	36	12.671	29	1	37.940	9712049.664	725393.086	1041.619
G104	-2	36	10.017	29	1	59.104	9712130.166	726047.148	1153.520
G105	-2	36	2.242	29	2	10.927	9712368.450	726412.833	1240.349
G106	-2	36	10.546	29	2	27.109	9712112.518	726912.401	1149.878
G107	-2	35	59.960	29	2	44.834	9712436.873	727460.596	1300.727
G108	-2	36	39.033	29	3	5.037	9711235.404	728082.871	1268.070
G109	-2	36	58.151	29	1	2.536	9710654.172	724296.961	1105.580
G110	-2	36	37.464	28	58	48.534	9711296.303	720157.754	1649.656
G111	-2	33	25.190	28	58	43.527	9717203.545	720012.246	1986.776
G112	-2	33	1.231	29	2	17.654	9717929.289	726629.554	1241.532
G113	-2	35	0.379	29	1	3.821	9714272.357	724342.431	1171.290

Source: JICA study team

2) Data processing and analysis method

i) Data processing

Some necessary corrections were applied to the acquired data at each station to calculate Bouguer anomaly values at each station. Fig.3-2.94 shows the procedure used for the gravity data processing.

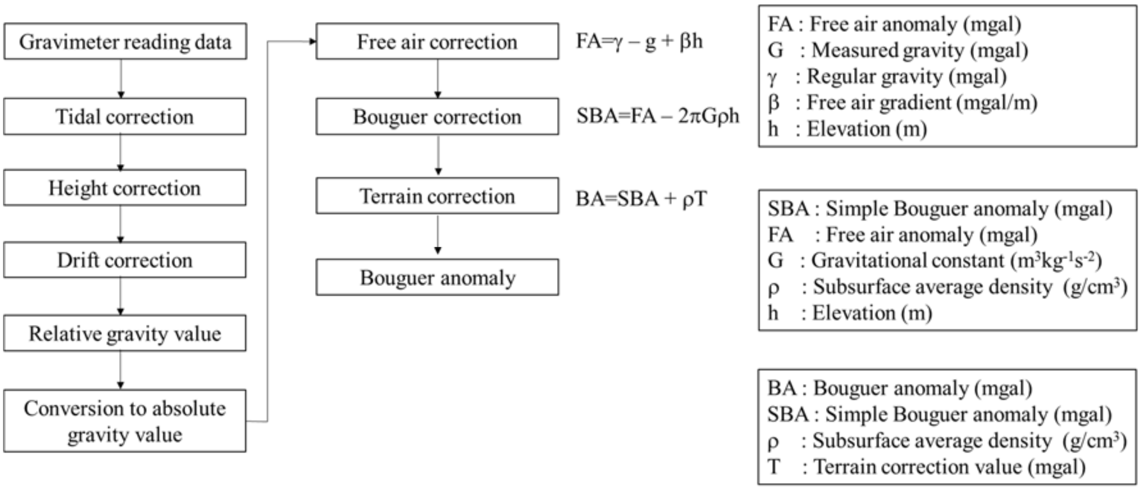

Source: JICA study team

Fig. 3-2.94 The procedure of data processing

a) Tidal correction

A gravimeter is sensitive enough to record the gravity changes caused by the movements of the Sun and the Moon, which vary according to latitude and time. Tidal correction is conducted to eliminate the influence of the attraction caused by the movement of the Sun and the Moon. In this survey the Scintrex CG-5 gravimeter was used. The Scintrex CG-5 utilizes an analytical program to correct for tidal values, which is automatically performed during gravity measurements.

b) Height correction

Correction of gravimeter height from the ground surface is necessary since gravity value decreases when increasing the distance between station and the datum surface. This is done using vertical gravity gradientheight correction (0.3086 mgal/m), which is expressed by the following equation:

$$V_{hi} = 0.3086 \times Hi$$

V_{hi} : height correction value（mgal）

Hi : the height of the gravimeter from the surface（m）

c) Drift correction

The spring in the gravimeter extends by itself with time, and the measured gravity value is influenced by this extension of the spring. The error of gravity value caused by the extension of the spring length with time is called “drift”. When the spring length increases, the measured gravity value becomes larger than the value without drift. This gravity change caused by drift is corrected by drift correction. Error caused by the rapid change of temperature and by impacts on the gravimeter during transport are also removed by the drift correction. In order to determine the level of drift, a base station for gravity measurement is established. Next, gravity measurements are taken at multiple locations, starting and ending at the base station. The gravity difference at the base station between start point and end point is regarded as the drift value because no gravity difference would occur at same station without drift effects. The drift value at each station is prorated depending on the elapsed time since the first measurement of the day occurred.

d) Free air correction

Free air correction is to correct the influence caused by the difference between the measurement elevation and the geoid level. The vertical gravity gradient is not necessarily constant, but in this survey an average value of 0.3086 mgal/m was used. The equation is shown below:

$F = 0.3086 \times h$

F : free air correction value (mgal)

h : elevation of the stations (m)

e) Bouguer correction

The Bouguer correction accounts for the gravity attraction of the material between the station and the datum plane that is ignored in the free air correction. The Bouguer correction is conducted by using the equation shown below. The estimated density is included in the equation. The method used to determine the estimated density is shown in a following section. In this survey, 2.64 g/cm^3 was used as the value of the estimated density.

$B = 2\pi G\rho h$

B : Bouguer correction value (mgal)

G : Gravitational constant ($6.67 \times 10^{-11} m^3 kg^{-1} s^{-2}$)

ρ : Estimated density (g/cm^3)

H : elevation of the stations (m)

f) Terrain correction

Terrain correction is used to eliminate the influence of the undulation of terrain on the measured gravity value. In this survey, the effect of terrain within a 60 km radius centering on the measuring station was calculated by using the digital elevation data of the SRTM (Shuttle Radar Topography Mission). This circular range is divided into four zones depending on the distance from the measuring stations;

extremely near zone (0~500m), near zone (500m~4km), medium zone (4~16km) and far zone (16~60km). The terrain correction value was calculated in each zone using the analytical program for terrain correction developed by Komazawa (1980)

g) Calculation of the Bouguer anomaly

After calculating each correction, the Bouguer anomaly is formulated by the following equation:

$$\Delta B = g_{obs} - \gamma + \beta h - 2\pi G\rho h + \rho T$$

ΔB : Bouguer anomaly (mgal)

g_{obs} : Measured gravity value (mgal)

γ : Regular gravity (mgal)

β : Free air gradient (mgal/m)

h : Elevation (m)

G : Gravitational constant ($6.67 \times 10^{-11} m^3 kg^{-1} s^{-2}$)

ρ : Estimated density (g/cm^3)

T : Terrain correction value (mgal)

ii) Evaluation of the estimated density

There are various methods which can be used to estimate surface density such as directly measuring the density of core samples, comparing the distribution of the Bouguer anomaly with a topography map, the G-H correlation method, etc. In this survey, a CVUR method was used to mathematically compare the distribution of the Bouguer anomaly with a topography map (Komazawa, 1995). In this method, the upward-continuation residual between 2 points at different heights which express the shortwave component of the Bouguer anomaly, is calculated. The estimated density is determined when the residual variance becomes the smallest, because the minimum value of the residual variance reflects the smallest correlation between topography and the Bouguer anomaly. Upward-continuation at 0m and 200 m was completed and $2.64 g/cm^3$ was obtained as the average density within a 2 km radius centering on the area of the gravity survey as shown in Fig.3-2.95.

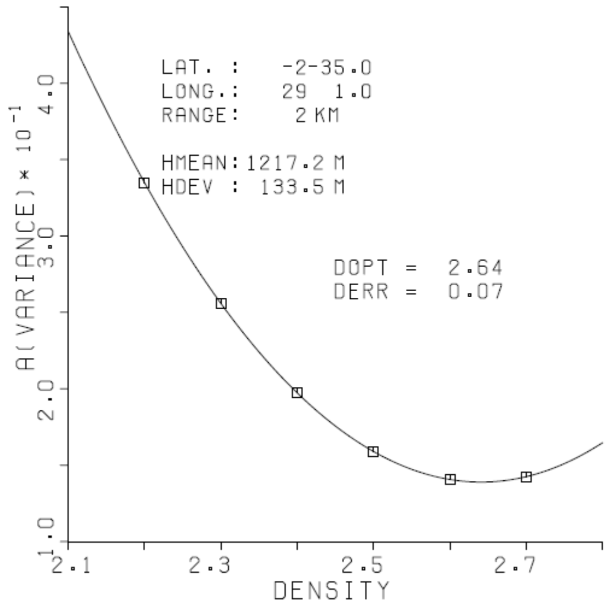

Source: JICA study team

Fig. 3-2.95 Result of CVUR method

iii) Bouguer anomaly

The Bouguer anomaly, caused by the heterogeneous character of the density distribution in the subsurface, is calculated in data processing. The distribution of the subsurface density can be estimated from the Bouguer anomaly. The gravity value is the net force, both the centrifugal force caused by the Earth's rotation and the attracting force occurring between the Earth, the Sun and the Moon. The magnitude of the centrifugal force by the Earth's rotation is at its maximum on the equator and at its minimum at the poles, which causes the gravity value to vary based on latitude. In addition, the gravity value at higher elevation decreases because the attracting force of the Earth becomes smaller. The tidal force depends on the position of the stations, relative to the Sun and the Moon, so the measured gravity changes with time at the measuring stations. The terrain effect is caused by the attracting force occurring near a body with large mass such as a mountain. Even if these corrections are conducted, the corrected gravity has different values at each of the stations. The difference between the corrected gravity and the average gravity is called the Bouguer anomaly. It is caused by the heterogeneous character of the density distribution in the subsurface and this is the purpose of the gravity survey.

iv) Trend surface analysis

The objective of trend surface analysis is to extract the longwave component of the Bouguer anomaly derived from the deep subsurface composition as shown in Fig.3-2.96. Trend surface is obtained by approximating the longwave component of the Bouguer anomaly by the n-order curved surface. Each coefficient is solved by applying least squares approximation to the Bouguer anomaly in the following equation:

- First order trend surface : $\Delta G_1(x,y) = a_0 + a_1 x + a_2 y$
- Second order trend surface : $\Delta G_2(x,y) = a_0 + a_1 x + a_2 y + a_3 x^2 + a_4 xy + a_5 y^2$

- N order trend surface :

$$\Delta G_n(x,y) = a_0 + a_1 x + a_2 y + a_3 x^2 + a_4 xy + a_5 y^2 + \cdots + a_{m-1} xy^{n-1} + a_m y^n$$

where m=n(n+3)/2

The n-order trend surface residual is obtained by subtracting n-th trend surface from the Bouguer anomaly value ($\Delta g(x,y)$ - $\Delta G(x,y)$)

v) Upward-continuation filter

The Bouguer anomaly at a given elevation is calculated by using the upward-continuation filter analysis. This process means that the Fourier coefficient of the wave number m of x direction and n of y direction is weighted by using the following equation.

$$w_{mn} = \exp\left(-\sqrt{\left(m^2 + n^2\right)}H\right)$$

The long wave component of the Bouguer anomaly can be extracted by using the upward-continuation filter analysis. The upward-continuation filter analysis at two different heights can play the role of the band pass filter

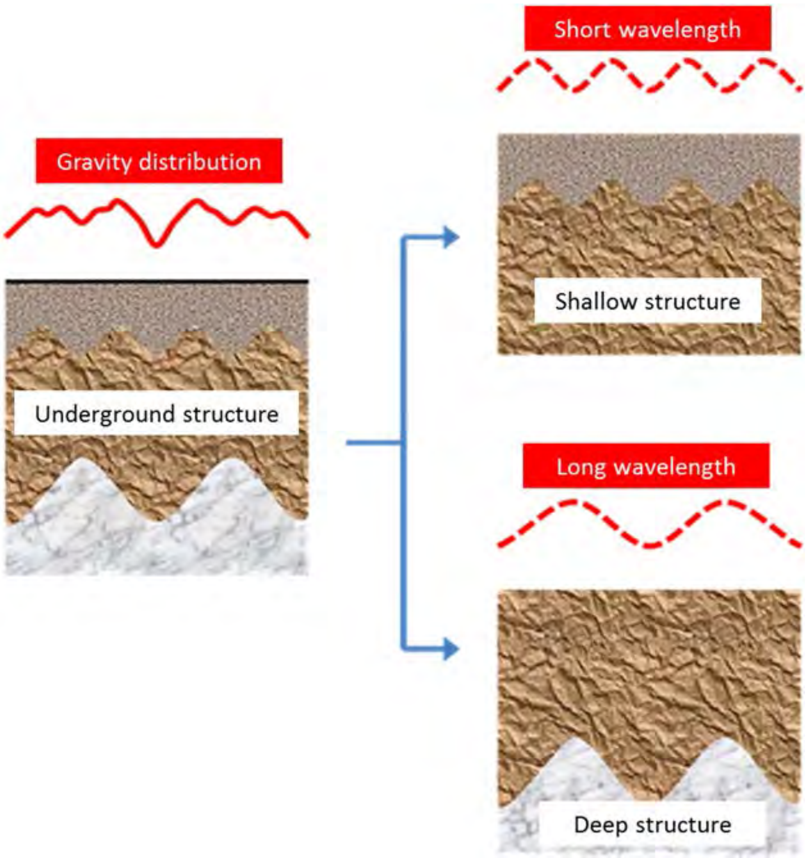

Source: JICA study team

Fig. 3-2.96 Conceptual diagram of trend surface analysis filter

vi) Horizontal first derivation and vertical second derivation filter analysis

Horizontal derivative filtering is one of the high-pass filtering processes which emphasize the boundaries of the structures, using the horizontal first derivative values of the Bouguer anomaly. Based on the result of the horizontal first derivation, faults and/or intrusive rock can be detected. However, since density boundaries situated at shallow depths create a remarkably high anomaly in the horizontal derivative distribution, and deep seated density boundaries only create slightly high anomaly, the deep seated density anomalies are easily overlooked. For this reason, the locations of points showing the maximum values of horizontal first derivative distribution were determined using a mathematical method, and the locations were used as additional information for detecting subsurface structures such as faults and/or intrusive rock (Fig.3-2.97).

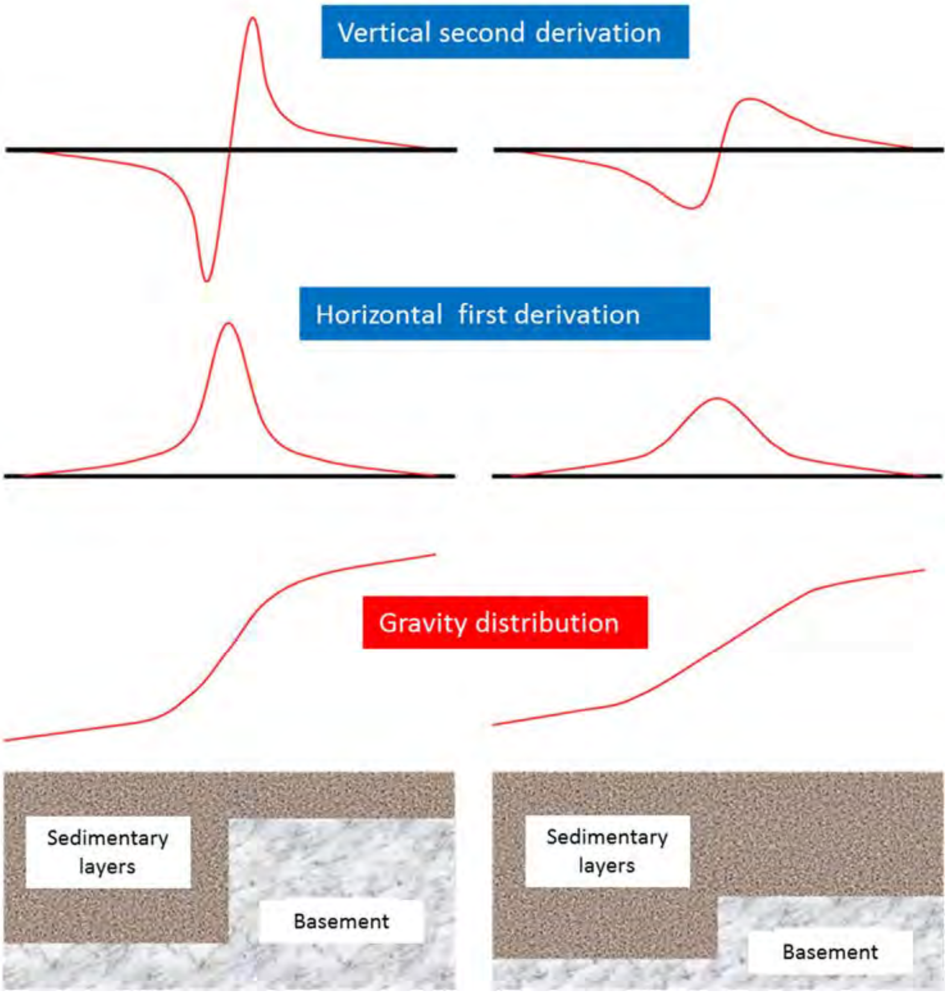

Source: JICA study team

Fig. 3-2.97 Conceptual diagram of vertical second derivation and horizontal first derivation

vii) Three-dimensional gravity inversion of basement relief

The illustration below demonstrates the gravity value, which is caused by the rectangular-shaped body infinitely extending downward vertically, at a specific point (A, B, C) (Fig.3-2.98) can be calculated using the following equation (1).

$$G = \gamma\rho\{F(X1,Y1,Z) - F(X2,Y1,Z) - F(X1,Y2,Z) + F(X2,Y2,Z)\} \quad \cdots\cdots (1)$$

Where,

$$X1 = A - x1, \quad X2 = A - x2$$
$$Y1 = B - y1, \quad Y2 = B - y2$$
$$Z = |z - C|$$

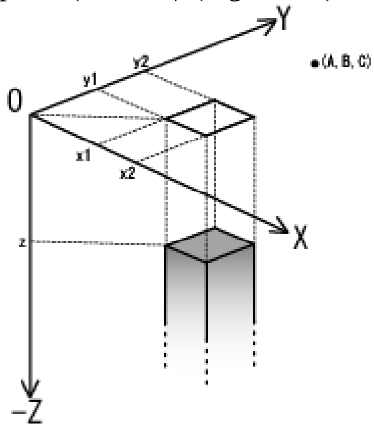

Fig. 3-2.98 Conceptual diagram of three-dimensional gravity inversion of basement relief

$$F(x,y,z) = -\iiint \frac{zdxdydz}{\left(x^2+y^2+z^2\right)^{3/2}}$$
$$= x\ln\left(\frac{y+\sqrt{x^2+y^2+z^2}}{\sqrt{x^2+z^2}}\right) + y\ln\left(\frac{x+\sqrt{x^2+y^2+z^2}}{\sqrt{y^2+z^2}}\right) - z\tan^{-1}\left(\frac{xy}{z\sqrt{x^2+y^2+z^2}}\right)$$

If the gravity stations and rectangular bodies representing the basement are aligned along the x and y coordinates in a grid system, a relative gravity anomaly, $\triangle G_{ij}(z)$ caused by the rectangular density body representing the basement relief can be calculated by the equation (2).

$$\Delta G_{ij}(z) = \sum_k \sum_l \left\{ G_{ij}^{\ kl}(z, D_{kl}) - G_{ij}^{\ kl}(z, D_0) \right\} \quad \cdots\cdot (2)$$

Where,

D_{kl} : a depth of top of a rectangular body

D_0 : an average depth of basement relief

G_{ij}^{kl} : gravity value caused by rectangular density bodies at a station (x_i, y_i, z)

The initial approximation of the basement relief, D_{kl} is set using the equation (3) for the gravity inversion.

$$D_{kl}^{\ (1)} = D_0 + \lambda \delta g_{ij} * / 2\pi\gamma\rho \quad \cdots\cdot (3)$$

Where,

δg* = observed gravity value – average value of all the observed gravity values

The gravity anomaly values at each station are determined by the initial density model and are calculated by using the following equation.

$$g_{ij}^{\ (1)} = \Delta G_{ij}(z_{ij}) = \sum_k \sum_l \left\{ G_{ij}^{\ kl}\left(z_{ij}, D_{kl}^{\ (1)}\right) - G_{ij}^{\ kl}(z_{ij}, D_0) \right\} \quad \cdots\cdot (4)$$

If an error sum of squares for $\delta g_{ij}^{(1)}$and δg* is sufficiently small, the D_{kl} will be a final density in the gravity inversion process. If the sum of squares is not sufficiently small, the equation (3) is used to obtain the second approximation for the final density model.

$$D_{ij}^{\ (2)} = D_{ij}^{\ (1)} + \lambda\left(\delta g_{ij} * - \delta g_{ij}^{\ (1)}\right) / 2\pi\gamma\rho \quad \cdots\cdot (5)$$

Where

$\delta g_{ij}^{(1)} = g_{ij}^{(1)}$ – (an average value of $g_{ij}^{(1)}$)

After combining the equation (5) with equation (2), the following equation is derived.

$$g_{ij}^{(2)} = \Delta G_{ij}(z_{ij}) = \sum_k \sum_l \left\{ G_{ij}^{kl}\left(z_{ij}, D_{kl}^{(2)}\right) - G_{ij}^{kl}\left(z_{ij}, D_0\right) \right\}$$

Iterative least-square method is employed to determine the final basement relief model (depth of the top of each rectangular body, D_{kl}) until the error sum of squares for $\delta g_{ij}^{(1)}$ and δg^* become sufficiently small.

3) Analysis results

i) Bouguer anomalies

A Bouguer gravity anomaly map is shown in Fig.3-2.99. As previously described, a rock density of 2.64g/cm^3 was used for calculating Bouguer anomaly values. Bouguer anomaly values at each stations are attached as an Appendix 2-3.

High-gravity anomaly zones are identified around the south-western and the eastern part of the survey area. On the other hand, a low-gravity anomaly zone is distributed in and around the Cyamura field and the low anomaly zone extends to the north and north-eastern sectors of the entire survey area. This low-gravity anomaly zone is considered to reflect a graben.

ii) Trend surface analysis

Trend surface analysis was applied to obtain the regional trend of the gravity distribution. After utilizing five different orders of polynomial equations for estimating the regional trend of the gravity distribution, the regional trend derived from the second order equation was considered to be the most effective for separating the regional trend and the residual anomaly.

A trend surface map and a residual gravity map based on the results derived from the trend surface analysis are shown in Fig.3-2.100 and Fig.3-2.101 respectively. According to the trend surface map shown in Fig.3-2.100, the low-gravity anomaly is identified in and around the southern part of the survey areas, and the low-gravity anomaly probably reflects an approximate shape of the gravity basement structure situated at depth.

The residual gravity values were calculated by deducing values of trend surface from Bouguer anomaly values. The residual gravity distribution is considered to reflect density distribution above the basement structure (Fig.3-2.101). Based on the distribution of this residual gravity map, a low-gravity anomaly zone is distributed in the region from the central to the north-eastern part of the survey area, and a high-gravity anomaly zone is identified in the south-western, northern and eastern parts of the survey area. The zone showing a steep gradient in residual gravity is located in between these low and high anomalies and the zone suggests a linearly distributed subsurface density discontinuity.

This kind of gravity discontinuity, linearly distributed, often reflects a fault or a fracture zone. For this reason, horizontal first derivative values were calculated using the residual gravity values. A map showing horizontal first derivative values of residual gravity is depicted in Fig.3-2.102. High anomaly zones of the horizontal first derivative values indicate structures with large changes in density. Therefore, if a high anomaly zone of the horizontal first derivative values extends in a certain direction, a fault can be deduced around the high anomaly zone. On the basis of the distribution of the horizontal first derivative map, the following nine gravity lineaments were detected.

- A clear gravity lineament which extends roughly in a N-S direction and is located in the northern portion of the survey area (G1).
- A clear gravity lineament which extends roughly in a N-S direction and is located in the eastern portion of the survey area (G2).
- A clear gravity lineament which extends roughly in a ENE-WSW direction and is located in the central portion of the survey area (G3).
- A clear gravity lineament which extends roughly in a NNW-SSE direction and is located in the western portion of the survey area (G4).
- A clear gravity lineament which extends roughly in a N-S direction and is located in the southern portion of the survey area (G5).
- A clear gravity lineament which extends roughly in a E-W direction and located in the south-eastern portion of the survey area (G6).
- A gravity lineament which extends roughly in a ENE-WSW direction and is located in the north-western portion of the survey area (G7).
- A clear gravity lineament which extends roughly in a N-S direction and is located in the western portion of the survey area (G8).
- A gravity lineament which extends roughly in a ENE-WSW direction and is located in the southern portion of the survey area (G9).

iii) Upward continuation analysis

The upward continuation method is a filtering technique which is different from the above-mentioned trend surface analysis. However, the purpose of the upward continuation is similar to the trend surface analysis, that is to separate a residual gravity anomaly from the original Bouguer anomaly distribution. In this study, the upward continuation method was applied to the Bouguer anomaly data to extract middle-scale and large-scale structures. The upward continuation method calculates a potential field at an elevation which is higher than the actual elevation where the gravity field was measured. Upward continuation is a kind of smoothing process to eliminate small-scale, near-surface density effects. Therefore, this analysis can remove small-scale noise structures at shallow depths from the Bouguer anomaly and thus the middle to large-scale structures are easily detected in the survey area. In this data analysis, the upward continuation was calculated at elevations of 100m and 3,000m above the gravity stations. The values between 100m and 3000m were then determined by subtracting the values at 100m from the values at 3000m. This analysis has the effect of a band-pass filter removing both effects caused by the small-scale noise structures at shallow depths and the large-scale regional structures in and around the survey area. An upward continuation map (100m to 3,000m) is shown in Fig.3-2.103.

The distribution of the upward continuation values shown in Fig.3-2.103 is similar to that in the above-mentioned residual gravity map (Fig.3-2.101). In this map, a low-gravity anomaly zone is distributed in an area from the central to the north-eastern part of the survey area, and a high-gravity anomaly zone is identified in the south-western and eastern portions of the survey area. In the same way as the above-mentioned trend surface analysis, the horizontal first derivative values were calculated using the upward continuation values for the purpose of extracting fault structures. The horizontal first derivation map calculated from the upward continuation is shown in Fig.3-2.104. From this distribution of the horizontal first derivative map, the following gravity lineaments were detected.

- A clear gravity lineament which extends roughly in a N-S direction and is located in the northern portion of the survey area (G1).
- A clear gravity lineament which extends roughly in a N-S direction and is located in the eastern portion of the survey area (G2).
- A clear gravity lineament which extends roughly in a ENE-WSW direction and is located in the central portion of the survey area (G3).
- A clear gravity lineament which extends roughly in a NNW-SSE direction and is located in the western portion of the survey area (G4).
- A clear gravity lineament which extends roughly in a N-S direction and is located in the southern portion of the survey area (G5).
- A clear gravity lineament which extends roughly in a E-W direction and located in the south-eastern portion of the survey area (G6).
- A gravity lineament which extends roughly in a ENE-WSW direction and is located in the north-western portion of the survey area (G7).
- A clear gravity lineament which extends roughly in a N-S direction and is located in the western portion of the survey area (G8).
- A gravity lineament which extends roughly in a ENE-WSW direction and is located in the southern portion of the survey area (G9).

The above-mentioned gravity lineaments detected in the distribution of the horizontal first derivative using upward continuation (100m to 3,000m) are almost same as those detected in the distribution of the horizontal first derivative using the residual gravity data derived from trend surface analysis. This fact means that the same gravity lineaments were detected by different data analyses, and therefore these gravity lineaments are reliable and possibly indicate faults.

A graben was deduced in the central portion of the survey area and based on geological studies, Cenozoic volcanic rock is infilled in the graben. The gravity lineaments, G1 and G3 are approximately situated in the area around the western edge portion of the graben, and the gravity lineament G2 is approximately situated in the area around the eastern the edge portion of the graben. Therefore, the gravity lineaments, G1, G2 and G3 are probably indications of faults located at the west and east edges of the deduced graben.

In addition, Mashyuza hot spring is located close to the center portion of the gravity lineament, G3, and thus the gravity lineament G3 is likely to indicate a fault and geothermal fluids possibly migrate in fracture zones existing along the fault.

The other gravity lineaments have the possibility of reflecting faults controlling geothermal fluids, but further geoscientific information is required to identify whether or not geothermal fluids migrate along and around the gravity lineaments.

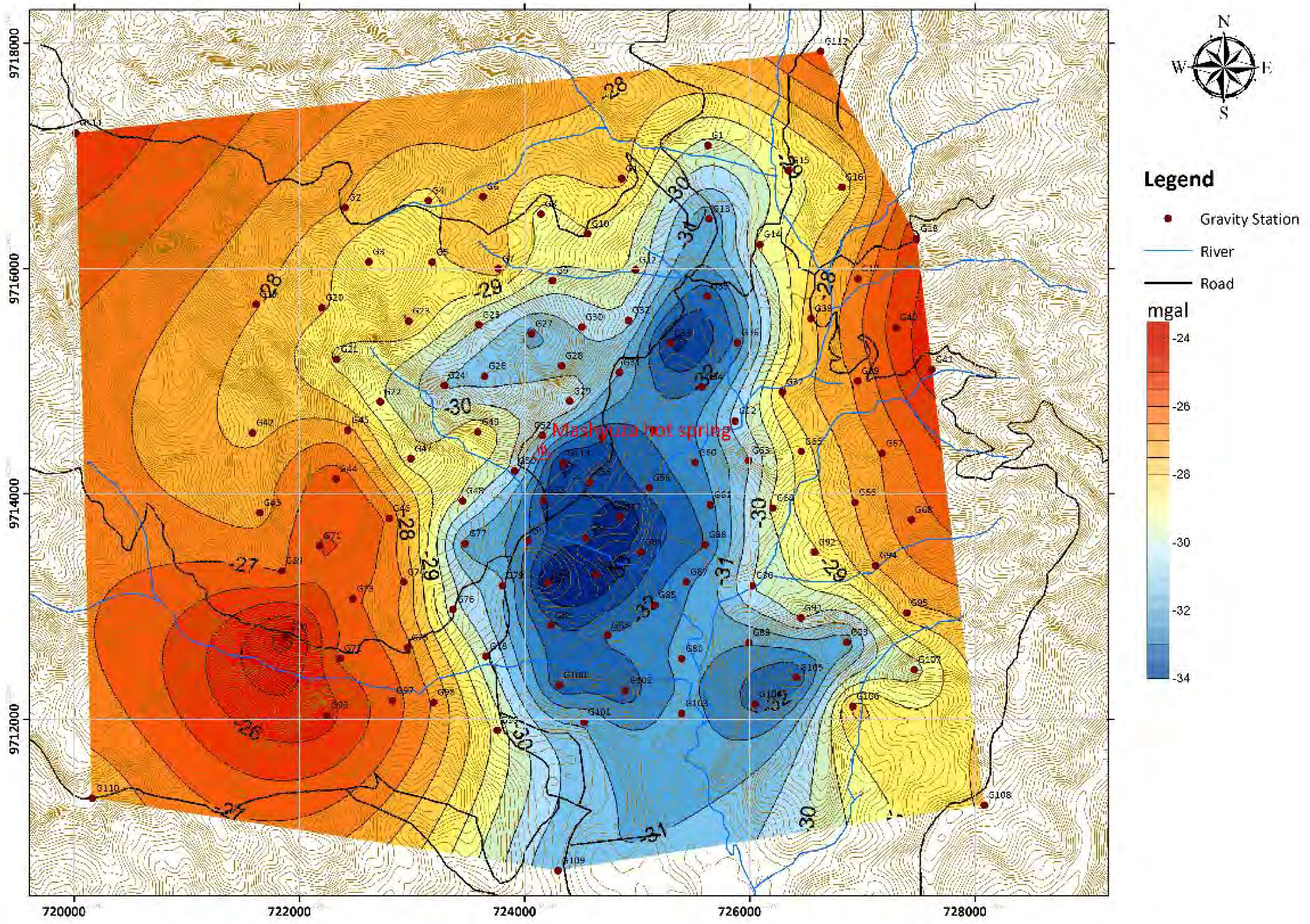

Source: JICA study team

Fig. 3-2.99 Bouguer anomalies map（Density：2.64g/cm^3）

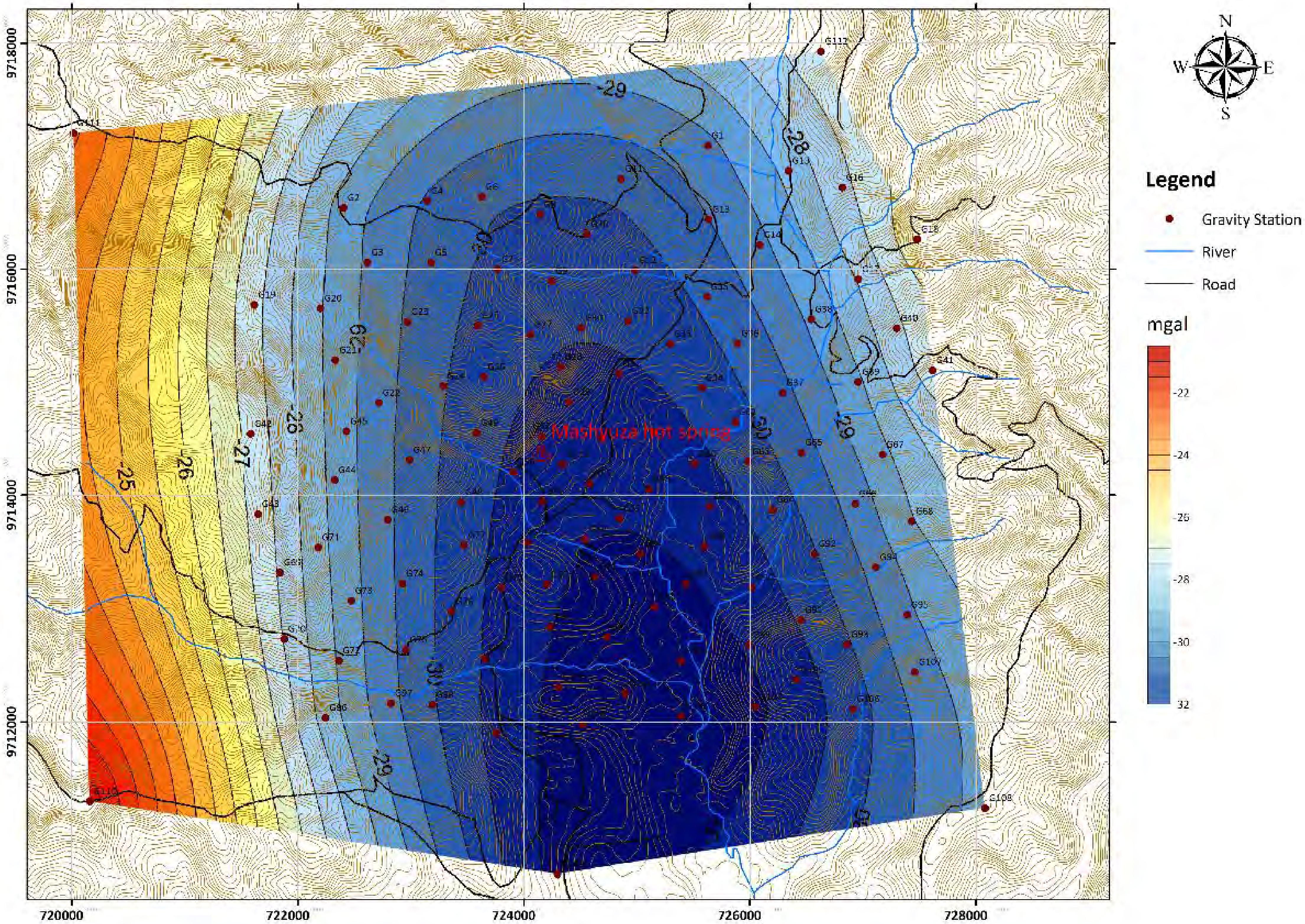

Source: JICA study team

Fig. 3-2.100 2nd Trend surface map

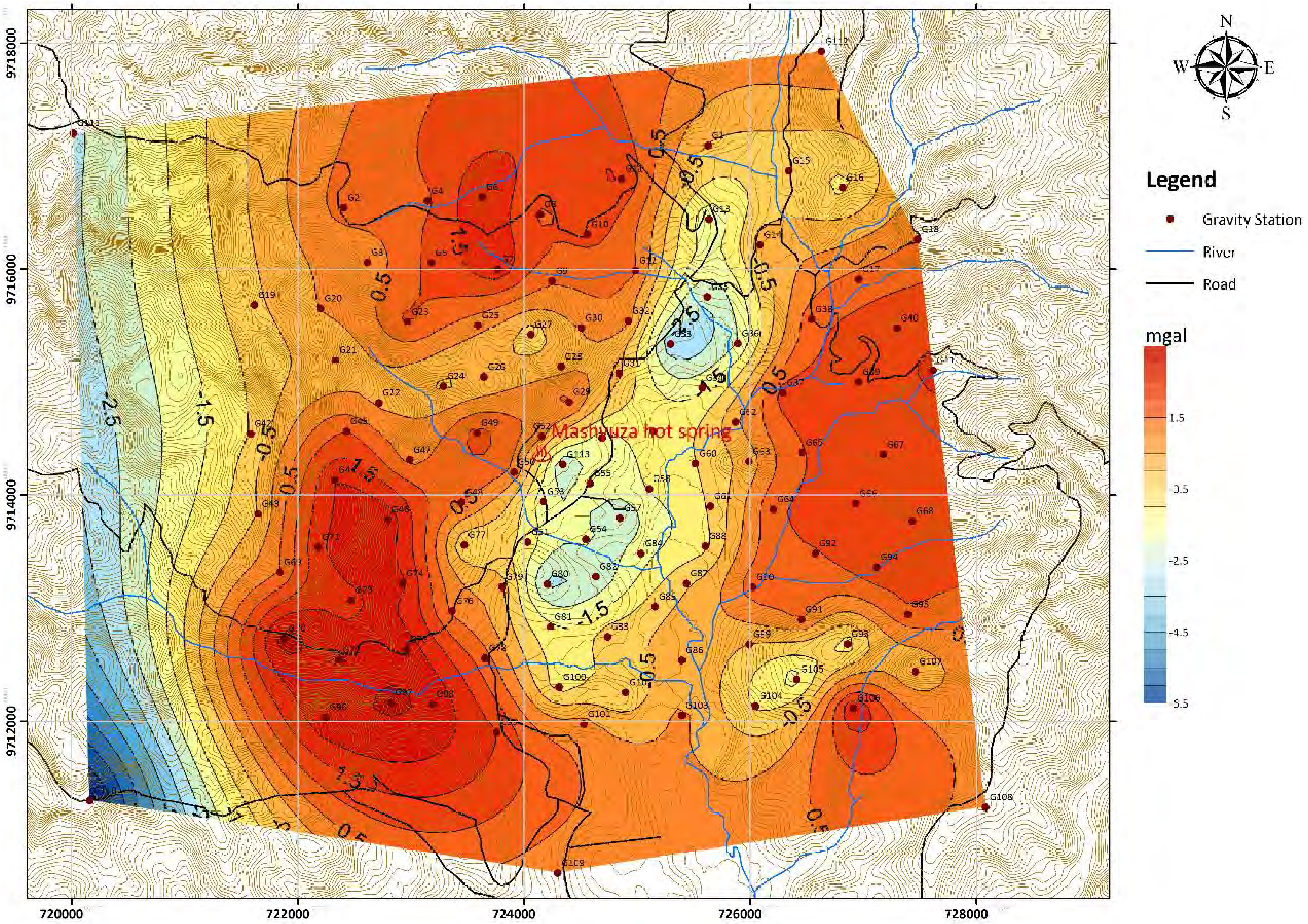

Source: JICA study team

Fig. 3-2.101 Residual of 2nd trend surface map

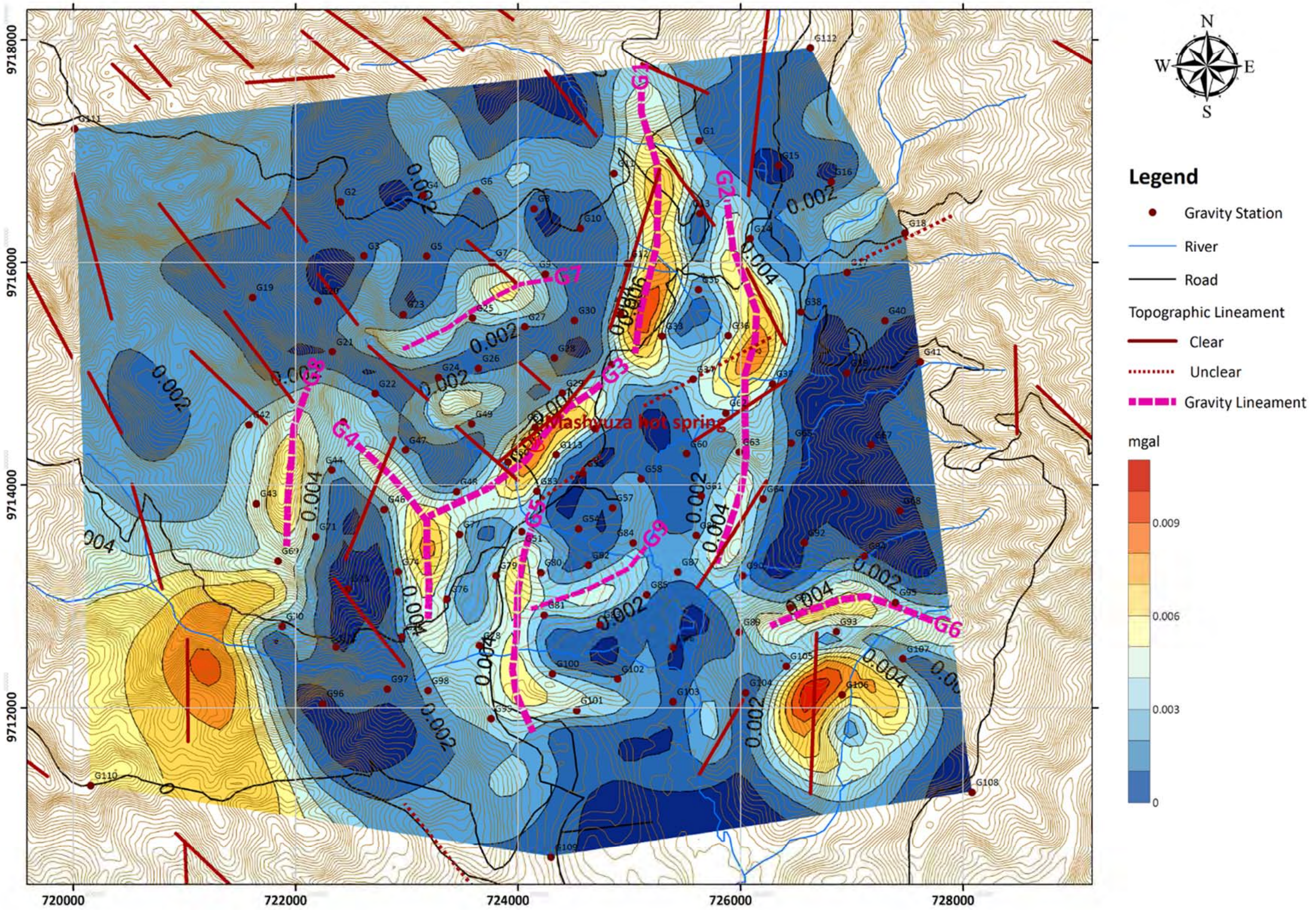

Source: JICA study team

Fig. 3-2.102 Horizontal first derivation of residual of 2nd trend surface map（ S=200m）

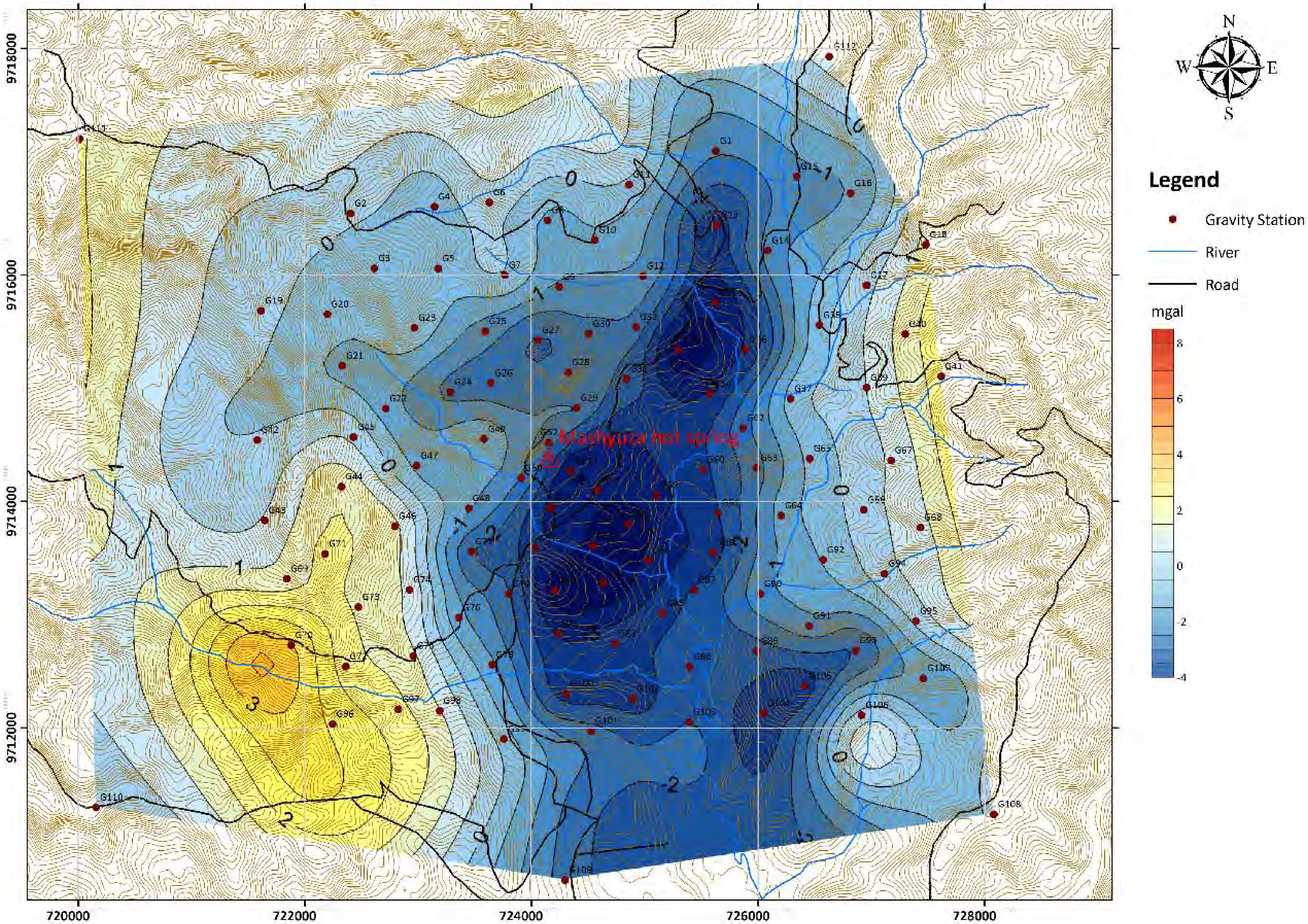

Source: JICA study team

Fig. 3-2.103 Upward continuation map（100~3000m）

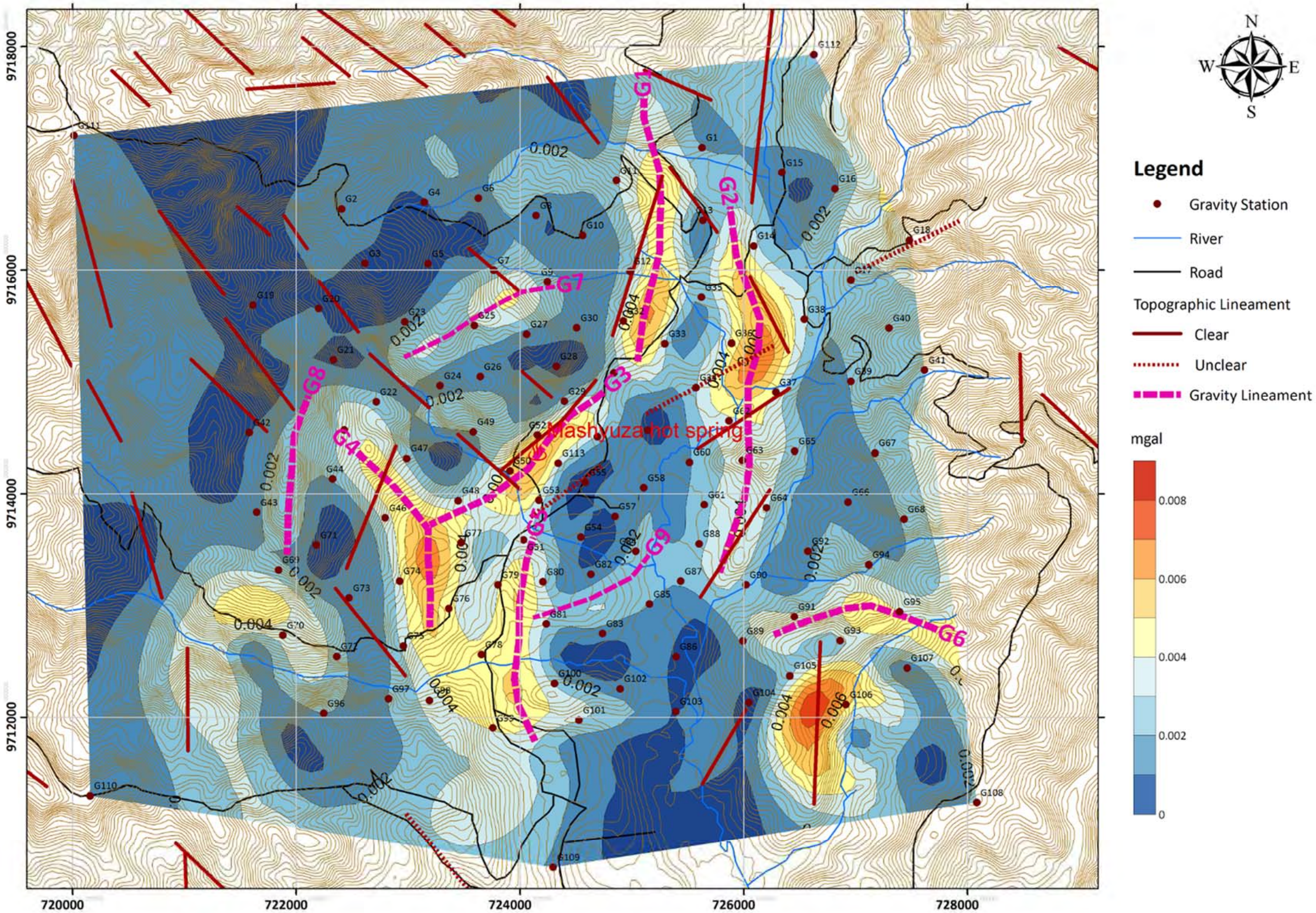

Source: JICA study team

Fig. 3-2.104 Horizontal first derivation map（S=200m）of upward continuation（100~3000m）

iv) Gravity inversion of basement relief

A gravity inversion of basement relief was conducted to estimate the depth distribution of deep-seated basement rock in the survey area. During the inversion process, the value of the density difference between the basement rock and volcanic rocks overlaying the basement is required to estimate a proper basement relief. However, no information is available for densities of rock in and around the survey area. Therefore, geophysical papers describing rock density, derived from other gravity surveys in African countries, were examined. In the paper “Integrated Geophysical Study of Lake Bogoria Basin, Kenya: Implications for Geothermal Energy Prospecting, Josphat Mulwa et al., Proceedings World Geothermal Congress 2010”, rock densities were determined by data analysis. Based upon those rock densities, the density difference was assumed to be 0.3g/cm^3 in the Bugarama field.

Applying the results of the gravity inversion of basement relief (see Fig.3-2.105), an area indicating deep basement relief was identified in and around the above-mentioned deduced graben located in the central portion of the survey area. In addition, steep gradient zones of the basement relief can be seen around the gravity lineaments G1, G2 and G3 located around the edge portions of the graben. This fact support that the gravity lineaments G1, G2 and G3 are probably indicative of faults.

Since the precise density difference between the basement and volcanic rocks overlying the basement is unknown, and no control point for basement depth is available, the distribution of the basement depth was not accurately determined in the gravity inversion process. Based on the basement depth distribution derived from the gravity inversion with the above-mentioned assumption of the density difference, an average basement depth in the graben is estimated to be approximately 2,000 m from the ground surface.

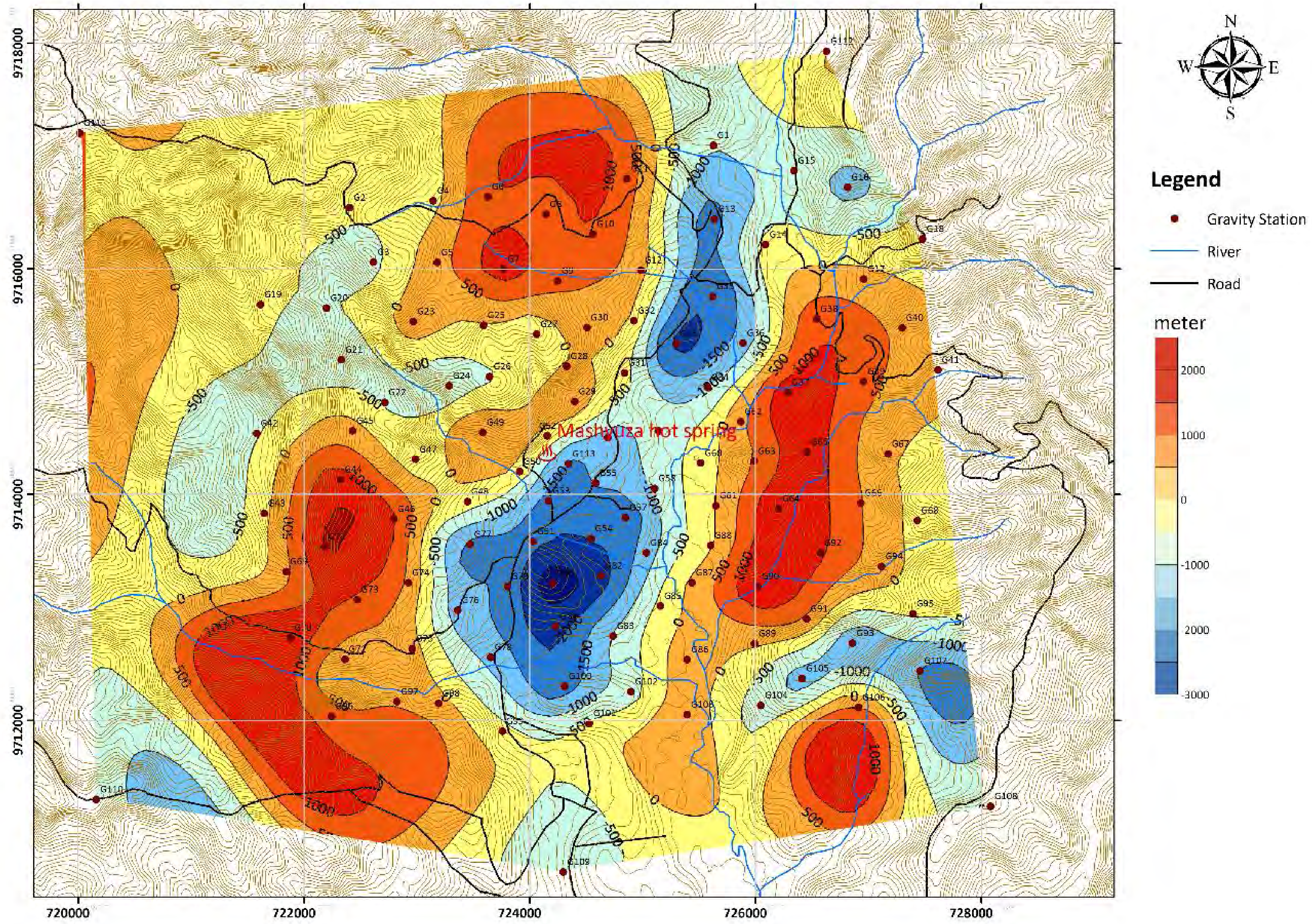

Source: JICA study team

Fig. 3-2.105 Basement relief derived from gravity inversion

3.2.4. Geothermal Resource Assessment

(1) Geothermal conceptual model

The geothermal conceptual models for selected fields are constructed based on geoscientific data described in sections 3.2.2 and 3.2.3. In general, a geothermal conceptual model is constructed through the integration of various geoscientific data, including geological, geochemical, geophysical, well-logging and well-testing data. The conceptual model is improved and updated in the course of resource study. At the initial stage of resource study, a surface resource study is conducted to confirm the possible presence of a geothermal resource and to delineate the geothermal reservoir in outline using geological and geochemical techniques (including geophysical survey such as gravity and other surveys to cover a wide area). A geothermal conceptual model including geological structure model and fluid flow model (geochemical model) is prepared in order to understand the characteristics and potential of the geothermal resources in the objective area. At this stage, the possible presence of a geothermal resource is discussed and the geothermal reservoir is roughly delineated. Based on the conceptual model, the development study area is narrowed down and the most promising areas are detected.

The geothermal conceptual models for selected fields constructed in this study are based on surface geoscientific data, with the exception of Karisimbi, where the geothermal conceptual model has been constructed based on the results of exploratory well drilling. These initial conceptual models should be improved and updated during the course of resource study.

1) Karisimbi field

The resistivity section, geological cross section and the conceptual model of the geothermal system in Karisimbi field are shown in Fig. 3.2-106, Fig.3.2-107 and Fig.3.2-108, respectively.

The north part of Karisimbi field is located in Virunga Volcano Range (VVR), whereas the southern part is in the Butare Horst composed of Proterozoic mylonitised granitic and phyllitic complexes. The geothermal conceptual model for Karisimbi field models the two fields separately as “the Karisimbi field”, the northern part of Karisimbi field, and “the Karago field”, the southern part of Karisimbi field.

The Karisimbi field is located close to Karisimbi volcano, which erupted in the late Quaternary. This late Quaternary volcanic activity of Karisimbi volcano is one of the candidate heat sources for the geothermal system in the Karisimbi field. However, no data or information indicating high temperature conditions in the subsurface in and around exploratory wells KW-01 and KW-02 have been obtained in the course of the well drilling.

Cap rock, which prevents cold groundwater from invading high temperature reservoirs, is an important constituent element of a geothermal reservoir supporting sustainable power generation. Few altered minerals are found in the exploratory wells. No low resistivity zones of less than 25 ohm-m are detected in the Karisimbi field by the 3D MT inversion. These facts suggest that geothermal activity in the Karisimbi field is relatively weak and that the hydrothermal alteration zone functioning as a cap rock of the geothermal reservoir is not well developed.

Permeable zones in the reservoir generally correlate with passages for the geothermal fluid and well productivity. In the Karisimbi field, it seems that permeability is strongly controlled by faults, considering that this field is comprised of hard rock of Proterozoic age. Considering the geological structures of the Proterozoic basement in the Butare Horst, fractures seems to be developed in the basement rocks seated below the Quaternary volcanic rocks in the Karisimbi field. However, no highly permeable structures have been identified by well drilling, or by geological and geophysical investigation in the Karisimbi field.

Although the high resistivity zone distributed in the southern portion of the Karisimbi field at depths between 1,000 m and 2,500 m shows extremely high resistivity values greater than 640 ohm-m, this high resistivity zone is not likely to be the result of high-temperature alteration minerals such as illite and/or chlorite, but instead is likely the result of a less permeable rock body where fractures are not well developed.

Exploratory well KW-01 has a linear relationship between temperature and depth; temperature increases at a steady rate with increasing depth (Fig.3.1-7 and Fig.3.1-10). It is considered that conductive heat flow is dominant in this layer, giving a linear temperature increase.

In conclusion, geothermal activity in the Karisimbi field is likely to be relatively weak compared with other geothermal fields where geothermal power stations have been installed and are being operated. It is considered that a geothermal system exploitable for power generation is not well developed in the Karisimbi field.

There are two hot springs in the Karago field, Karago and Mbonyebyombi hot springs. Considering the geology, geological structures and distribution of thermal manifestations in the area, it seems that the flow of hot fluid is strongly controlled by permeable zones related to faults and fractures. In general, faults play an important role in ensuring vertical permeability in a geothermal system. In the Karago field, NW-SE trending topographic lineaments are well detected, which implies the presence of faults. These inferred faults are considered to be permeable zones related to the path of fluid flows in the Karago field.

The Karago field is situated in the Proterozoic basement (granite), and there is no recent volcanism in or around the area. It is supposed that thermal springs in the area are associated with the deep circulation of natural waters across faults, and the high temperature results from the relatively high geothermal gradient, or the conductive heat of the magmatic materials situated in a deeper part of the crust, or the conductive heat of intrusive rocks. Although the subsurface resistivity structure around the Karago field could not be defined properly, a relatively low resistivity zone is detected below the Karago field at greater depth (Fig.3-2.77 and Fig.3-2.106). There is a possibility that a relatively high-temperature zone is present at depth in the Karago field.

From the hydrogen and oxygen isotopic composition and Cl concentration of the spring waters, it appears likely that the discharging hot spring water in the Karago field originates in meteoric water. The hot spring water is classified as HCO_3 type, a conductively heated type (Fig.3-2.38). The diagram of temp-SiO_2 and Cl concentration (Fig.3-2.41) shows a mixing correlation between Karago and Mbonyebyombi water that implies that those waters are diluted from the same parental fluid.

The fluid flow model for the Karago field suggests that meteoric water is penetrating into the deep levels of the mountainous area at a higher elevation than the Karago field, where it is heated by conductive heat. Hot fluids are stored in a permeable zone developed in granite that trends NW-SE. The geothermometry temperatures for spring water suggest that the temperature of the hot water aquifer is around 81^{o}C. The hot fluid ascending along fractures yields the hot springs of Karago and Mbonyebyombi. Considering the Cl concentration in the hot spring water, the parental fluid is likely to be present at greater depth in the Karago field (Fig. 3-2.108). In general, geothermometry based on geochemistry is a powerful tool in estimating reservoir temperatures at greater depth. However, it is difficult to estimate reservoir temperature at depth because the reliability of geothermometry in this area is very limited (only the silica geothemometer is reliable). Therefore, more detailed geoscientific study is required to examine the possible presence of a deeper reservoir and to establish its temperature.

Although the accuracy of the estimates is not high due to the shortage of subsurface geoscientific information such as geophysical and well-logging data, the geothermal resource area for geothermal resource evaluation (using the Stored Heat Method) is estimated based on the conceptual model constructed for the Karago field. An field is determined considering the distribution of permeable zones which control geothermal fluid flow and thermal manifestations. This area includes permeable zones assumed along NW-SE trending faults and the thermal manifestation of Karago, as shown in Fig.3-2.109. The thickness of the geothermal reservoir is assumed from consideration of the drilling depth.

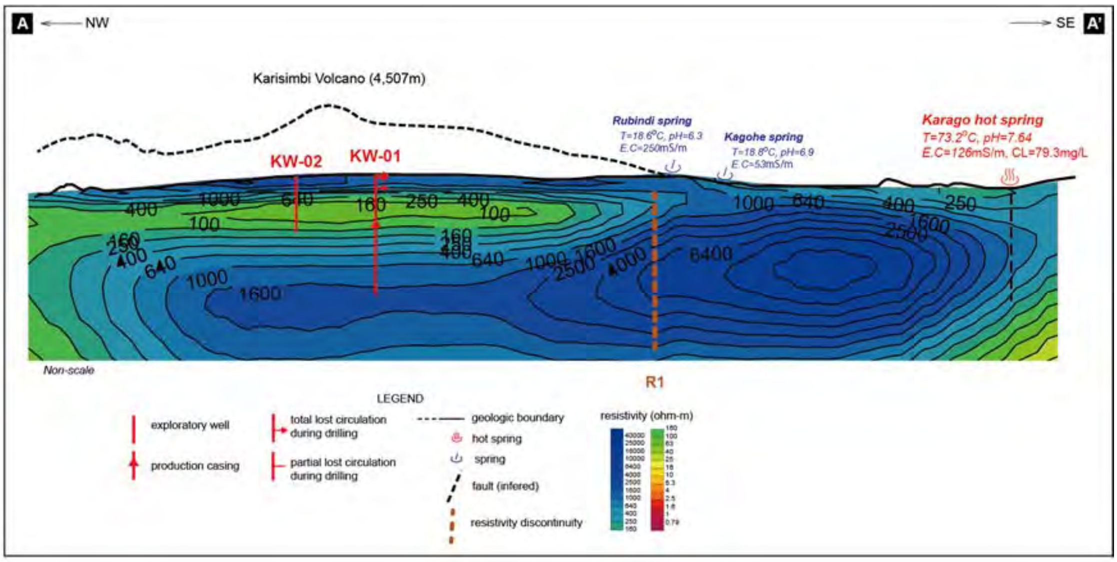

Source: JICA study team

Fig. 3-2.106 Resistivity section for Karisimbi field

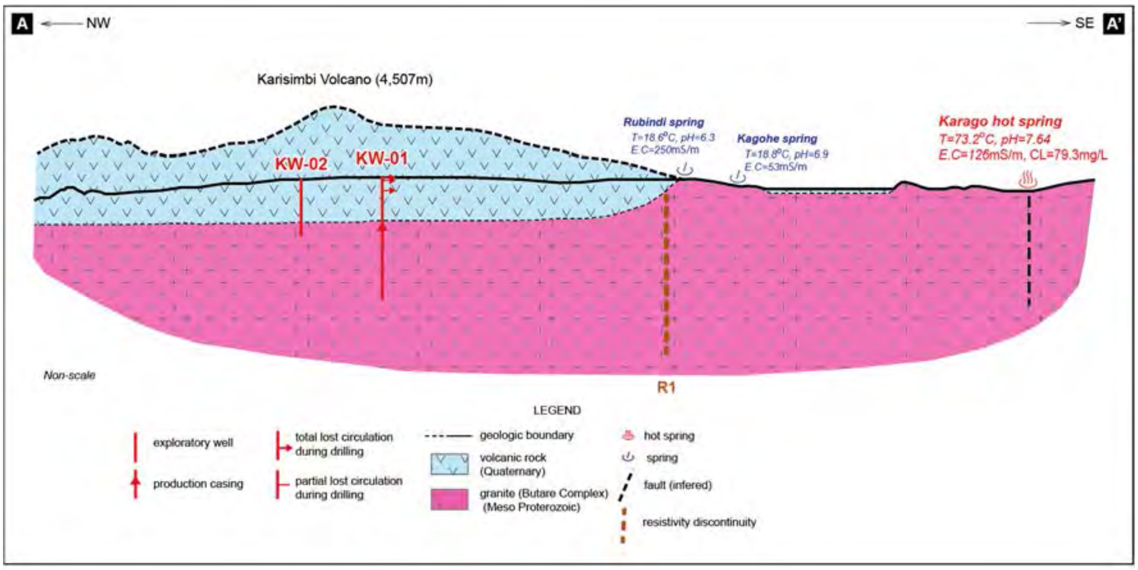

Source: JICA study team

Fig. 3-2.107 Geological section for Karisimbi field

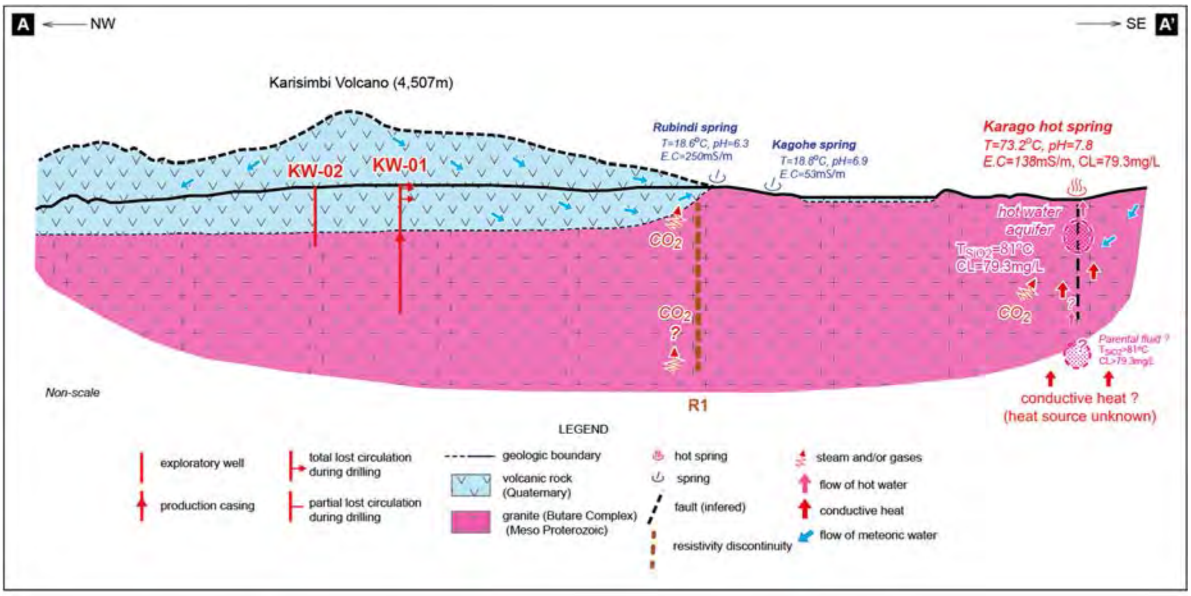

Source: JICA study team

Fig. 3-2.108 Conceptual model for Karisimbi field

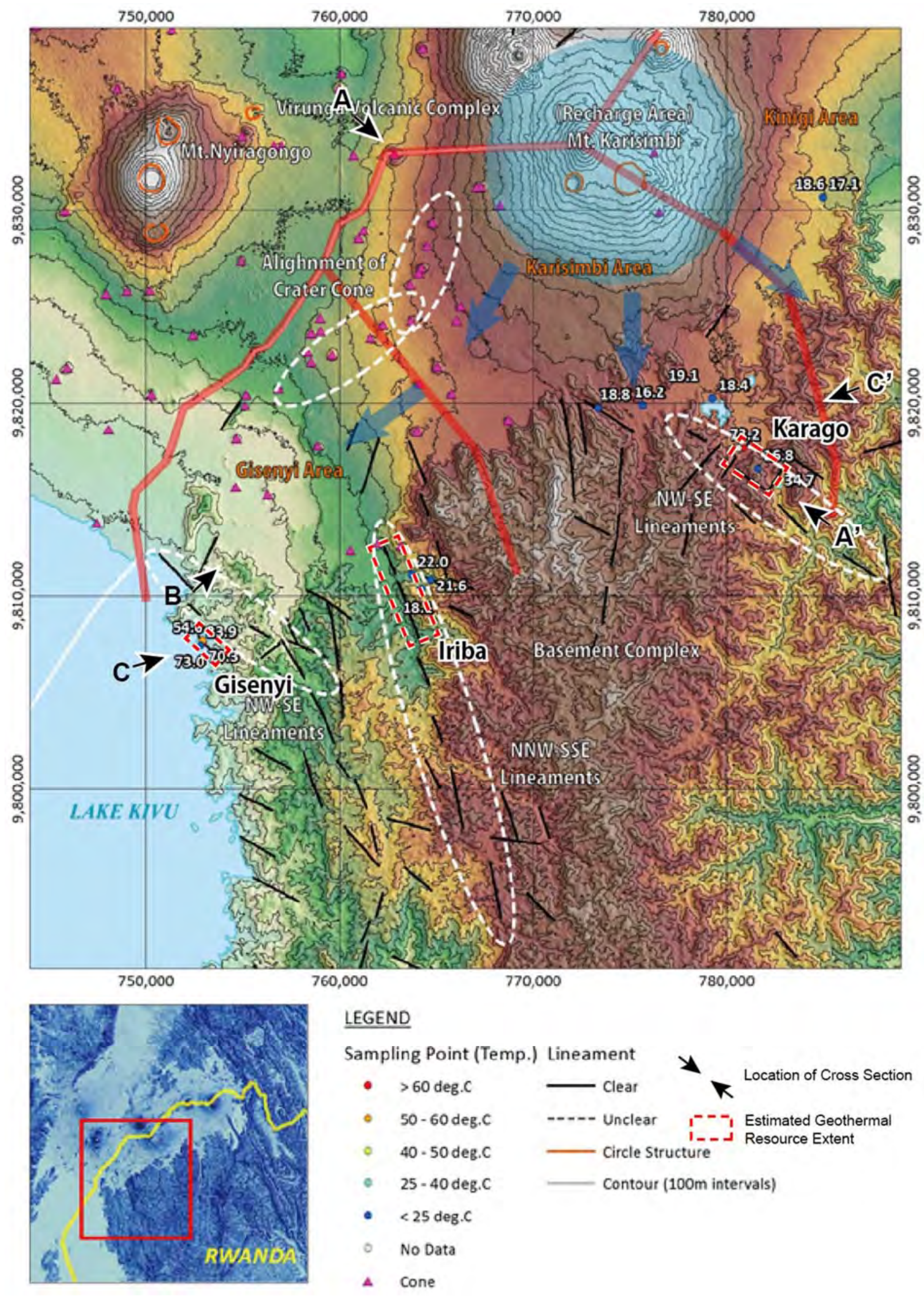

Source: JICA study team

Fig. 3-2.109 Estimated geothermal resource extent area in Karisimbi and Gisenyi fields

2) Kinigi field

The resistivity section, geological cross section and the conceptual model of the geothermal system in Karisimbi – Kinigi fields are shown in Fig. 3.2-110, Fig. 3.2-111 and Fig. 3.2-112, respectively.

The northern part of the Kinigi field is situated in Virunga Volcano Range (VVR), where there are some late quaternary volcanoes. The southern part of the field is in the Butare Horst, which is composed of Proterozoic mylonitised granitic and phyllitic complexes.

The northern part of Kinigi is located close to the Karisimbi, Visoke, Sabinyo, Gahinga and Muhavura volcanoes that erupted in the Quaternary. Southern flank of Mt. Sabinyo is composed of andesite. In general, andesitic volcanic activity is accompanied by magma chamber at relatively shallower depth, which will be candidate heat source of geothermal system. K-Ar rock dating of the andesite is obtained as 0.5 ± 0.1 Ma as described in 3.2.2. These analytical results inferred a possibility of that magma chamber in late Quaternary to be a heat source of geothermal system exist at relatively shallower depths in and around Mt. Sabinyo. The heat source of the Kinigi geothermal system is assumed to be related to the Quaternary activity of Sabinyo volcanoes. While K-Ar rock dating and petrographic information of Mt. Sabinyo is limited (analysed number of sample is one), further analysis is required to assess the heat source of geothermal system in Kinigi field.

No geothermal manifestations such as fumaroles, hot springs, or altered ground have been recognized in the Kinigi field. Cold springs such as Rubindi, Mubona, Cyabararika, etc. occur at the topographic boundary of the volcanic region in the north and in the Butare Horst in the south. The cold spring water contains CO_2 gas.

A widely distributed low resistivity zone is clearly detected at a depth of 2,000 m and deeper in the northern portion of the Kinigi field (Fig.3-2.86 through Fig.3-2.90). In addition, two remarkable resistivity discontinuities, R2 and R3 were identified at a depth of 1,500 m and deeper. Geological structures in the southern part of Kinigi (in the Butare Horst) are characterized by the presence of NNW-SSE trending faults. Considering these geological structures, R2 and R3 delineated by 3D MT inversion show the presence of NNW-SSE trending faults developed in the Proterozoic basement seated below the volcanic rock. It is still uncertain whether a geothermal reservoir at greater depth can be expected or not, but relatively high-temperature geothermal fluids may possibly ascend in the fracture zones around resistivity discontinuities R2 and R3, and these geothermal fluids may migrate in and around the low resistivity zone. Although it is difficult to judge that this low resistivity zone is related with geothermal activity or not at present, there is apossibility of that this low resistivity is related with geothermal activity considering geological data and information such as the presence of andesitic volocanic activity in late Quaternary.

Although uncertainty concerning the presence of a geothermal reservoir remains, the geothermal resource area for geothermal resource evaluation (using the Stored Heat Method) is estimated on the basis of the conceptual model constructed for the Kinigi field. The minimum area is that of the low resistivity zone at a depth of 3,000m (Fig. 3.2-113). The maximum area is determined as lying between R2 and R3, and includes the low resistivity zone at a depth of 3,000m, as shown in Fig.3-2.113. The upper boundary of the reservoir is assumed to be at a depth of 1,500m, based on the resistivity distribution. The thickness of the geothermal reservoir is assumed from a consideration of the drilling depth.

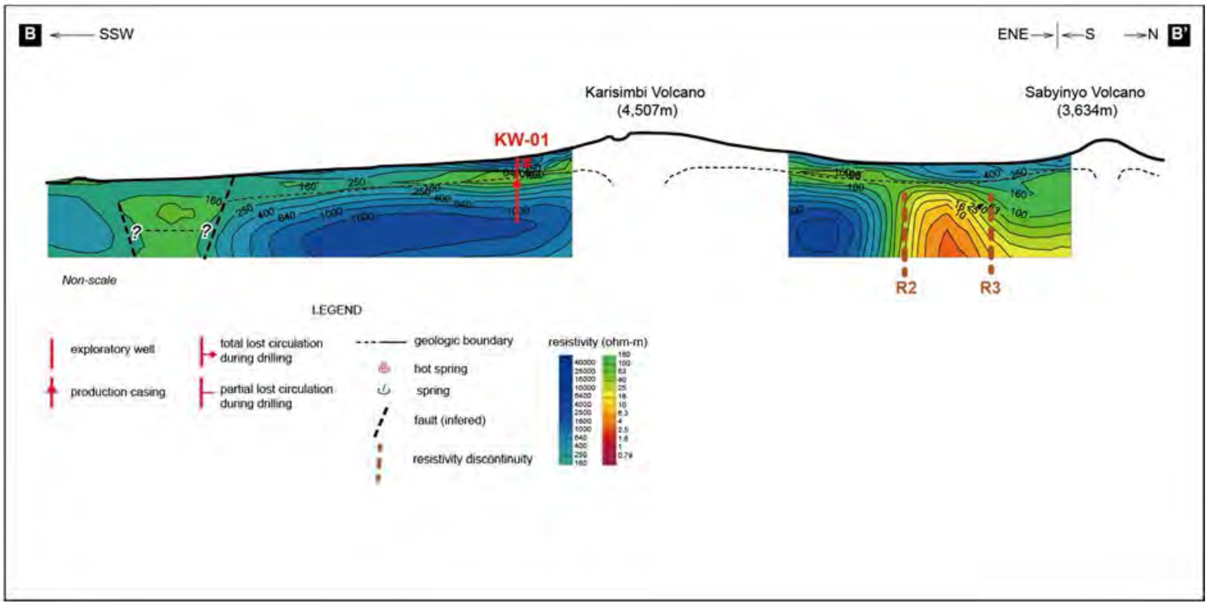

Source: JICA study team

Fig. 3-2.110 Resistivity section for Karisimbi - Kinigi fields

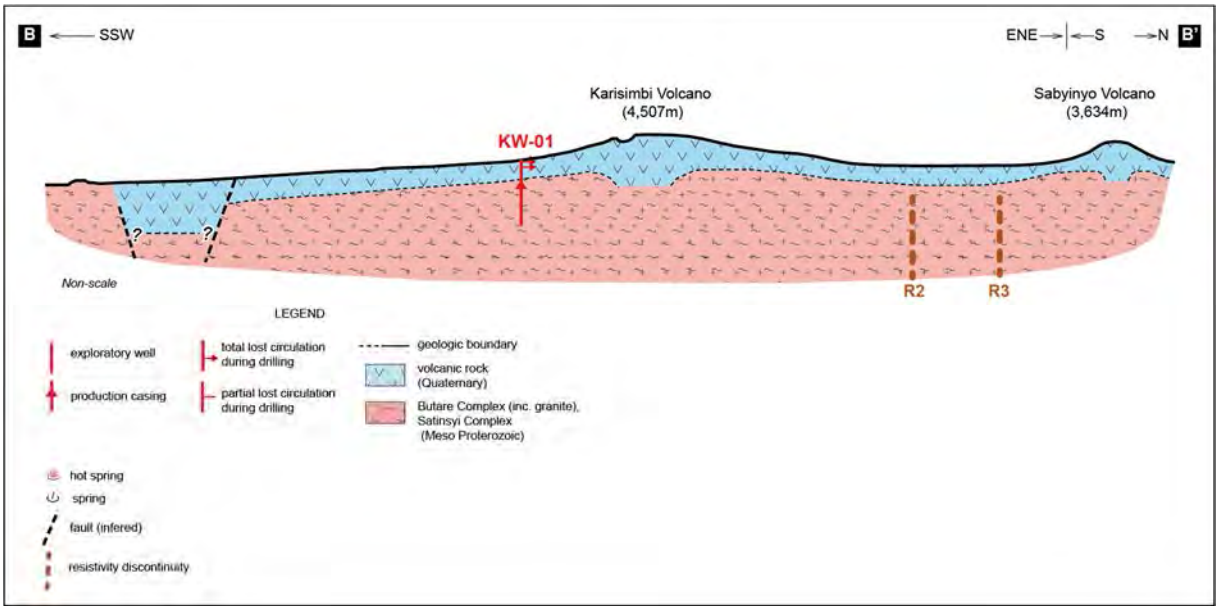

Source: JICA study team (created in March 2015)

Fig. 3-2.111 Geological section for Karisimbi - Kinigi fields

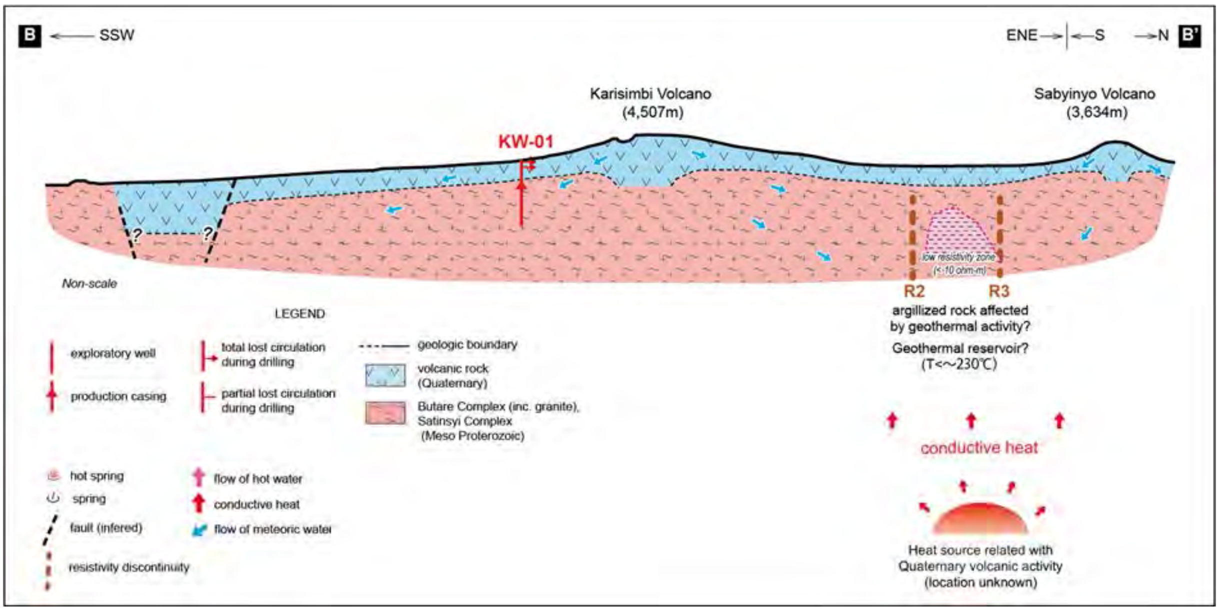

Source: JICA study team (created in March 2015)

Fig. 3-2.112 Conceptual model for Karisimbi - Kinigi fields

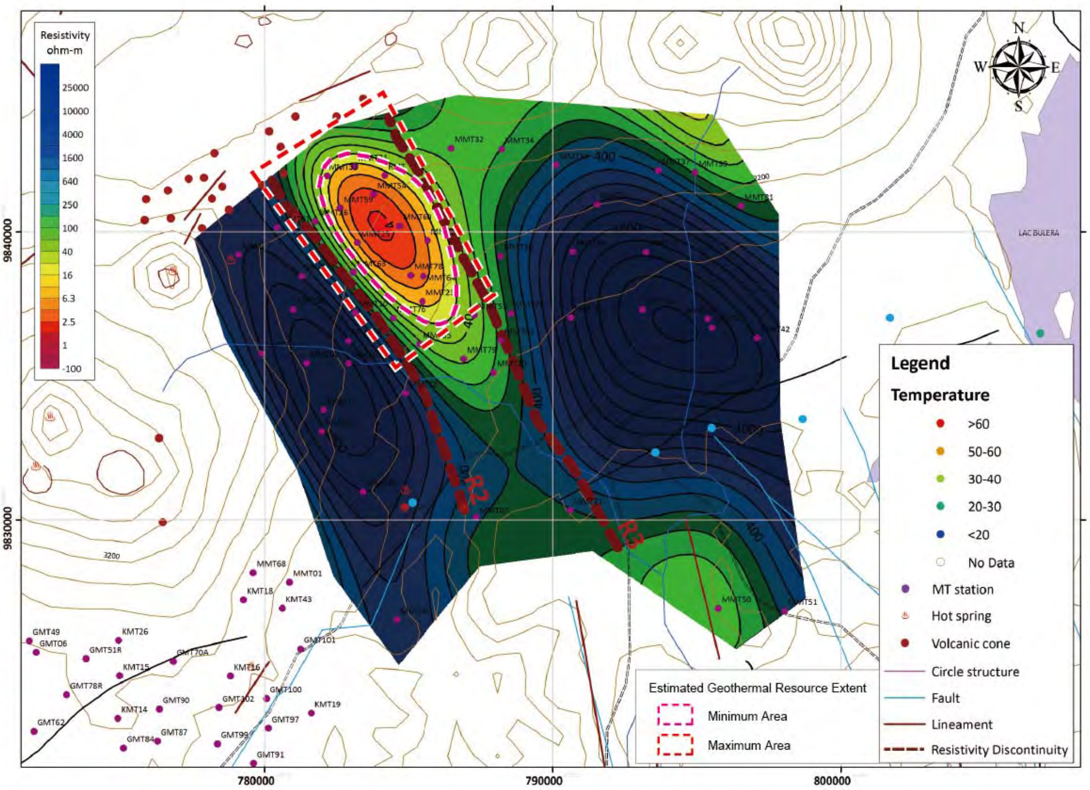

Source: JICA study team (created in March 2015)

Fig. 3-2.113 Estimated geothermal resource area extent in Kinigi field

3) Gisenyi field

The resistivity section, geological cross section and the conceptual model of the geothermal system in Gisenyi field are shown in Fig. 3.2-114, Fig. 3.2-115 and Fig. 3.2-116, respectively.

The northern part of the Gisenyi field is situated in Virunga Volcano Range (VVR) where there are some late Quaternary volcanoes. The southern part of Gisenyi field is in the Butare Horst, which is composed of Proterozoic mylonitised granitic and phyllitic complexes.

Permeable zones in a geothermal system are generally related to passages of the geothermal fluid and to well productivity. Considering the stratigraphy and geological structures of the field and the distribution of thermal manifestations in the field, it seems that fluid flow is strongly controlled by permeable zones related to faults. In general, faults play an important role in the vertical permeability of a geothermal system. In the Gisenyi field, NNW-SSE trending and NW-SE trending faults are inferred from satellite imagery analysis and geological survey (Fig.3-2.33). In and around Gisenyi hot springs, NW-SE trending topographic lineaments are well-recognized as implied faults which are considered to play a role as an upflow zone for hot fluid.

Although the "Recent" Border Fault, which trends N-S, and the Accommodation Zone, which trends NE-SW, have been mapped by BGR (2009) as major geological structures in Gisenyi field, there is no data or information indicating that these structures control geothermal activity. The "Recent" Border Fault reported by BGR (2009) is well-recognized by satellite imagery analysis as topographic scarps and lineaments. Resistivity discontinuity R1 (Figs.3-2.69 to 3-2.77) can be correlated with the Accommodation Zone (BGR, 2009) trending NE-SW. Some volcanic craters and cones, as well as cold springs are distributed along the Accommodation Zone, indicating that this is a highly fractured zone.

Although hot springs and Quaternary volcanism are present in Gisenyi field, no low resistivity zone of less than 40 ohm-m has been detected from the ground surface level down to a depth of 5,000 m over the whole area of the Gisenyi field, even around Gisenyi hot spring and resistivity discontinuity R1 (Figs.3-2.67 to 3-2.77). This suggests that geothermal activity in the Gisenyi field is likely to be relatively weak compared with other geothermal fields where geothermal power stations have been installed and are being operated.

From the hydrogen and oxygen isotopic composition and Cl concentration of the spring waters in Gisenyi field, it appears likely that the discharging hot spring water in the area originates in meteoric water. The hot spring water is classified as HCO_3 type, which is a conductively heated type (Fig.3-2.51). The relatively high Cl concentration implies some mixing of deep high-temperature reservoir water in Gisenyi hot spring.

The fluid flow model in and around Gisenyi hot spring shows meteoric water penetrating into the deeper level in the mountainous area above Gisenyi hot spring area, where it is heated by conductive heat.

Hot fluids are stored in a permeable zone trending NW-SE developed in the Proterozoic basement. The geothermometry for the spring water suggests that the temperature of the hot water aquifer is around 80^{o}C. The hot fluid ascending along the fractures gushes out as the hot springs of Gisenyi. The Cl concentration in the hot spring water suggests the presence of a parental fluid at deeper depth in Gisenyi, as shown in Fig. 3-2.116. In general, geothermometers based on geochemistry are powerful tools in estimating reservoir temperatures at greater depth. However, it is difficult to estimate reservoir temperature at depth because the reliability of geothermometry in this area is very limited (only the silica geothermometer is reliable in this area). Therefore, more detailed geoscientific study is required to examine the possible presence of a deeper reservoir and establish its temperature.

Although the accuracy is not high due to the shortage of subsurface geoscientific information such as geophysical and well-logging data, the geothermal resource area for geothermal resource evaluation (using the Stored Heat Method) is estimated based on the conceptual model constructed for Gisenyi hot spring area. The area is determined considering the distribution of permeable zones which control geothermal fluid flow and thermal manifestations and includes the permeable zones assumed along the NW-SE trending faults shown in Fig.3-2.109. The thickness of geothermal reservoir is assumed from a consideration of the drilling depth.

Although the temperature of discharged water in Iriba is low (22^{o}C), the Cl concentration of the discharged water reaches a maximum of 320 mg/L, implying some mixing of deep high-temperature reservoir water. The estimated geothermometry temperature is 79 ^{o}C in Iriba, which is considered to indicate the temperature of a shallow hot water aquifer (Fig. 3.2-116). The Cl concentration in the hot spring water indicates a possibility that parental fluid of a higher temperature may be present below the Iriba field at depth (Fig. 3-2.116). A NNW-SSE trending inferred fault is mapped in Iriba. This fault is considered to control fluid flow in Iriba. K-Ar rock dating of basalt in Gikombe crater situated near Iriba spring is obtained as 1.0 ± 0.4 Ma as described in 3.2.2. The heat source of the Iriba geothermal system is assumed to be related to the late Quaternary volcanic activity in this area.

Although the accuracy is not high due to shortage of subsurface geoscientific information such as geophysical and well-logging data, the geothermal resource area for geothermal resource evaluation (using the Stored Heat Method) is estimated based on the conceptual model constructed for the Iriba field. The field is determined considering the distribution of permeable zones which control fluid flow and includes permeable zones assumed along the NNW-SSE trending faults shown in Fig.3-2.109. The thickness of geothermal reservoir is assumed from a consideration of the drilling depth.

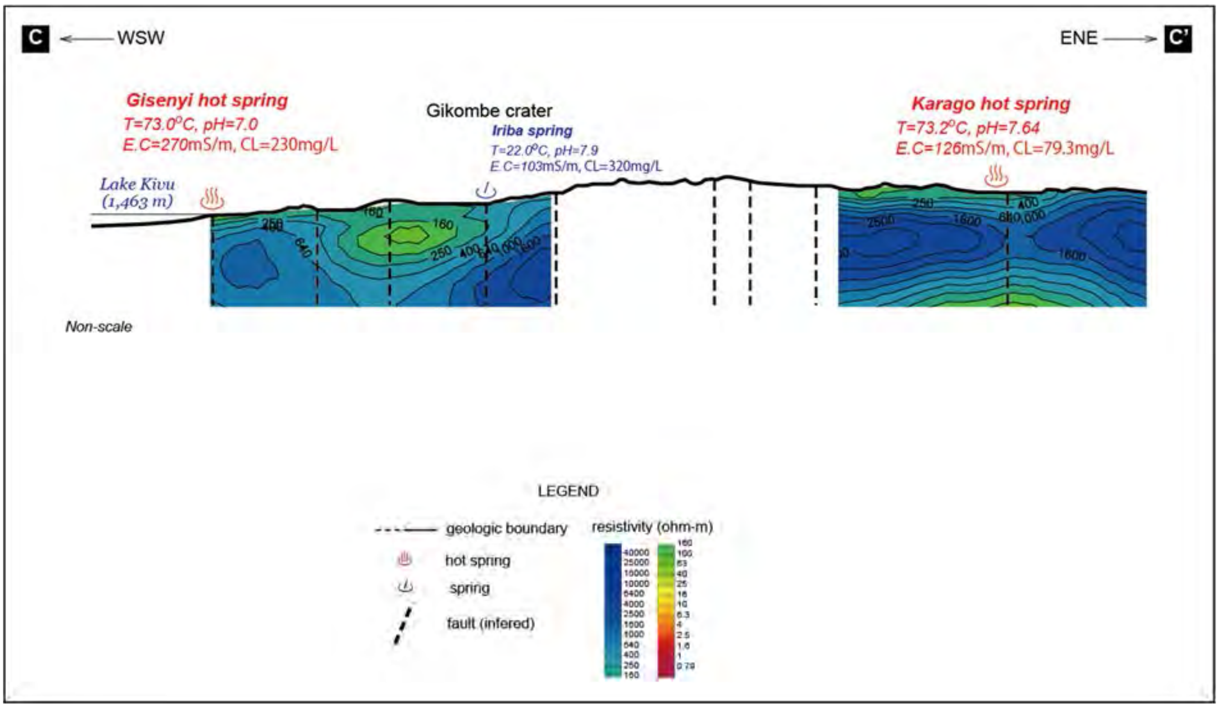

Source: JICA study team

Fig. 3-2.114 Resistivity section for Gisenyi - Karisimbi fields

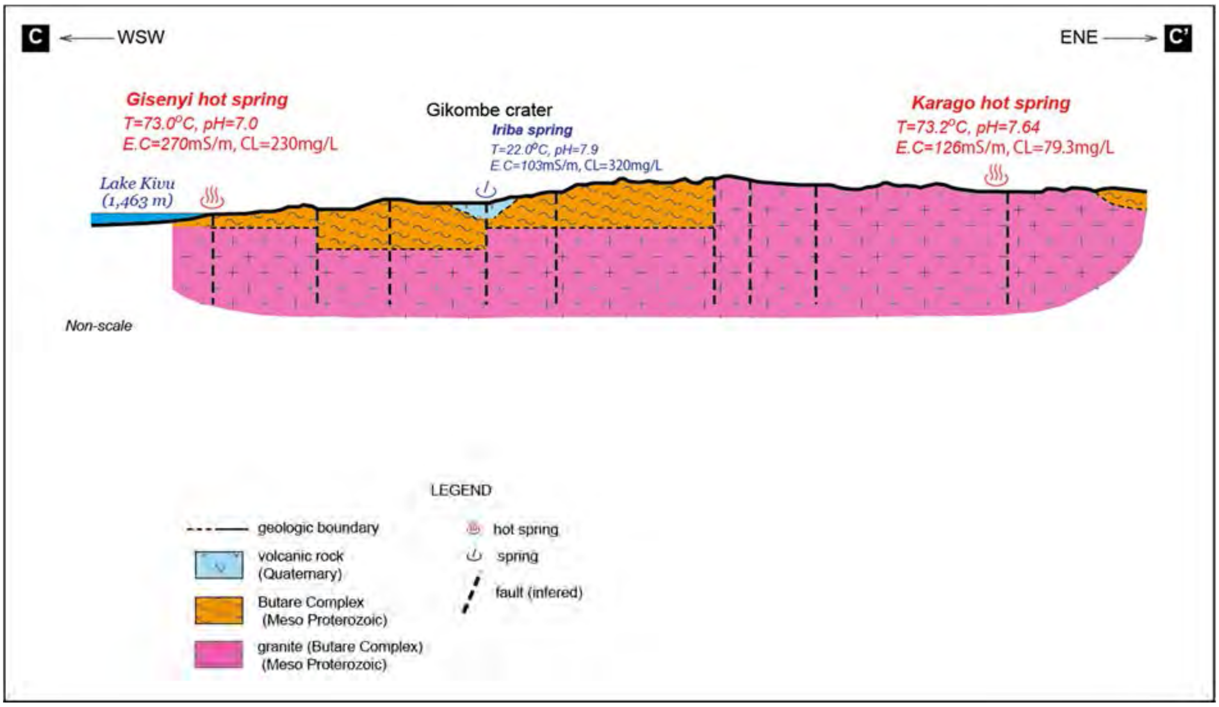

Source: JICA study team

Fig. 3-2.115 Geological section for Gisenyi - Karisimbi fields

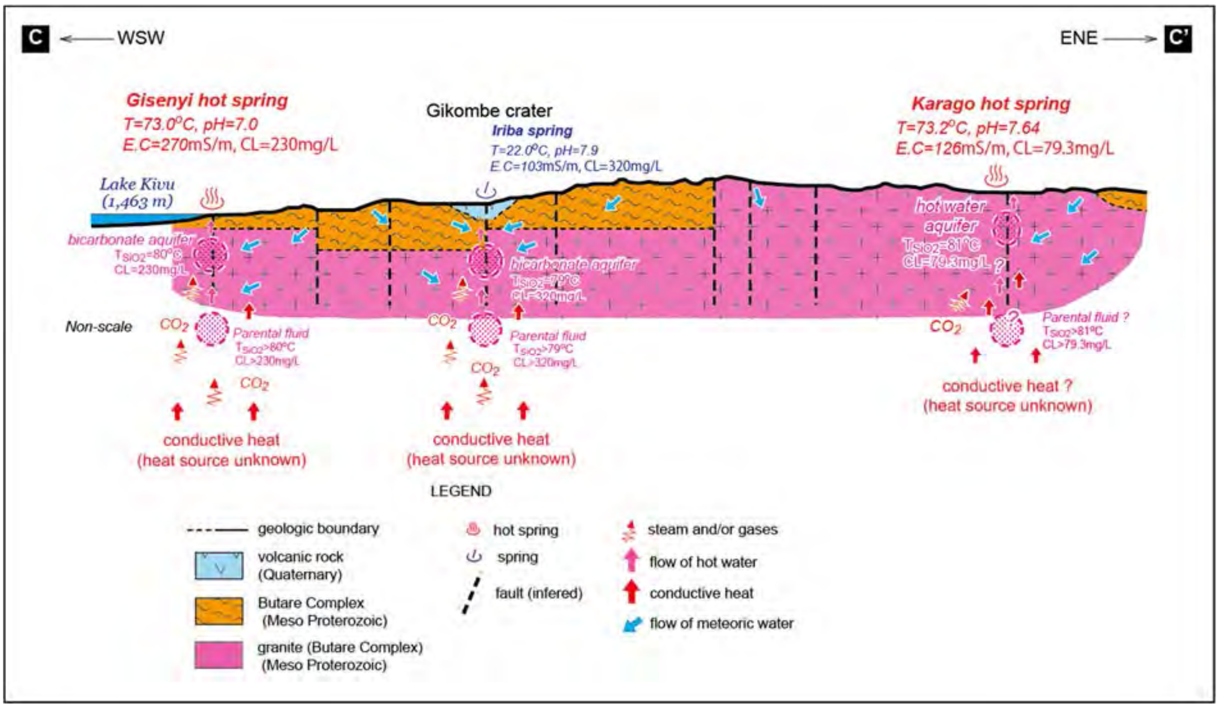

Source: JICA study team

Fig. 3-2.116 Conceptual model for Gisenyi - Karisimbi fields

4) Bugarama field

The geological section and conceptual model of the geothermal system in the Bugarama field (in and around Mashyuza hot spring) is shown in Fig.3-2.117 and Fig.3.2-118. The Bugarama field is comprised of Proterozoic basement, Tertiary basaltic rocks and Quaternary alluvials. K-Ar rock dating of basalt in Bugarama is obtained as 12.2 ± 0.4 Ma. There do not appear to be any young volcanoes related to the magmatic heat source in and around Bugarama field. The heat source of the Bugarama geothermal system is considered to be the conductive heat of the magmatic materials situated in a deeper part of the crust, or the conductive heat of intrusive rocks.

Permeable zones in a geothermal system are generally related to passages for the geothermal fluid and well-productivity. Considering the stratigraphy, geological structures, distribution of thermal manifestations and results of gravity survey in the area, it seems that the geothermal fluid flow is strongly controlled by permeable zones related to faults. In general, faults play an important role in the vertical permeability of a geothermal system. Geological structures in the Bugarama field are characterized by the presence of graben structures, which are delineated in the gravity survey. A low Bouguer anomaly zone extends over the north and northeastern sectors of the entire survey area. Faults or fracture zones are delineated at the subsurface in the gravity survey. The distribution of the delineated faults indicates that the graben is bounded by faults on both sides. Mashyuza hot spring is located close to the central portion of gravity lineament G3, where a topographic lineament is in evidence. Thus, gravity lineament G3 is likely to indicate a fault where geothermal fluids may migrate in fracture zones existing along the fault. The other gravity lineaments may reflect faults controlling geothermal fluids, but further geoscientific information is required to clarify whether or not geothermal fluids migrate along and around those gravity lineaments.

From the hydrogen and oxygen isotopic composition and Cl concentration of the spring waters, it appears likely that the geothermal reservoir water in the field originates in meteoric water. The Cl concentration reaches a maximum of 150 mg/L, implying some mixing of deep high-temperature reservoir water. The diagram of temp-SiO_2 and Cl concentration (Fig.3-2.60) shows the mixing correlation between Bize and Mashyuza water, which implies that those waters are diluted from the same parental fluid.

The fluid flow model for the Bugarama field shows meteoric water penetrating into the deep level in the mountainous area at a higher elevation to the west and northwest of the Mashyuza hot spring area, where it is heated up to over 63^{o}C by conductive heat. The thermal fluid at depth in the area is considered to be up-flowing through the permeable zones found mainly along gravity lineament G4 trending NW-SE and gravity lineament G3 trending NE-SW. Up-flowing thermal fluid is stored in the fractures developed in metamorphic and volcanic rocks. The hot water, having ascended to the shallow level mainly along G3, is likely diluted and cooled by cold shallow groundwater and/or river water, and stored in these permeable zones at relatively shallower depth. The geothermometry for spring water estimates the temperature of the shallow aquifer to be 63^{o}C. Warm water resulting from the dilution and cooling discharges to the surface at Mashyuza.

As shown in Fig. 3-2.119, there is a possibility that a relatively higher temperature geothermal reservoir may be present below the Bugarama field at depth, but the presence of this deeper geothermal reservoir is still uncertain. In general, geothermometers based on geochemistry are powerful tools in estimating reservoir temperatures at greater depth. However, it is difficult to estimate reservoir temperature at depth because the reliability of geothermometry in this area is very limited (only the silica geothermometer is reliable). Therefore, more detailed geoscientific study is required to examine the possible presence of a deeper reservoir and to estimate its temperature.

Although the accuracy is not high due to shortage of subsurface geoscientific information such as geophysical and well-logging data, the geothermal resource area for geothermal resource evaluation (using the Stored Heat Method) is estimated based on the conceptual model constructed for the Bugarama field. The field is determined considering the distribution of permeable zones which control geothermal fluid flow and thermal manifestations. The minimum assumed area is located along gravity lineaments G4, G3 and G1, which are considered to represent the main permeable zone. The maximum area includes gravity lineaments G4, G3, G1 and G7. The eastern boundary of the maximum area is determined by the eastern margin of the graben. The thickness of geothermal reservoir is assumed from a consideration of the drilling depth.

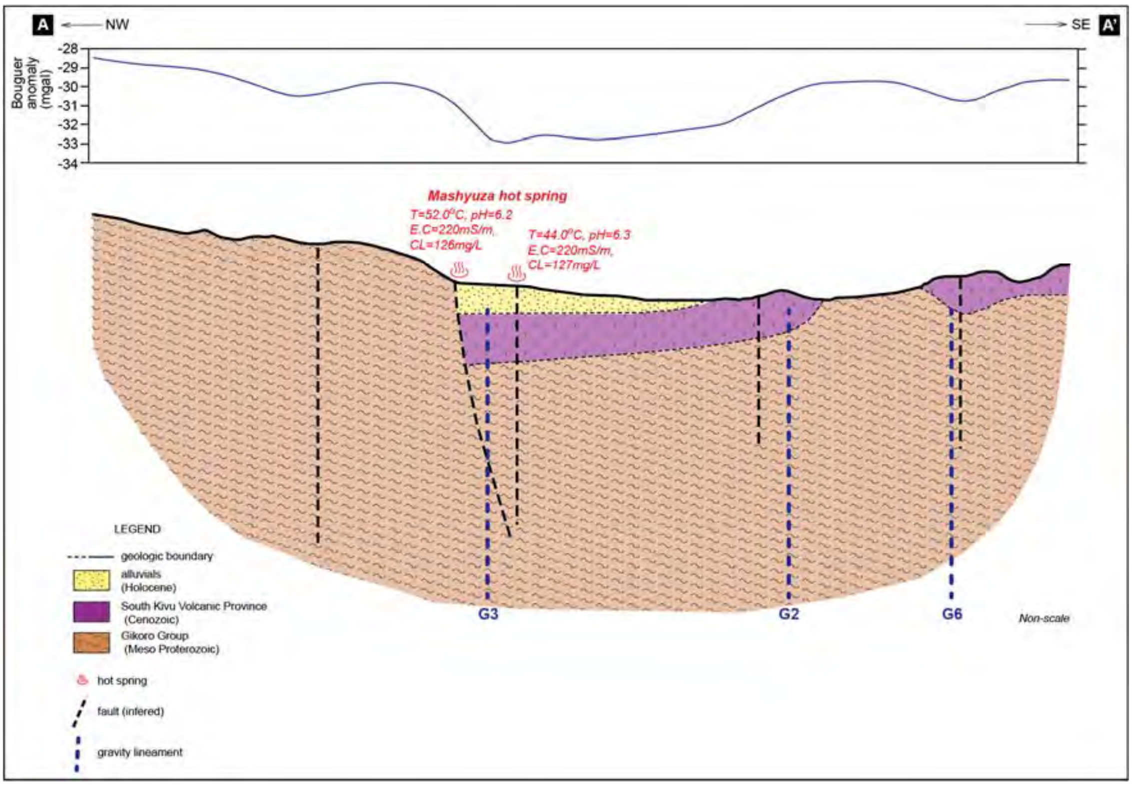

Source: JICA study team

Fig. 3-2.117 Geological section for Bugarama field

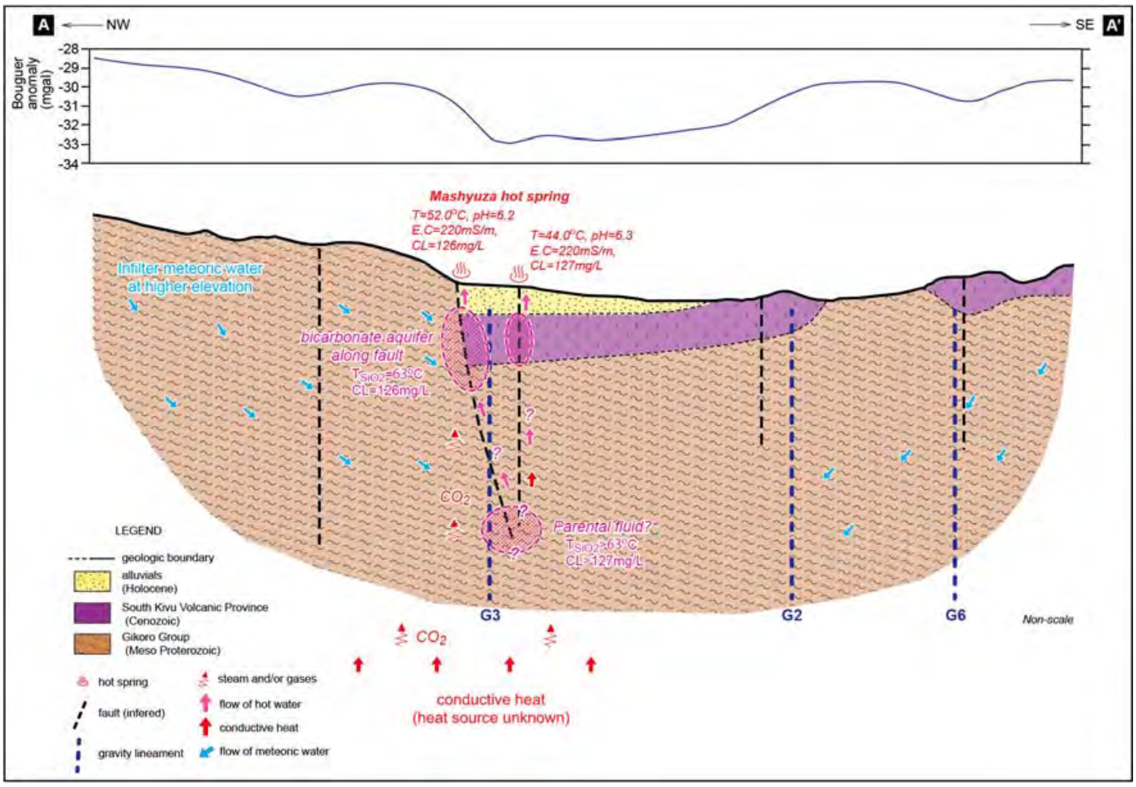

Source: JICA study team

Fig. 3-2.118 Conceptual model for Bugarama field

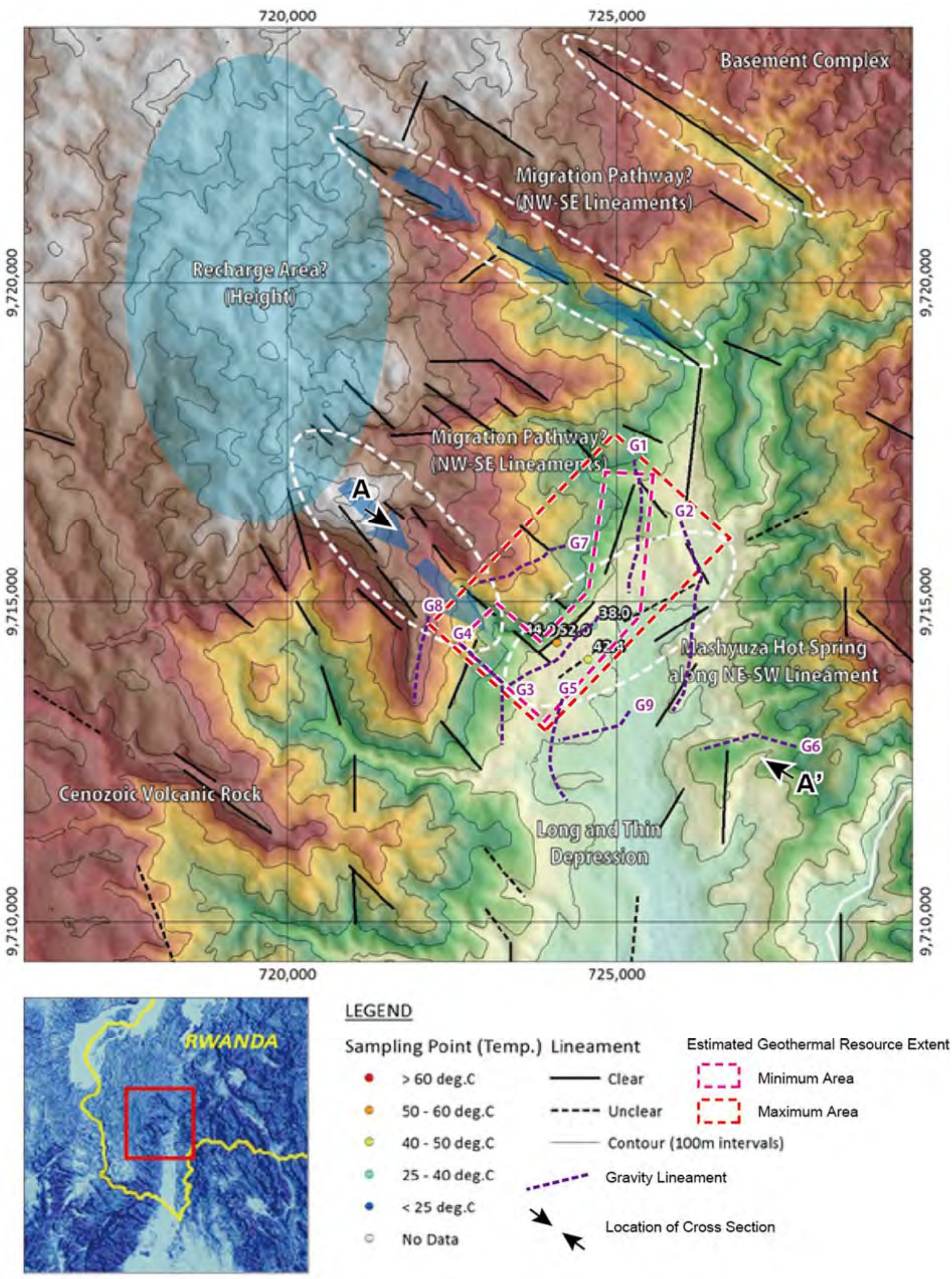

Source: JICA study team

Fig. 3-2.119 Estimated geothermal resource extent area in Bugarama field

(2) **Resource potential evaluation**

1) Methodology

The geothermal resource potential of the detailed geoscientific survey field was estimated by the volumetric method from some parameters necessary for the calculation. The volumetric method is a method for calculating the heat energy stored underground, then calculating the energy available for power generation and finally converting that energy into power output. In the volumetric method of calculation, the geothermal resource potential can be determined with statistical probability by applying the Monte Carlo analysis technique. For a specified plant life, the power output of the field in MWe can be derived as follows.

$$\text{Power Output [MWe]} = (Tr - Ta) \times \{(1-\varphi) \times Cpr \times \rho r + \varphi \times Cpw \times \rho w\} \times V \times RF \times CE / (LF \times PL)$$

ρr、ρw : rock density and fluid density（kg/m^3）

Cpr、Cpw : rock specific heat and fluid specific heat（kJ/kg-ºC）

Tr、Ta : reservoir temperature and abandonment temperature（ºC）

φ : porosity（%）

V : reservoir volume（km^3）

RF : recovery factor（%）

CE : conversion efficiency（%）

LF : load factor（%）

PL : plant life（years）

Using a distribution of the probable values for each of the parameters relevant to the estimation of the geothermal potential, Monte Carlo analysis is used to statistically estimate the most probable power output of the field by trying all possible combinations of these parameters. The distribution of parameters may include values that are not precisely known but can be part of the probability distribution. Triangular distribution or quadrilateral distribution (see Fig. 3-2.120) is generally chosen as a probability distribution for this estimation.

Reservoir Volume

The thickness of each field is assumed to be as follows: the minimum is 1,000m and the maximum is 2,000m assuming rectangular uncertainty distribution. The assumed maximum and minimum area of a given field can be estimated assuming rectangular uncertainty distribution from the distribution of geothermal manifestations and so on. The reservoir volume can then be obtained by multiplying the thickness by the area. Later verification of the reservoir volume based on further detailed survey will be necessary, however, because the values used here are just estimates.

Reservoir Temperature and Abandonment Temperature

The average reservoir temperature for each area is assumed principally based on the geochemical data concerning the hot springs and the geothermal conceptual model. Minimum and maximum temperatures are assumed for each field, which makes the probability distribution triangular. The abandonment temperature is assumed to be an invariable 80 ^{o}C for a binary-type installation. (Generally, it is 180 ^{o}C for a flash type installation).

Rock Density

The minimum rock densities are assumed to be 2,500kg/m^3 in Karago which consists of granite, and 2,600kg/m^3 in the other areas which consist of Proterozoic metamorphic rock. The maximum rock density is 3,000kg/m^3, assuming a rectangular uncertainty distribution.

Rock Specific Heat

The rock specific heat is assumed to range from 0.8 to 1.0 kJ/kg- ^{o}C based on the general value of rock assuming a rectangular uncertainty distribution.

Porosity

1% and 5% are assumed as minimum and maximum values for areas whose formation antedates the Proterozoic. 1% and 10% are assumed as minimum and maximum values for areas whose formation antedates both the Cenozoic and the Proterozoic.

Fluid Density and Specific Heat

The fluid density and specific heat are obtained from the steam tables assuming a rectangular uncertainty distribution.

Recovery Factor

The recovery factor is assumed to be 2.5 times the porosity value from the rectangular uncertainty distribution.

Conversion Efficiency

Minimum and maximum values of conversion efficiency are assumed to be 5.0% and 10.0% for a binary type installation assuming a rectangular uncertainty distribution.

Plant Life and Load Factor

The plant life and load factor are assumed to be an invariable 30 years and 85%, respectively.

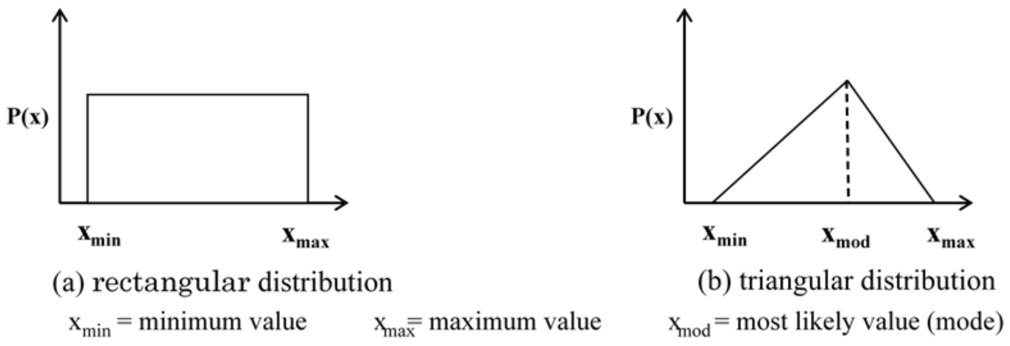

Source: JICA study team

Fig. 3-2.120 Assumed Probability Distribution

2) Estimation results

The computed resource potential distributions of the 5 survey fields, considering minimum and maximum values for each of the parameters, are shown in Figs. 3-2.121 to 3.2-125. Since the computed resource potentials of the fields are distributed over a wide range, the potentials at the 80 % and 50% confidence levels are chosen as representative of the potential value of the field.

The results are summarized in Table 3-2.24. The total geothermal power generation potential of the 5 fields is estimated to be about 47.3 MWe at the 80% confidence level, and 89.5 MWe at the 50 % confidence level.

Table 3-2.24 Summary of resource evaluation for 5 fields

Field name	Resource Potential at 80% Confidence Level (MWe)	Resource Potential at 50% Confidence Level (MWe)
Kinigi	32.6	58.6
Bugarama	6.6	15.1
Gisenyi	1.9	3.7
Karago	2.5	4.9
Iriba	3.7	7.2
Total	**47.3**	**89.5**

Source: JICA study team (created in March 2015)

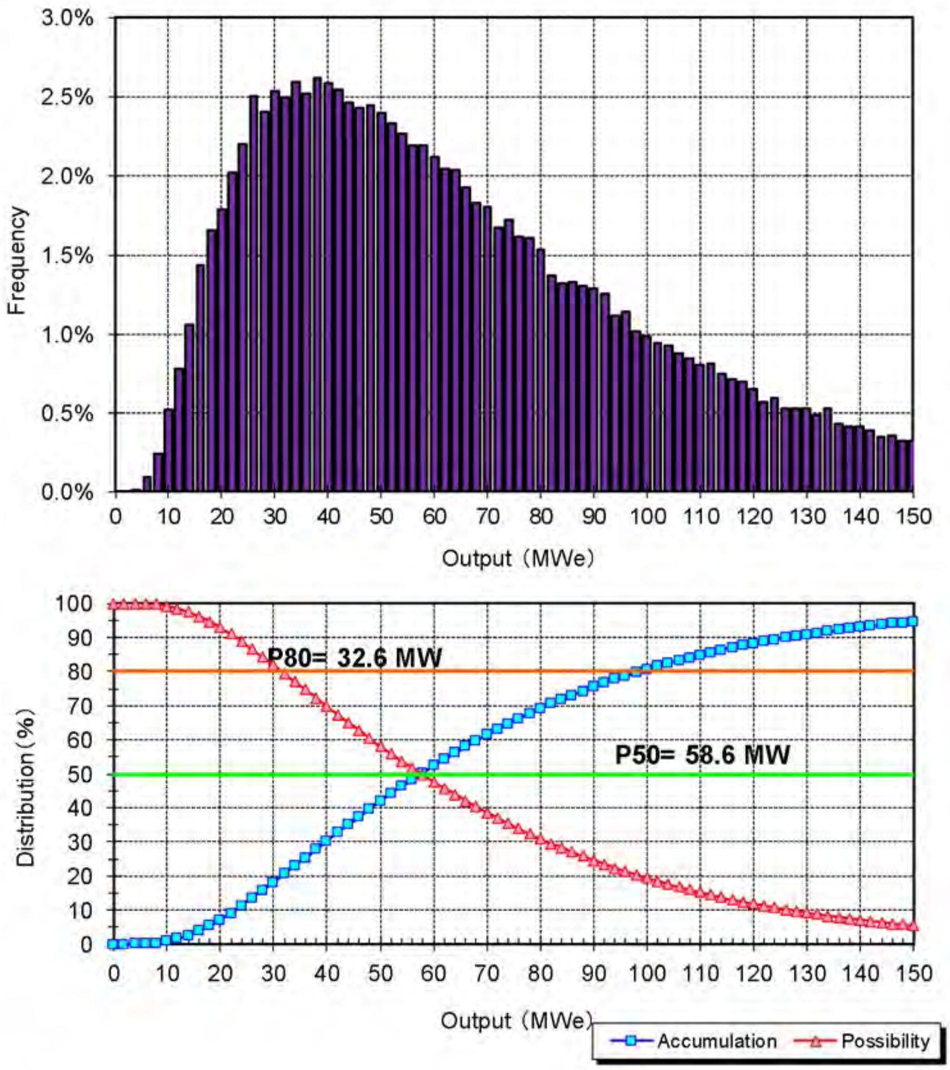

Input

Parameter	min.	most likely	max.
Reservoir Area (km^2)	17.83	-	35.93
Reservoir Thickness (m)	1000	-	2000
Rock Density (kg/m^3)	2600	-	3000
Porosity (-)	0.01	-	0.05
Recovery factor (-)	0.025	-	0.125
Rock Specific Heat (kJ/kg^oC)	0.80	-	1.00
Reservoir Average Temperature (^oC)	150	-	230
Reservoir Average Pressure (MPa)	-	22.5	-
Heat-Electricity Conversion Factor (-)	0.02	0.065	0.11
Plant Life (year)	-	30	-
Load Factor (-)	-	0.85	-
Abandonment Temperature (^oC)	-	80	-

Source: JICA study team (created in March 2015)

Fig. 3-2.121 Probability distribution of the geothermal potential for Kinigi field

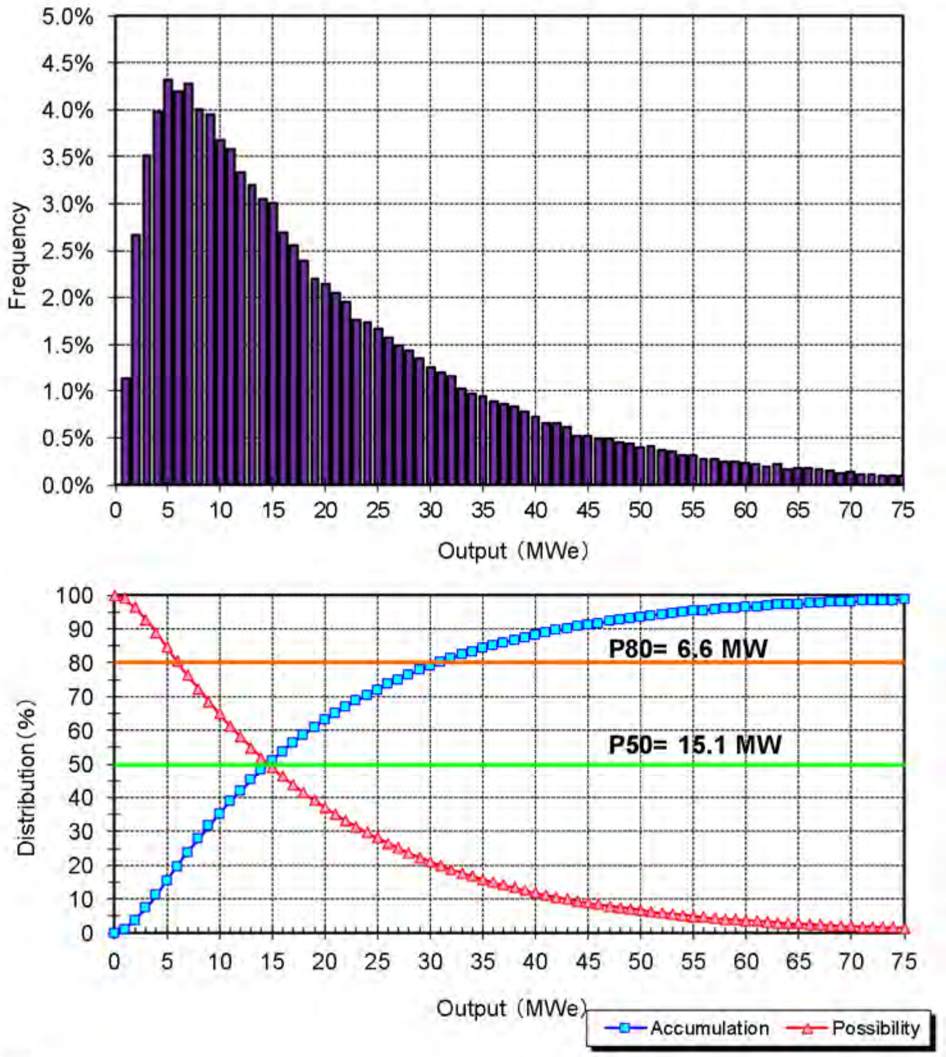

Input

Parameter	min.	most likely	max.
Reservoir Area (km^2)	3.40	-	8.30
Reservoir Thickness (m)	1000	-	2000
Rock Density (kg/m^3)	2600	-	3000
Porosity (-)	0.01	-	0.10
Recovery factor (-)	0.025	-	0.250
Rock Specific Heat (kJ/kg°C)	0.80	-	1.00
Reservoir Average Temperature (°C)	100	-	220
Reservoir Average Pressure (MPa)	-	12.5	-
Heat-Electricity Conversion Factor (-)	0.02	0.065	0.11
Plant Life (year)	-	30	-
Load Factor (-)	-	0.85	-
Abandonment Temperature (°C)	-	80	-

Source: JICA study team

Fig. 3-2.122 Probability distribution of the geothermal potential for Bugarama field

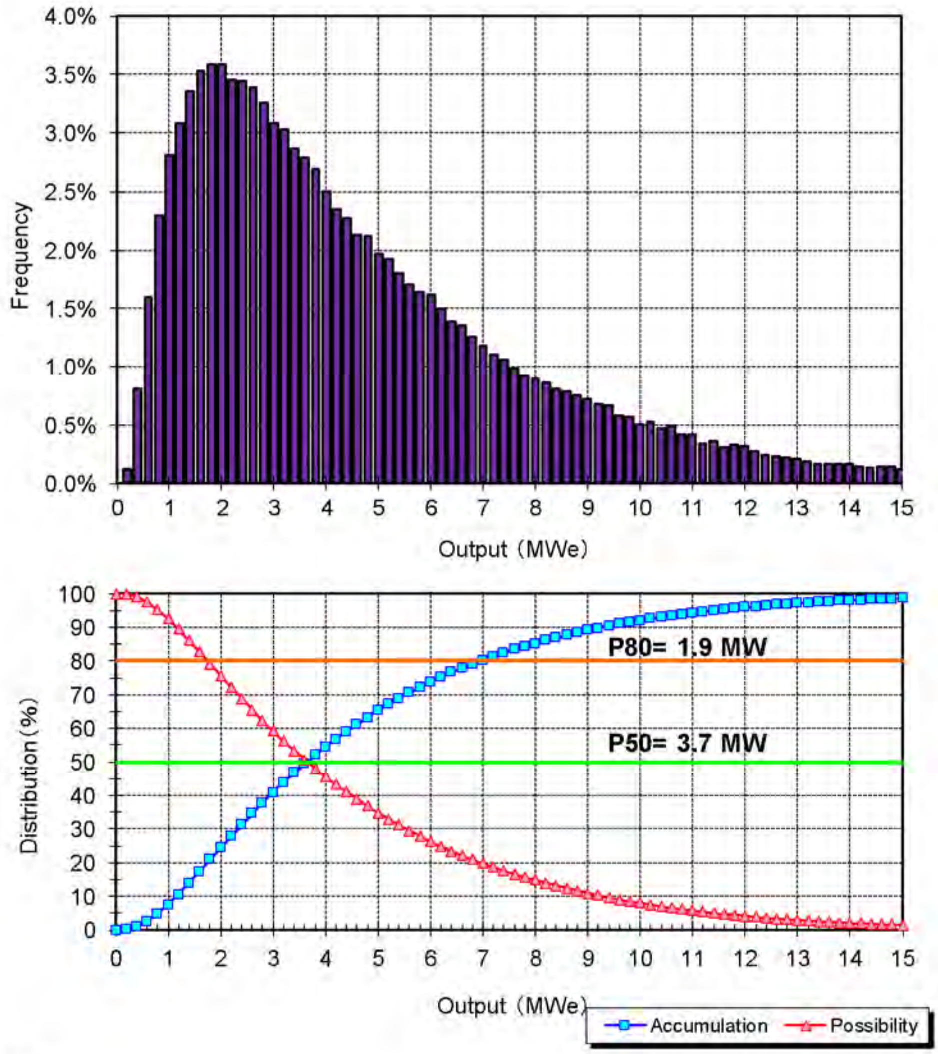

Input

Parameter	min.	most likely	max.
Reservoir Area (km^2)	-	2.50	-
Reservoir Thickness (m)	1000	-	2000
Rock Density (kg/m^3)	2600	-	3000
Porosity (-)	0.01	-	0.05
Recovery factor (-)	0.025	-	0.125
Rock Specific Heat (kJ/kg$^{\circ}$C)	0.80	-	1.00
Reservoir Average Temperature ($^{\circ}$C)	100	-	220
Reservoir Average Pressure (MPa)	-	12.5	-
Heat-Electricity Conversion Factor (-)	0.02	0.065	0.11
Plant Life (year)	-	30	-
Load Factor (-)	-	0.85	-
Abandonment Temperature ($^{\circ}$C)	-	80	-

Source: JICA study team

Fig. 3-2.123 Probability distribution of the geothermal potential for Gisenyi field

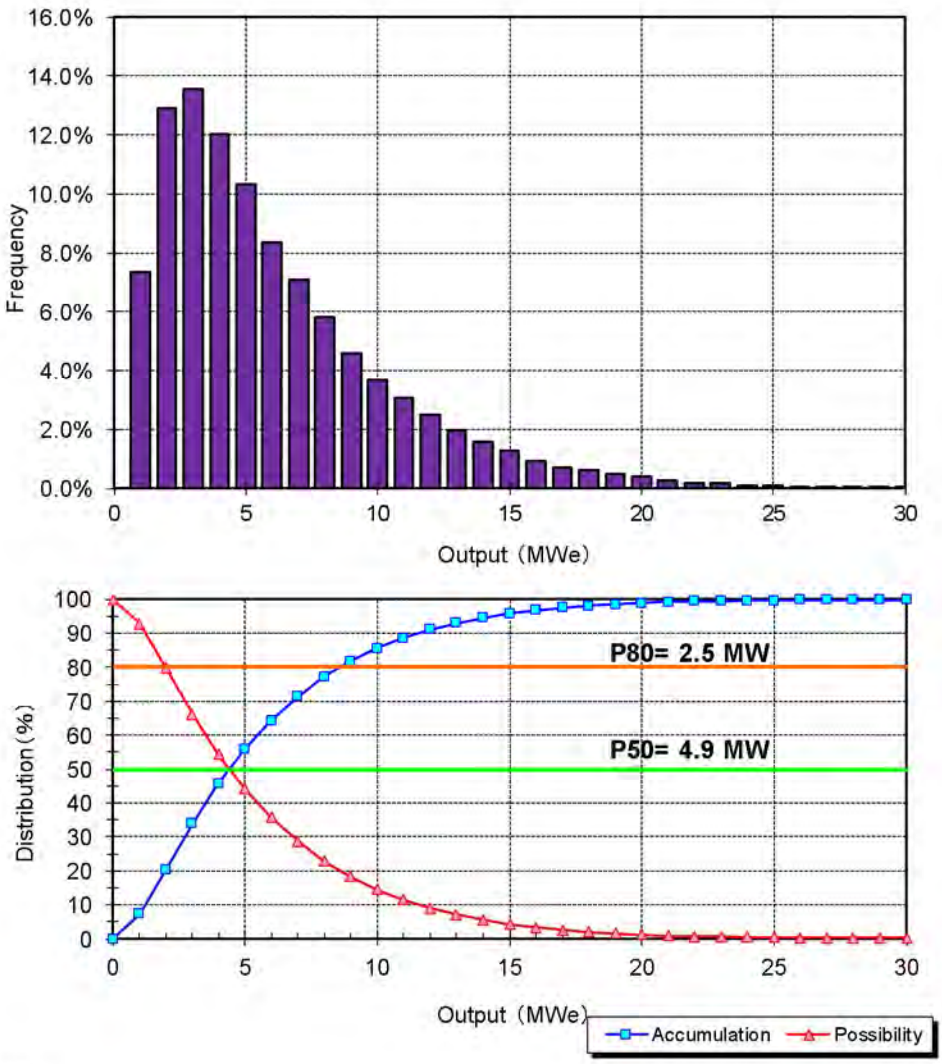

Input

Parameter	min.	most likely	max.
Reservoir Area (km^2)	-	3.75	-
Reservoir Thickness (m)	1000	-	2000
Rock Density (kg/m^3)	2500	-	3000
Porosity (-)	0.01	-	0.05
Recovery factor (-)	0.025	-	0.125
Rock Specific Heat (kJ/kg^{o}C)	0.80	-	1.00
Reservoir Average Temperature (^{o}C)	100	-	200
Reservoir Average Pressure (MPa)	-	12.5	-
Heat-Electricity Conversion Factor (-)	0.02	0.065	0.11
Plant Life (year)	-	30	-
Load Factor (-)	-	0.85	-
Abandonment Temperature (^{o}C)	-	80	-

Source: JICA study team

Fig. 3-2.124 Probability distribution of the geothermal potential for Karago field

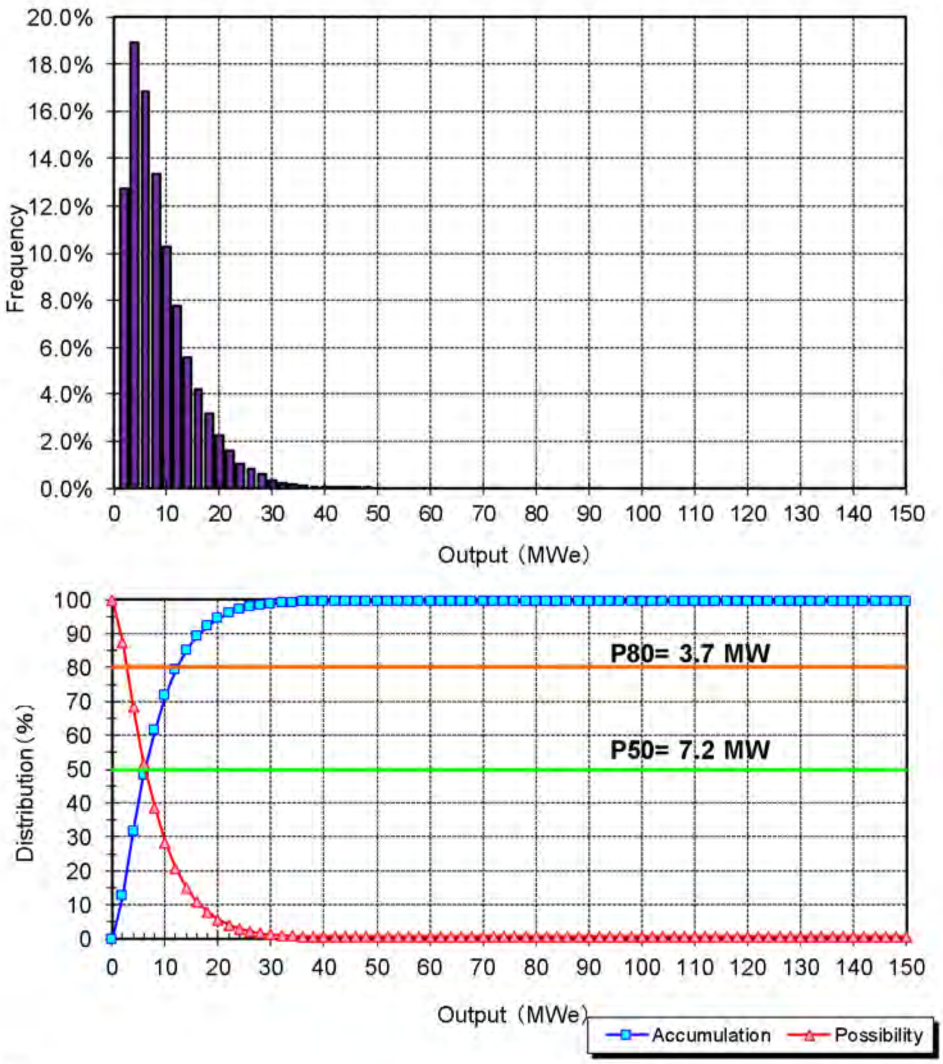

Input

Parameter	min.	most likely	max.
Reservoir Area (km^2)	-	6.25	-
Reservoir Thickness (m)	1000	-	2000
Rock Density (kg/m^3)	2600	-	3000
Porosity (-)	0.01	-	0.05
Recovery factor (-)	0.025	-	0.125
Rock Specific Heat (kJ/kg^{o}C)	0.80	-	1.00
Reservoir Average Temperature (^{o}C)	100	-	180
Reservoir Average Pressure (MPa)	-	12.5	-
Heat-Electricity Conversion Factor (-)	0.02	0.065	0.11
Plant Life (year)	-	30	-
Load Factor (-)	-	0.85	-
Abandonment Temperature (^{o}C)	-	80	-

Source: JICA study team

Fig. 3-2.125 Probability distribution of the geothermal potential for Iriba field

3) Discussion of estimated geothermal resource potential in Rwanda

Using the volumetric method and applying a Monte Carlo method, the amount of geothermal resource potential stored in each geothermal field was estimated. The geothermal resource potential calculated using the Monte Carlo method is represented by a probability distribution.

As a result of the calculation, the total geothermal resource potential of the five fields was estimated to be about 47.3 MWe at the 80% confidence level, and 89.5 MWe at the 50% confidence level. Kinigi was evaluated to be the field with highest priority for detailed investigation and development among the five fields because an obvious low-resistivity structure was detected. The geothermal resource potential of the Bugarama field, also characterized by a low-resistivity structure, was estimated to be higher than that of Gisenyi, Karago and Iriba. The geothermal resource potential of Karago, Iriba and Gisenyi was estimated to be in the range of 1.9MWe and 3.7MWe for each field at the 80% confidence level.

Each parameter used for estimation of the geothermal resource potential in so far as possible was set based on the data collected and analyzed. However, since exploratory wells drilled in the Karisimbi field showed low temperatures right down to depth, and no wells have yet been drilled in the other fields, it was difficult to evaluate the geothermal temperature structure in the deeper zones. Therefore, the geothermal reservoir temperature for the purposes of the resource potential calculation was set based on the assumption that the geothermal fluid stored at depth has a temperature of about 200 ^{o}C.

Accordingly, in order to validate the parameter values used for estimation of the geothermal resource potential and to improve evaluation accuracy, the drilling of exploratory wells to obtain detailed information concerning the geothermal structure (temperature and geological structures) will be indispensable in the near future.

4) Evaluation of productivity of geothermal well

To define the mass output from one standard production well in each field, the wellbore simulator “WELLFLOW” (developed by West JEC in conjunction with Kyushu Univbersity) was used. The main input parameters for the simulator were the depth of the feed point, reservoir temperature, reservoir pressure, and formation permeability (known as the “kh value”).

The depth of feed point is assumed to be 3,000 m in Kinigi, 2,000 m in Bugarama respectively, depending on the conceptual model of each field. The assumed reservoir temperature were set as 220 ^{o}C and 230^{o}C in Kinigi and 210^{o}C and 220^{o}C in Bugarama, respectively, which was used for the resource potential evaluation. In Kinigi, the reservoir pressure was set based on water level in exploratory wells in Karisimbi (at depth of 600 m). The reservoir pressure in Bugarama was set two case assumed by that the water level are at depths of 300m and 600m. The minimum and maximum kh value were set to be 5 darcy-m and 10.0 darcy-m, respectively, Using these condition, the average mass production for a well in each field were calculated. In the calculation, specification of binary cycle type plant manufactured by Fuji Electric are referred (the wellhead pressure: 3.0 bar, steam flow: 21.6 t/h, brine flow: 147.6 t/h). The calculated amount of steam and separated brine at 3 bar are summarized in Table

3-2.25.

Obtained results of steam in Kinigi and Bugarama (at condition of water level as 300 m) are almost same value. Calculated average mass production is double value of required amount of steam for 2,000kW. Therefore, output from one well is estimated as consistent with about 4,000kW.

Table 3-2.25 Summary of calculated mass output per well in Kinigi and Bugarama fields

Field Name	Water level (m)	Steam (t/h)	Brine (t/h)
Kinigi	600	34.0 - 56.5	152.1 - 219.1
Bugarama	300	37.4 - 63.7	194.7 - 287.3
	600	20.9 - 40.8	109.2 - 184.0

Source: JICA study team (created in March 2015)

3.3. Formulation of Geothermal Development Plan

3.3.1 Prioritization of the Development of Geothermal Fields

Prospective areas for geothermal power development in Rwanda were selected on the basis of temperatures expected from the chemistry of thermal water, geological and geophysical information and the present state of exploration of each field. Based on a review of the geothermal resource characteristics and natural/social issues, the JICA study team prioritized the fields for geothermal exploration.

Some technical tasks in the assessment of the geothermal resource remain because an exploitable geothermal reservoir has not been confirmed by drilling in all geothermal fields in Rwanda. Data presently available for Kinigi and Bugarama fields are not sufficient to evaluate the geothermal resource, and the presence of a geothermal reservoir adequate for power generation has not yet been confirmed. Thus, prioritization in this study aims to select the highest priority fields where further exploration activity should be conducted.

In the prioritization, several factors that are important for future geothermal power development and also for the execution of additional detailed surface geoscientific study were chosen, considering the current situation of geothermal development and resource potential in Rwanda (Table 3-3.1). The items evaluated include resource potential, topography, accessibility and protected areas.

Table 3-3.1 Summary of geothermal resources, natural/social environmental constraints and topography/accessibility in the five fields

Field Name	Altitude (m. a.s.l.)	Base camp (hours to the site)	Site Condition	Topography	Natural/Social and Environmental Constraints	Hot Spring		Geological structures controlling geothermal activity	Heat source of geothermal system	Host rock of reservoir	Possibility of existence of geothermal reservoir	Estimated reservoir temperature	Resource Potential	
						Tmax	Clmax						at 80% Confidence Level (MWe)	at 50% Confidence Level (MWe)
Kinigi	2,576 m (at the proposed drilling site No.1)	30 minutes from Ruhengeri city by car (20 km). 5 km to the site, unpaved road	Few residents	Flat location and gentle slope	Close to the Volcanoes National Park. Following constraints are arised: 1) resettlement of residents 2) compensation of cultivated area	N/A	N/A	NNW-SSE trending faults inferred from 3D MT inversion analysis	Related with Quaternary volcanic activity	Proterozoic basement	Although uncertainly of presence geothermal reservoir remains, there is a possibility of that geothermal reservoir extent in and around low resistivity zone detected at a depth of 2,000 m and deeper and along resistivity discontinuity R2 and R3	Assumed to be around 200 oC	32.6	58.6
Bugarama	1,180 m (at hot spring site)	50 minutes from Cyangugu city by car (15 km). From Kibangiro town to the site, unpaved road	No resident. Hot spring is located close to cement factory. Bath use of the hot spring	Flat location. Hot spring is located at topographic boundary of graben (flat) and steep slope of the mountain	-	52 oC	127 mg/L	N-S to NE-SW trending faults bounds westrern margin of Bugarama graben (gravity lineaments G1, G2 and G3) and NW-SE trending fault (gravity lineament G4 etc.)	Conductive heat of the magmatic materials situated at deeper part of the crust, or conductive heat of intrusion rocks.	Tertiary basaltic rocks and Proterozoic basement	There is uncertainly whether geothermal reservoir at deeper depth exist or not, Cl concentration in hot spring water suggests that a possibility of presence of parental fluid at deeper depth.	Shallow aquifer: 63 oC Parental fluid: > 63oC	6.6	15.1
Gisenyi	1,470 m (at hot spring site)	25 minutes from Gisenyi city by car (6 km).	Hot spring is close to residensial area (distance: 100m) Bath use of the hot spring	High relief topography at the coast of Kivu lake	-	73 oC	230 mg/L	NW-SE trending faults inferred from topographic lineaments	Related with Quaternary volcanic activity in and around Virunga volcanic region	Proterozoic basement	There is uncertainly whether geothermal reservoir exist or not, Cl concentration suggests a possibility of presence of parental fluid at deeper depth	Shallow aquifer: 80 oC Parental fluid: > 80oC	1.9	3.7
Karago	2,278 m (at hot spring site)	1 hour from Gisenyi city by car. 30 minutes on foot to the hot spring from parking point.	Hot spring is located valley floor close to the Karago lake.	High relief topography	-	73.2 oC	79.3 mg/L	NW-SE trending faults inferred from topographic lineaments	High geothermal gradient, or conductive heat of the magmatic, or conductive heat of intrusion rocks	Proterozoic basement (granite)	There is uncertainly whether geothermal reservoir exist or not, Cl concentration suggests a possibility of presence of parental fluid at deeper depth	Shallow aquifer: 81 oC Parental fluid: > 81 oC	2.5	4.9
Iriba	1,961 m (at spring site)	30 minutes from Gisenyi city by car. 30 minutes on foot to the spring from parking point.	Spring is located valley floor	Moderate or relatively high relief topography	-	22.0 oC	320 mg/L	NNW-SSE trending faults inferred from topographic lineaments	Related with Quaternary volcanic activity, such as Gikombe crater	Proterozoic basement	There is uncertainly whether geothermal reservoir exist or not, Cl concentration suggests a possibility of presence of parental fluid at deeper depth	Shallow aquifer: 79 oC Parental fluid: > 79oC	3.7	7.2

Source: JICA study team (created in March 2015)

For prioritization, we evaluate the criteria for each of the respective evaluation items. The criteria for ranking are shown in Table 3-3.2. At the current stage of exploration, the highest emphasis in prioritizing geothermal fields for future exploration activity was placed on the geothermal resource potential in each geothermal field. The second highest emphasis was given to the progress of geothermal exploration and topographic conditions, considering not only the future development itself but also the field work in the exploration stage.

The results of the ranking are presented in Table 3-3.2. In light of the results of the ranking and given the present status of each field among the 5 fields described in the sections above, the Kinigi and Bugarama fields can be regarded as the most prospective ones (highest priority). The remaining 3 fields are of secondary priority.

Table 3-3.2 Criteria of evaluation and results of evaluation

Evaluation Item		Rank	Criteria	Kinigi	Bugarama	Gisenyi	Karago	Iriba
Geothermal resource	Estimated Resource Potential	A	at 80% Confidence Level : > 10 MWe	A	B	C	C	C
		B	at 80% Confidence Level : > 5 MWe					
		C	at 80% Confidence Level : < 5 MWe					
	Hot spring	A	Temp.: > 50 oC and Cl max: > 100 mg/l	C	A	A	B	B
		B	Temp.: > 50 oC or Cl max: > 100 mg/l					
		C	Temp.: < 50 oC and/or Cl max: < 100 mg/l					
	Heat source	A	Presence of Quaternary volcanoes in and around the field	A	C	A	C	A
		B	-					
		C	Absense of Quaternary volcanoes in and around the field					
	Geological structures controlling geothermal activity	A	Detected by geological and geophycial study	B	A	B	B	B
		B	Detected by geological study or geophysical study					
		C	unknown					
Topography		A	Flat or small valley with calm slope	A	B	C	C	B
		B	Partially steep slope					
		C	Deep valley with steep slope					
Protected area etc.		A	None	B	A	A	A	A
		B	Within the non-strictly protected area / near the strictly protected area					
		C	Very Close to the strictly protected area					
Exploration Stage		A	Stage Phase 2: MT survey done	A	B	C	C	C
		B	Stage Phase 2: Gravity or MT survey done					
		C	No gravity and MT survey done or partly covered					

Source: JICA study team (created in March 2015)

3.3.2 Formulation of Geothermal Development Plan

(1) Possible geothermal power development in Rwanda

Even in the Kinigi and Bugarama fields, the presence of a geothermal reservoir adequate for power generation has not yet been confirmed, so the resource development risk is thought to be relatively high. However, a tentative geothermal development plan is formulated as a reference for Kinigi and Bugarama fields, which are ranked as having the highest priority for exploration activity. It should be noted that the details of geothermal power plant projects will be formulated in a feasibility study, which will be carried out later on the basis of the geothermal resource study (Phase 3).

The development scale, namely the output capacity of the geothermal power plant for Kinigi and Bugarama fields, is proposed based on the estimated resource potential. A binary cycle type plant is considered optimal in both fields, considering the resource potential and its characteristics. The required number of geothermal wells is estimated according to the results of evaluation of well productivity. The main specifications for possible power development in the fields are shown in Table 3-3.3.

Table 3-3.3 Main specifications for possible power development in the promising fields

Field Name	Resource Potential P80 (MWe)	Plant Capacity (MWe)	Power Unit	Number of Production Wells	Number of Reinjection Wells
Kinigi	32.6	20	5MW x 4	5	3
Bugarama	6.6	5	5MW x 1	2	1
Total	39.2	25	-	-	-

Source: JICA study team (created in March 2015)

The power output capacity is assumed based on the resource potential at an 80% confidence level with allowance of some margin. The number of required production wells in each project (excluding make-up wells drilled during the plant operation period) is estimated based on the following assumed conditions:

- Mass output from one well in each field: 4,000kW

In estimating the required number of wells, it is thought that 2 exploratory wells will be utilized for the operation (one a production well, the other a reinjection well) in each field. The number of reinjection wells required for each project is estimated based on the number of production wells required, the amount of produced brine, which depends on the brine productivity of the production wells, and the estimated reinjection capacity per well (300 t/h).

According to the conceptual model of the geothermal system in each promising field, the Kinigi field will require wells to be drilled to a depth of 3,000 m for production wells and 1,500m for reinjection wells. In Bugarama field, both production and reinjection wells will need to be 2,000-2,500 m deep.

(2) **Development plan and schedule**

1) Process of geothermal power development

As development risk (leading to an unfavorable result) is not negligible in steam field development, a phased process of steam field development is usually adopted. One typical process of steam field development is a development process composed of the following four stages:

1st Stage	Exploration Stage
2nd Stage	Feasibility Study Stage
3rd Stage	Project Implementation Stage
4th Stage	Operation and Maintenance Stage

The goal of the First Stage (Exploration Stage) is to confirm the presence of a geothermal resource, to identify the chemical and physical properties of the geothermal resource and to estimate the resource capacity (optimum output to maintain sustainable operation). The exploration stage is subdivided into the following three phases:

Phase 1 Regional Exploration Phase, to select a prospective area (or areas)

Phase 2 Detailed Exploration Phase, to clarify the presence of a geothermal resource, to identify the geothermal structure and to select drilling targets

Phase 3 Resource Evaluation Phase, to identify the chemical and physical properties of a targeted geothermal reservoir by well-drilling and to evaluate resource capacity

In Phase 1 (Regional Exploration Phase), exploration is carried out over the whole of an objective field to select a prospective area (highest priority area to study in detail). In Phase 2 (Detailed Exploration Phase), detailed exploration of sufficient accuracy to permit selection of drilling targets is carried out. In Phase 3 (Resource Evaluation Phase), several exploratory wells (more than three wells is desirable) are drilled to tap the selected targets, and production (discharge) tests are carried out. Moreover, resource evaluation to estimate the optimum sustainable geothermal power generation output is conducted through reservoir simulation using a 3-D numerical model based on the results of the production tests and exploration.

A conceptual model of geothermal resources is usually constructed at the end of each phase, to draw up a revised strategy for the development. In this model, information about the distribution of geological elements controlling geothermal activity, the extent of high-temperature anomalies and the flow pattern of geothermal fluid, which are sometimes referred to as "geothermal structure", are represented in a way that is easy to understand. There are many kinds of geothermal exploration technologies contributing to this estimation of geothermal structure for modeling, but no single technology is sufficient on its own.

Therefore, a variety of exploration technologies must be applied in order to prepare an adequate model for geothermal development. However, the best combination of technologies to be applied depends on the particular field, as an objective field has unique geothermal resource characteristics and surrounding geological conditions differing from other fields. Although geological, geochemical and MT surveying are rather commonly conducted, consideration of the suitable combination of technologies for the objective field is required at the planning stage. Furthermore, comprehensive analysis and integrated interpretation of the obtained geothermal exploration results will be required.

The work of Phases 1 and 2 in private geothermal development can be undertaken either by the Government or by the private sector. Phase 2 work is of particular importance and is believed to significantly affect the outcome of the geothermal power development project.

In the Second Stage (Feasibility Study Stage), the conceptual design of the future geothermal power station is elaborated, based on estimated optimum output and steam quality as clarified by production tests. At this stage, economic and financial evaluation of the proposed geothermal project is also carried out. It is desirable that a full environmental assessment, including the power plant and associated transmission line, should be completed before the inception of the following stage (Project Implementation Stage).

In the Third Stage (Project Implementation Stage), a detailed design of the power plant and FCRS (Fluid Collection and Reinjection System) is prepared. If the power plant, including pipelines, is constructed using a competitive tendering system to select an EPC contractor, bidding documents for procurement are prepared based on information in the detailed design. Then, the power plant and FCRS are constructed. During construction, the necessary number of additional production and reinjection wells to meet the power plant operation requirements are constructed. Those wells are also subject to long term production tests, following which a review of the geothermal reservoir simulation is conducted.

In the Fourth Stage (Operation and Maintenance Stage), ongoing refinement of the conceptual model on the basis of data accumulated through steam field operation will be required to maintain sustainable steam production (reservoir management).

Based on this phased process of the development, a development plan and schedule have been formulated for both Kinigi and Bugarama fields.

2) Development plan and schedule for Kinigi and Bugarama fields

As mentioned above, the resource development risk is thought to be relatively high in both Kinigi and Bugarama fields. In order to reduce this fatal risk to the economical development of geothermal power, it is indispensable to further confirm the structure and extent of the geothermal reservoir, the physical and chemical characteristics of the geothermal fluids and so on.

Considering the present status of both fields described in the previous section, the geoscientific studies and surveys necessary for a geothermal resource feasibility study including exploratory well-drilling can be summarized as follows.

Phase 2: Surface Study

- Supplemental geological and geochemical study
- Geophysical survey
- Resource assessment/planning

Phase 3: Exploratory well drilling/testing and evaluation

- Field development, access road, mobilization
- Exploratory well drilling & testing
- Production test
- Resource assessment/planning/basic design etc.

The main objectives of this Resource Feasibility Study are as follows:

- To reduce geothermal resource development risks
- To confirm the presence of the geothermal resource (geothermal fluid reservoir)
- To make clear the resource potential and characteristics affecting power generation

Project Feasibility Study

On the basis of the optimum resource development plan determined from the results of resource studies, a basic design of the power plant can be drafted. In general, on the basis of the results of economic and financial analysis at this stage, the economic and financial viability of the project will be judged. After fundamental decisions on the geothermal power development project are taken, the following stages of work, such as the detailed design of the power plant, additional well drilling, and construction work for the fluid collection and reinjection system, will be undertaken. After the submission of feasibility study report, approval and permissions required for power plant construction will be obtained.

In the Construction Stage, the consultant will first be selected, and then procurement of a well drilling/testing contractor will proceed in parallel. Commencement of commercial operation will follow immediately on the completion of the project.

The details of both Kinigi and Bugarama geothermal power plant projects will be formulated in a feasibility study, which will be carried out on the basis of the geothermal resource study (Phase 3).

For a geothermal power plant project, the development work items listed below will need to be completed by the commencement of power plant operation.

<u>Construction Stage:</u>

- Engineering Services by Consultant
- Steam Field Development
- Fluid Collection and Reinjection System Construction
- Power Plant Construction
- Transmission Line and Switchyard Construction

Geothermal power development plans for Kinigi and Bugarama fields are shown in Tables 3-3.4 to 3-3.7. Development plans are shown for two different cases: using an ODA Yen Loan or using other financing.

Table 3-3.4 Kinigi Geothermal Power Plant Construction Project Overall Schedule: 5MW x 4 units (as Yen Loan Project)

Activity	Duration (month)
Exploration Stage	
Phase 2	12
Engineering Services by Consultant	12
Surface Study	11
Judgement to Progress Next Stage (Phase 3)	
Environmental Study, Acquisition of Permission etc.	2
Finance Procurement of Phase 3	3
Phase 3	33
Engineering Services by Consultant	33
Resource FS in Kinigi	32
Exploratory Well Test Study/Evaluation	32
Judgement to Progress Next Stage (Exploitation)	
Environmental Impact Asssessment, Feasibility Study	
Environmental Impact Asssessment, Feasibility Study	12
Appraisal Mission, E/N, L/A	
Appraisal Mission, E/N, L/A	12
Construction Stage	
Procurement Engineering Consultant	9
Procurement Engineering Consultant	9
Engineering Services by Consultant	55
Engineering Services by Consultant	55
Procurement of Contractor	17
Procurement of Contractor	17
Steam Field Development (for 20 MW)	22
Survey, Design	4
Field Development, Rig Mobilization	6
Drilling & Testing (5 production wells, 3 reinjection wells)	16
Fluid Collection and Reinjection System (5MW x 4)	23
Survey, Basic design	6
Design, Fabrication & Delivery, Construction/Installation	20
Power Plant (5MW x 4)	26
Survey, Basic design	6
Design, Manufacturing, Delivery, Construction/Installation	20
Commissioning	3
Transmission Line and Switchyard	20
Survey, Basic design	6
Design, Manufacturing, Delivery, Construction/Installation	17
Post Construction Stage	12
Warranty Period (inc. Operation and Training)	12

Source: JICA study team (created in March 2015)

Table 3-3.5 Kinigi Geothermal Power Plant Construction Project Overall Schedule: 5MW x 4 units (using other financing)

Activity	Duration (month)
Exploration Stage	
Phase 2	12
Engineering Services by Consultant	12
Surface Study	11
Judgement to Progress Next Stage (Phase 3)	
Environmental Study, Acquisition of Permission etc.	2
Finance Procurement of Phase 3	3
Phase 3	33
Engineering Services by Consultant	33
Resource FS in Kinigi	32
Exploratory Well Test Study/Evaluation	32
Judgement to Progress Next Stage (Project FS)	
Environmental Impact Asssessment, Feasibility Study	
Environmental Impact Asssessment, Feasibility Study	12
Judgement to Progress Next Stage (Exploitation)	
Finance Procurement of Exploitation	12
Construction Stage	
Procurement Engineering Consultant	6
Procurement Engineering Consultant	6
Engineering Services by Consultant	53
Engineering Services by Consultant	53
Procurement of Contractor	15
Procurement of Contractor	15
Steam Field Development (for 20 MW)	22
Survey, Design	4
Field Development, Rig Mobilization	6
Drilling & Testing (5 production wells, 3 reinjection wells)	16
Fluid Collection and Reinjection System (5MW x 4)	23
Survey, Basic design	6
Design, Fabrication & Delivery, Construction/Installation	20
Power Plant (5MW x 4)	26
Survey, Basic design	6
Design, Manufacturing, Delivery, Construction/Installation	20
Commissioning	3
Transmission Line and Switchyard	20
Survey, Basic design	6
Design, Manufacturing, Delivery, Construction/Installation	17
Post Construction Stage	12
Warranty Period (inc. Operation and Training)	12

Source: JICA study team (created in March 2015)

Table 3-3.6 Bugarama Geothermal Power Plant Construction Project Overall Schedule: 5MW x 1 unit (as Yen Loan Project)

Activity	Duration (month)
Exploration Stage	
Phase 2	12
Engineering Services by Consultant	12
Surface Study	11
Judgement to Progress Next Stage (Phase 3)	
Environmental Study, Acquisition of Permission etc.	2
Finance Procurement of Phase 3	3
Phase 3	30
Engineering Services by Consultant	30
Resource FS in Bugarama	29
Exploratory Well Test Study/Evaluation	29
Judgement to Progress Next Stage (Project FS)	
Environmental Impact Asssessment, Feasibility Study	
Environmental Impact Asssessment, Feasibility Study	12
Appraisal Mission, E/N, L/A	
Appraisal Mission, E/N, L/A	12
Construction Stage	
Procurement Engineering Consultant	9
Procurement Engineering Consultant	9
Engineering Services by Consultant	45
Engineering Services by Consultant	45
Procurement of Contractor	17
Procurement of Contractor	17
Steam Field Development (for 5 MW)	10
Survey, Design	3
Field Development, Rig Mobilization	6
Drilling & Testing (1 production well, 1 reinjection well)	4
Fluid Collection and Reinjection System (5MW x 1)	9
Survey, Basic design	3
Design, Fabrication & Delivery, Construction/Installation	8
Power Plant (5MW x 1)	16
Survey, Basic design	3
Design, Manufacturing, Delivery, Construction/Installation	12
Commissioning	3
Transmission Line and Switchyard	9
Survey, Basic design	3
Design, Manufacturing, Delivery, Construction/Installation	8
Post Construction Stage	12
Warranty Period (inc. Operation and Training)	12

Source: JICA study team

Table 3-3.7 Bugarama Geothermal Power Plant Construction Project Overall Schedule: 5MW x 1 unit (using other financing)

Activity	Duration (month)
Exploration Stage	
Phase 2	12
Engineering Services by Consultant	12
Surface Study	11
Judgement to Progress Next Stage (Phase 3)	
Environmental Study, Acquisition of Permission etc.	2
Finance Procurement of Phase 3	3
Phase 3	30
Engineering Services by Consultant	30
Resource FS in Bugarama	29
Exploratory Well Test Study/Evaluation	29
Judgement to Progress Next Stage (Project FS)	
Environmental Impact Asssessment, Feasibility Study	
Environmental Impact Assessment, Feasibility Study	12
Judgement to Progress Next Stage (Exploitation)	
Finance Procurement of Exploitation	12
Construction Stage	
Procurement Engineering Consultant	6
Procurement Engineering Consultant	6
Engineering Services by Consultant	40
Engineering Services by Consultant	40
Procurement of Contractor	12
Procurement of Contractor	12
Steam Field Development (for 5 MW)	10
Survey, Design	3
Field Development, Rig Mobilization	6
Drilling & Testing (1 production well, 1 reinjection well)	4
Fluid Collection and Reinjection System (5MW x 1)	9
Survey, Basic design	3
Design, Fabrication & Delivery, Construction/Installation	8
Power Plant (5MW x 1)	16
Survey, Basic design	3
Design, Manufacturing, Delivery, Construction/Installation	12
Commissioning	3
Transmission Line and Switchyard	9
Survey, Basic design	3
Design, Manufacturing, Delivery, Construction/Installation	8
Post Construction Stage	12
Warranty Period (inc. Operation and Training)	12

Source: JICA study team

The earliest commencement of power generation will be 2023 in Bugarama field. In Kinigi field, it is assumed that about 10 years will be necessary to commencement from the selection of the consultant for “Phase 2” (using other financing).

3.3.3 Action Plan for Each Field

A geothermal power development project is a typical example of a high-risk, low-return project. It is also characterized by a relatively long lead time. In order to establish the optimum output for sustained and stable power generation for the field, the following investigative steps are necessary. First, in order to identify promising areas, a regional survey (Phase 1) is necessary. Next, a detailed survey of areas shown to be promising in the regional survey is carried out, establishing drilling targets and the extent of the geothermal resource (Phase 2). The geothermal potential of the target area is roughly estimated by applying the stored-heat or volumetric method to the survey results. The estimated geothermal potential value is set as the provisional development goal. However, this provisional estimate does not always correctly indicate the sustainable optimum power output at that point. Geothermal resource evaluation based on exploratory well drilling and production testing in the next stage (Phase 3) is required to identify the optimum sustainable power output.

As indicated above, the expected power output is usually unknown at the early stage of development study. The three stages of investigation outlined above are required to ascertain the optimal sustainable power output, and a budget is necessary for these investigations. However, a project sometimes fails, even when the investigation is carried out stage by stage. Such development risks present a barrier to private sector entry. With the exception of the Karisimbi field (which is in the stages of Phase 3), most geothermal areas in Rwanda are still in Phase 1 or Phase 2. So the initial development risks constitute a significant factor interfering with private sector participation in geothermal development projects. Some countries have introduced incentives to promote the participation of the private sector. In Japan, surveys corresponding to the Phase 1 to Phase 3 stage have been carried out by government. In other words, government surveys reduce the development risk for the private sector and facilitate its entry. Even in Indonesia, surveys corresponding to phases 1 and 2 have been carried out by government, so the risk is reduced for the private sector, and this promotes development.

In Rwanda, considering of the lack of experience in geothermal development, government-led surveys corresponding to Phase 2 and Phase 3 are very much desired to confirm the presence of geothermal reservoirs and to promote geothermal development in this country. It is recommended that support by the donors in this situation is best directed to enabling these early-stage surveys by the government or governmental agencies (REG). In addition, support for capacity-building among policy makers and/or survey staff involved in early stage development is important. Considering the present situation of Rwanda, the following projects of Phase 2 and Phase 3 are listed up here. Tables 3-3.8 to 3-3.10 show possible projects in Kinigi and Fig. 3-3.1 shows the area of proposed exploration study in Kinigi. Tables 3-3.11 to 3-3.13 show possible projects in Bugarama and Fig. 3-3.2 shows the area of proposed exploration study in Bugarama. It must be noted that personnel costs of REG are not included in cost estimates. Likely sources of funding for these projects are JICA grants, or financing from AfDB, UNEP, EU and Geothermal Risk Mitigation Fund.

Table 3-3.8 Possible projects in Kinigi (Phase 2)

Project Name	Resource Exploration Survey in Kinigi (Phase 2)		
Field	Kinigi		
Area	Kinigi		
Project Outline	To carry out supplemental surface geoscientific surveying to update the geothermal conceptual model and select drilling targets in the Kinigi field.		
Details	➢ Supplemental geological and geochemical study ➢ Gravity survey (200 stations) ➢ Supplemental MT/TEM survey ➢ Resource Assessment/Planning (Integrated analysis) ➢ Study of multi-purpose utilization		
Beneficiary	REG		
Scheme	Development Study	Category	Resource survey
Project Scale	Approx. 1 year Approx. USD 0.8 million Supplemental geological geochemical study: 0.07 million (inc. lab. analysis) Gravity survey (200 stations) : 0.35 million Supplemental MT/TEM survey: 0.35 million Resource Assessment/Planning (Integrated analysis) : 0.05 million Study of multi-purpose utilization: 0.01 million		
Remarks	Permission for work in the National Park is required. Supplemental MT/TEM survey is recommendable in case of that the survey can be done in the National Park and area in Uganda.		

Source: JICA study team (created in March 2015)

Table 3-3.9 Possible projects in Kinigi (Phase 3)

Project Name	Resource Feasibility Study in Kinigi (Phase 3)		
Field	Kinigi		
Area	Kinigi		
Project Outline	To carry out an exploration survey including drilling three (3) exploration wells in the Kinigi field to confirm presence of a geothermal reservoir and to evaluate the geothermal resource.		
Details	➢ Exploratory Well Drilling & Testing (3,000m x 2 wells, 1,500m x 1 well) ➢ Production testing ➢ Resource Assessment/Planning/basic Design etc. ➢ Study of multi-purpose utilization		
Beneficiary	REG		
Scheme	Development Study	Category	Resource survey
Project Scale	Approx. 3 years Approx. USD 26 million		
Remarks			

Source: JICA study team (created in March 2015)

Table 3-3.10 Details and schedule of proposed exploration study in Kinigi

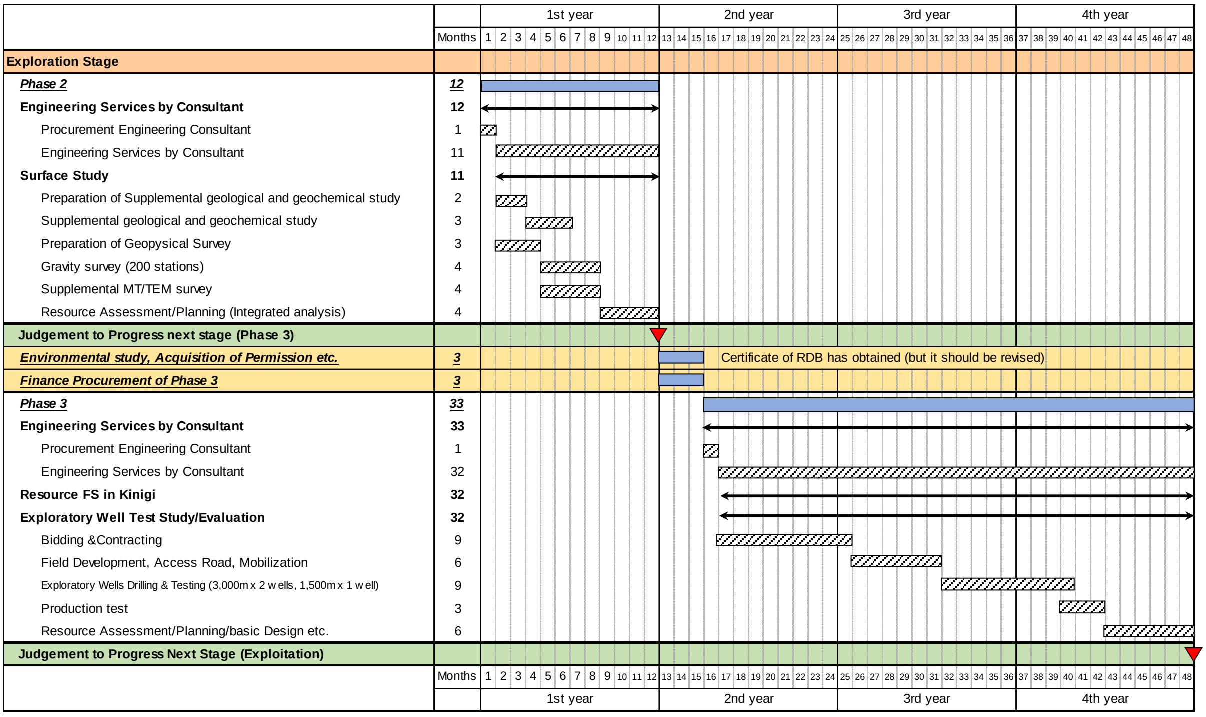

Source: JICA study team (created in March 2015)

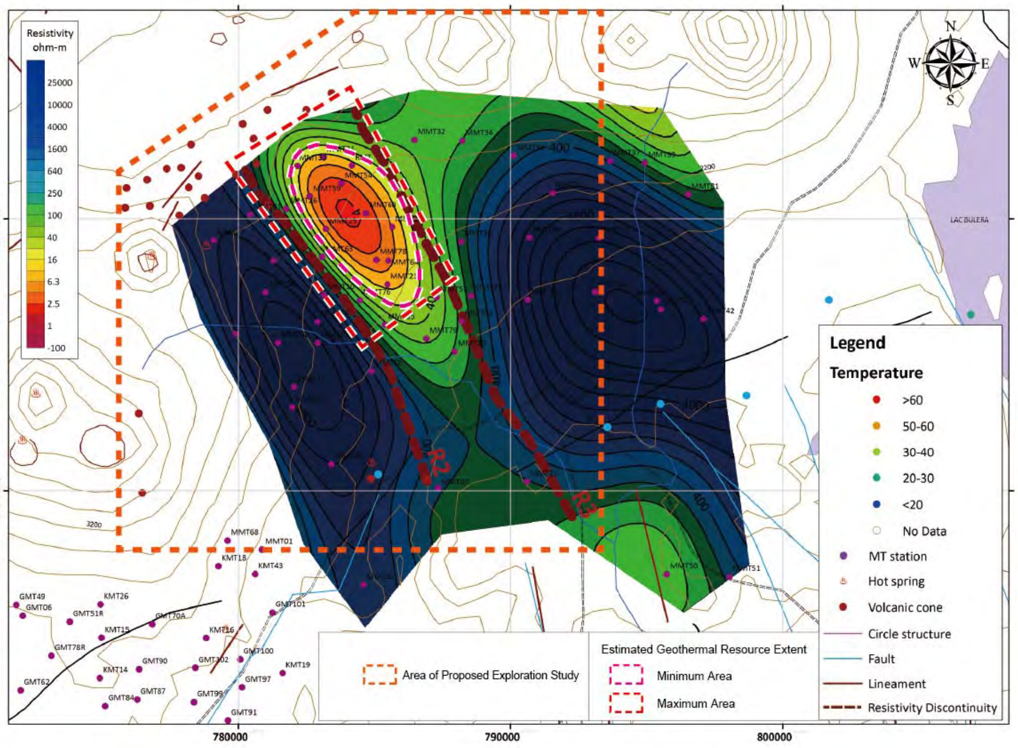

Source: JICA study team (created in March 2015)

Fig. 3-3.1 Area of proposed exploration study in Kinigi

Table 3-3.11 Possible projects in Bugarama (Phase 2)

Project Name	Resource Exploration Survey in Bugarama (Phase 2)		
Field	Bugarama		
Area	Mashyuza		
Project Outline	To carry out supplemental surface geoscientific surveying to update the geothermal conceptual model and select drilling targets in the Bugarama field.		
Details	➢ Supplemental geological and geochemical study ➢ Review of existing geophysical survey data (TEM, Magnetic etc.) ➢ Supplemental MT/TEM survey ➢ Resource Assessment/Planning (Integrated analysis) ➢ Study of multi-purpose utilization		
Beneficiary	REG		
Scheme	Development Study	Category	Resource survey
Project Scale	Approx. 1 year Approx. USD 0.5 million Supplemental geological and geochemical study: 0.07 million (inc. lab. analysis) Supplemental MT/TEM survey: 0.4 million Resource Assessment/Planning (Integrated analysis): 0.05 million Study of multi-purpose utilization: 0.01 million		
Remarks			

Source: JICA study team

Table 3-3.12 Possible projects in Bugarama (Phase 3)

Project Name	Resource Feasibility Study in Bugarama (Phase 3)		
Field	Bugarama		
Area	Bugarama		
Project Outline	To carry out an exploration survey including drilling two (2) exploration wells in the Bugarama field to confirm presence of a geothermal reservoir and to evaluate the geothermal resource.		
Details	➢ Exploratory Well Drilling & Testing (2,000-2,500 m x 2 wells) ➢ Production testing ➢ Resource Assessment/Planning/basic Design etc. ➢ Study of multi-purpose utilization		
Beneficiary	REG		
Scheme	Development Study	Category	Resource survey
Project Scale	Approx. 2.5 years Approx. USD 18 million		
Remarks			

Source: JICA study team

Table 3-3.13 Details and schedule of proposed exploration study in Bugarama

	Months	1st year (1–12)	2nd year (13–24)	3rd year (25–36)	4th year (37–48)
Exploration Stage					
Phase 2	**12**				
Engineering Services by Consultant	**12**				
Procurement Engineering Consultant	1				
Engineering Services by Consultant	11				
Surface Study	**11**				
Preparation of Supplemental geological and geochemical study	2				
Supplemental geological and geochemical study	3				
Preparation of Geopysical Survey	3				
MT/TEM survey (50-70 stations)	4				
Resource Assessment/Planning (Integrated analysis)	4				
Judgement to Progress next stage (Phase 3)					
Environmental study, Acquisition of Permission etc.	**3**			Certificate from RDB	
Finance Procurement of Phase 3	**3**				
Phase 3	**30**				
Engineering Services by Consultant	**30**				
Procurement Engineering Consultant	1				
Engineering Services by Consultant	29				
Resource FS in Bugarama	**29**				
Exploratory Well Test Study/Evaluation	**29**				
Bidding &Contracting	9				
Field Development, Access Road, Mobilization	6				
Exploratory Wells Drilling & Testing (2,000-2,500m x 2 wells)	6				
Production test	3				
Resource Assessment/Planning/basic Design etc.	6				
Judgement to Progress Next Stage (Exploitation)					

Source: JICA study team

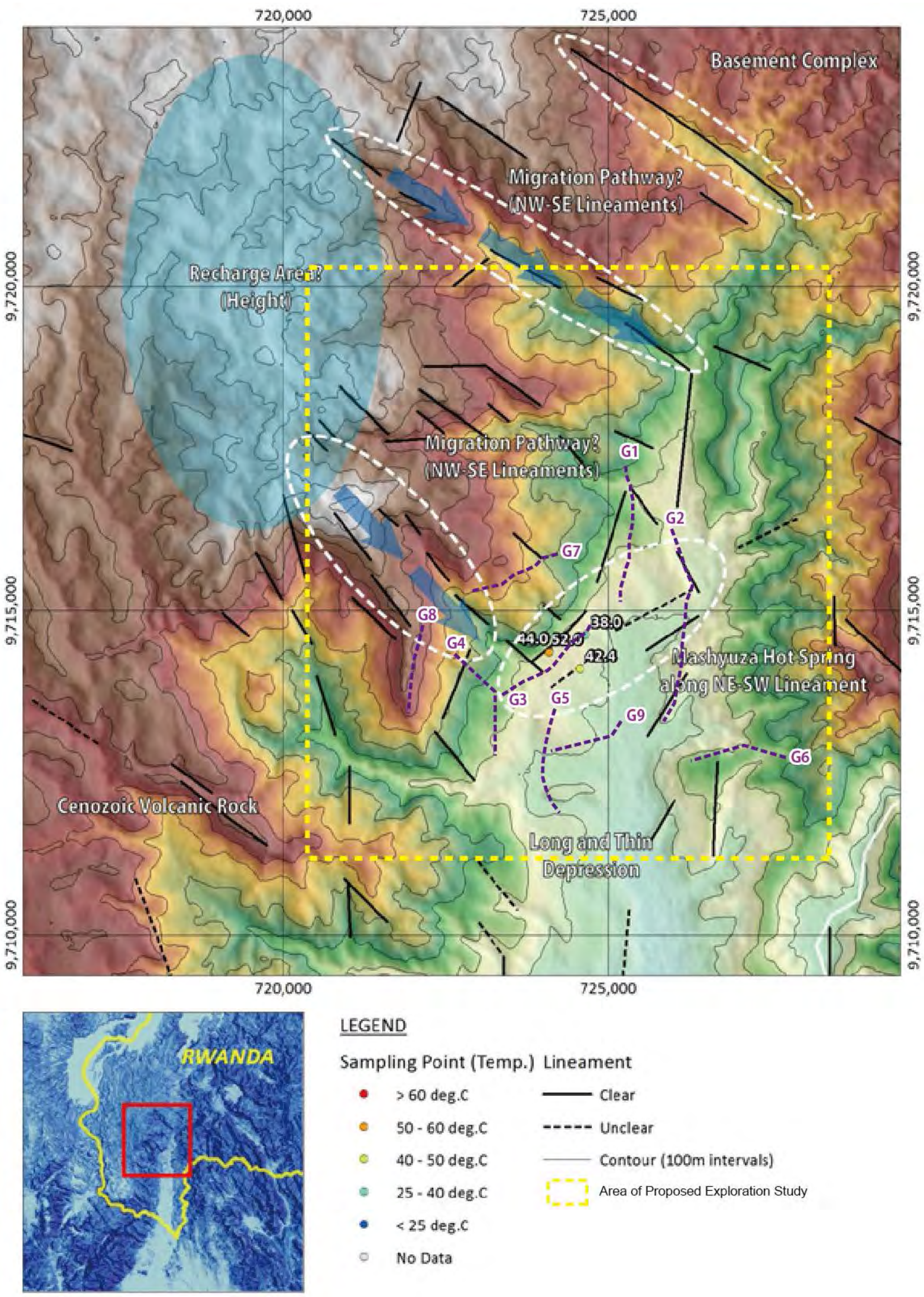

Source: JICA study team

Fig. 3-3.2 Area of proposed exploration study in Bugarama

The fields of second highest priority for exploration are Gisenyi, Karago and Iriba. These fields can be regarded as being in the Detailed Exploration Phase (Phase 2). As mentioned above, the risk for resource development is thought to be relatively high. Considering the present status of these 3 fields, it is impossible to discuss detailed development planning at present. Therefore, only exploration activity (Phase 2) including detailed geophysical surveying is planned. This Phase 2 exploration activity is required before a judgement can be made to progress to the next stage (Phase 3) and to ascertain the possible presence of an exploitable reservoir prior to resource development. Taking into consideration the above-mentioned field exploration situations as well as identified and estimated temperature conditions, exploration activity is proposed for each field and summarized in tables 3-3.14 to 3-3.17. Figure 3-3.3 shows areas of proposed exploration study in Karago field, Gisenyi hot spring area and Iriba-Mufumba cone area. Bize hot spring area in Bugarama field is considered to be Phase 1. Phase 1 study in Bize is shown in Table 3-3.17. Location of Bize is shown in Fig. 3-2.10.

Table 3-3.14 Possible projects in Karago (Phase 2)

Project Name	Resource Exploration Survey in Karago (Phase 2)		
Field	Karisimbi		
Area	Karago		
Project Outline	To carry out supplemental surface geoscientific surveying to update the geothermal conceptual model, for selection of drilling targets in the Karago field.		
Details	➢ Supplemental geological and geochemical study ➢ Supplemental MT/TEM survey (40-50 stations) ➢ Resource Assessment/Planning (Integrated analysis)		
Beneficiary	REG		
Scheme	Development Study	Category	Resource survey
Project Scale	Approx. 1 year Approx. USD 0.5 million		
Remarks			

Source: JICA study team

Table 3-3.15 Possible projects in Gisenyi hot spring area

Project Name	Study of Multi Purpose Utilization in Gisenyi hot spring area		
Field	Gisenyi		
Area	Gisenyi hot spring		
Project Outline	To carry out supplemental geological and geochemical surveying to update the geothermal conceptual model, and study of multi-purpose utilization in the Gisenyi hot spring area.		
Details	➢ Supplemental geological and geochemical study ➢ Resource Assessment/Planning (Integrated analysis) ➢ Study of multi-purpose utilization		
Beneficiary	REG		
Scheme	Development Study	Category	Resource survey
Project Scale	Approx. 1 year Approx. USD 0.3 million		
Remarks			

Source: JICA study team

Table 3-3.16 Possible projects in Iriba-Mufumba cone area (Phase 2)

Project Name	Resource Exploration Survey in Iriba-Mufumba cone area (Phase 2)		
Field	Gisenyi		
Area	Iriba-Mufumba cone area		
Project Outline	To carry out supplemental surface geoscientific surveying to update the geothermal conceptual model and to detect the prospective area		
Details	➢ Supplemental geological and geochemical study ➢ Regional gravity survey, covering Iriba and Mufumba cone area (200 stations with spatial interval of 1-2 km) ➢ Integrated analysis and selection of prospective area ➢ Formulation of detailed surface study in detected prospective area		
Beneficiary	REG		
Scheme	Development Study	Category	Resource survey
Project Scale	Approx. 1 year Approx. USD 0.5 million		
Remarks	Surface study including TEM and Magnetic will be conducted financed by EU. Iriba is not included.		

Source: JICA study team

Table 3-3.17 Possible project in Bize hot spring area (Phase 1)

Project Name	Resource Exploration Survey in Bize hot spring area (Phase 1)		
Prospect	Bugarama		
Field	Bize		
Project Outline	To carry out surface geoscientific survey to construct preliminary geothermal conceptual model and to detect prospective area		
Contents	➢ Supplemental geological and geochemical study ➢ Construction of preliminary geothermal conceptual model ➢ Planning of detailed geoscientific survey including geophysical survey		
Beneficiary	REG		
Scheme	Development Study	Category	Resource survey
Project Scale	Approx. 1 year Approx. USD 0.5 million		
Remarks			

Source: JICA study team

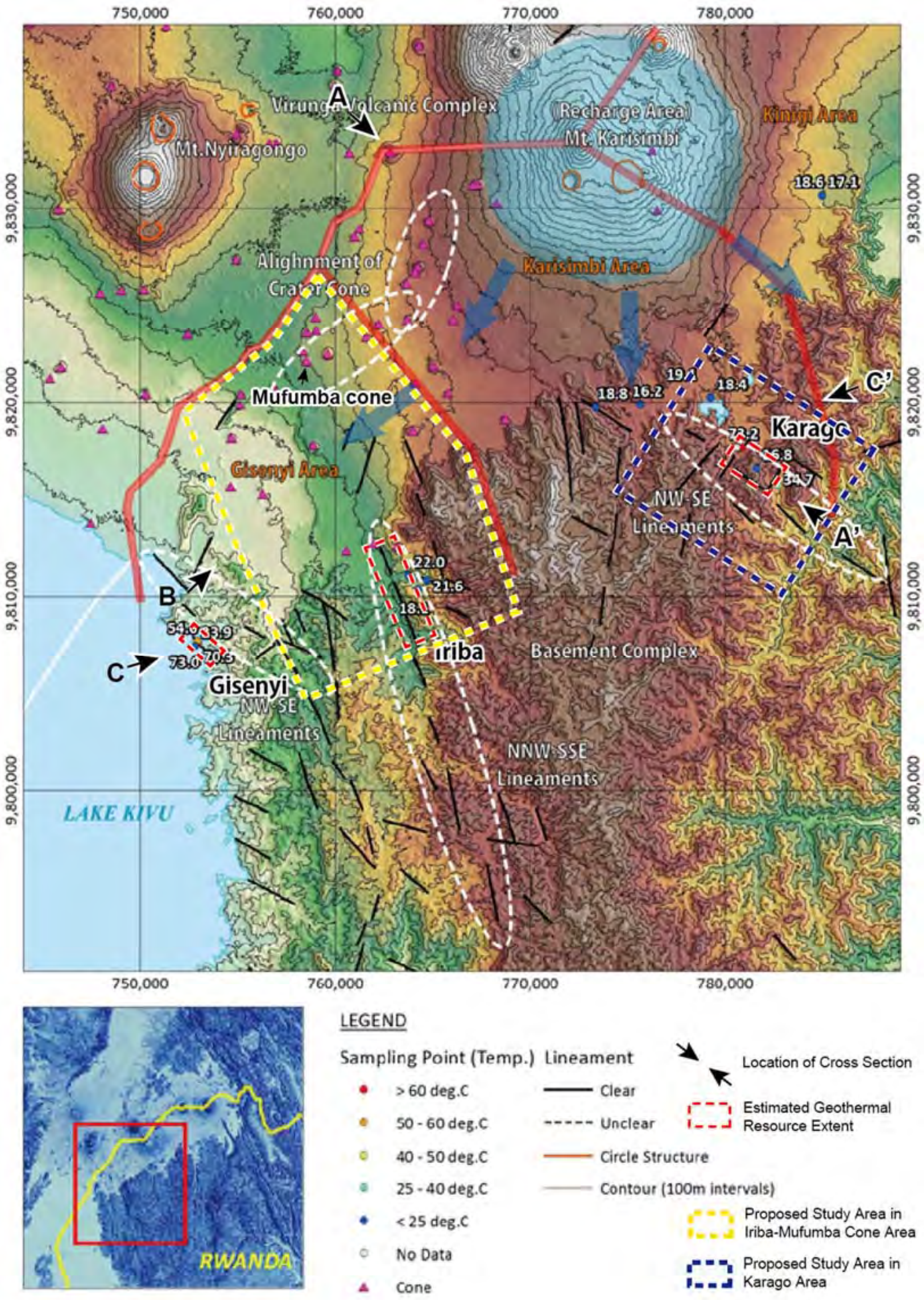

Source: JICA study team

Fig. 3-3.3 Areas of proposed exploration study in Karago field, Gisenyi hot spring area and Iriba-Mufumba cone area.

The implementation body for geothermal development in the governmental organization of Rwanda is the Geothermal Development Unit of REG/EDCL. Table 3-3.18 shows a list of staff of GDU as of February 2016. As mentioned above, the experience of experts in the governmental organization

(GDU) is insufficient in the area of resource development technologies including geothermal well-drilling and geothermal power plant technology, and capacity building in this area is barely existent. Therefore, technical advisory services by consultants and/or researchers who have knowledge of and experience in geothermal development are critical to the implementation of the exploration activities. Capacity building in GDU is expected to result from the collaborative work between the staff of GDU and consultants and/or researchers on exploration activities. Figure 3-3.4 shows an example of an implementation system for exploration activity. In strengthening the capacity of GDU, the following issues should be considered.

- Capacity building in geothermal exploration technology (geology, geophysics, geochemistry, reservoir engineering and environmental study) through geothermal exploration activity and through participation in training courses such as those held in Japan, New Zealand, Iceland, Kenya. Practical training through collaborative study is necessary.
- Management of geothermal resource and development database
- Capacity building and supervision of project planning and management including procurement procedure, financial aspects etc.
- Enrichment of basic survey equipment and software for geothermal investigation and analysis

Table 3-3.18 Staff of Geothermal Development Unit of REG/EDCL

(as of Feb 2016)

Assignment	Number of Staff
Head	1
Geochemist	2
Geophysicist	2
Reservoir Engineer	1
Drilling Engineer	1
Multi-purpose utilization	1

Source: JICA study team

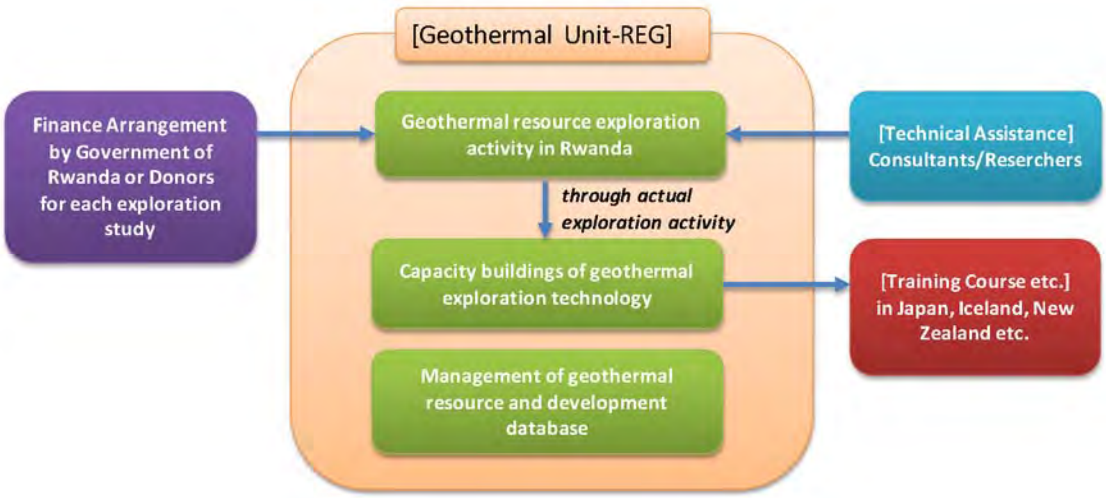

Source: JICA study team

Fig. 3-3.4 An example of an implementation system for exploration activity

3.3.4 Construction of a Geothermal Development Database

Collection and analysis of data related to the geothermal fields of Rwanda was carried out in this study. The geothermal development database was installed and introduced to REG in the 4th period of work in Rwanda to store and manage data and information related to geothermal development in Rwanda. The electricity development database is newly constructed in this study. The constructed electricity development database (POWER DB) can be utilized as a geothermal development database by adding other information about geothermal development. The database has been created using the MS-Access relational database system. In a relational database different categories of data and information are stored in a manner which allows for efficient and flexible data storage, with minimal duplication and considerable flexibility in data retrieval. The specifications and operation of the database are described in 2.7.1.

The geothermal development database not only focuses on specific geothermal fields to provide detailed information concerning the fields, but also provides general information on geothermal development in Rwanda and basic information for each geothermal field in the country. The geothermal development database can be utilized to search and update the necessary information regarding geothermal development in Rwanda. The database is expected to assist in accelerating geothermal development in Rwanda. The database was introduced and installed to the counterparts. It was confirmed that the database works well in the system in the counterparts.

3.4. Multi-Purpose Utilization of Geothermal Resources

3.4.1 Outline of Multipurpose Utilization of Geothermal Resources

Possible uses of geothermal resources at different temperatures are shown in Fig.3-4.1. In addition to their use in conventional and binary power plants, geothermal resources are used for spa treatment, swimming pools, snow melting, greenhouses, air conditioning, etc.

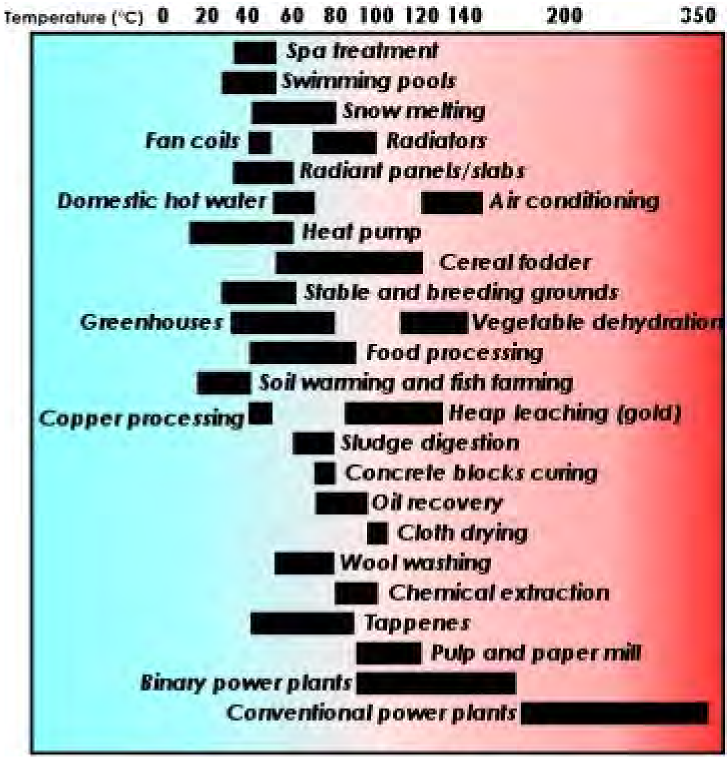

Source: http://www.unionegeotermica.it/What_is_geothermal_en.html

Fig. 3-4.1 Possible uses of geothermal resources at different temperatures

Figure. 3-4.2 below shows the changes in the amount of direct use of geothermal resources from 1995 to 2010. One direct use of geothermal resources, the heat pump, a system of cooling/heating utilizing geothermal heat maintained at constant temperature throughout the year, is spreading rapidly. Geothermal resources are also used for heating, spas and hot baths, agricultural greenhouses, cultivation, drying of crops, industry, air conditioning, snow melting, etc.

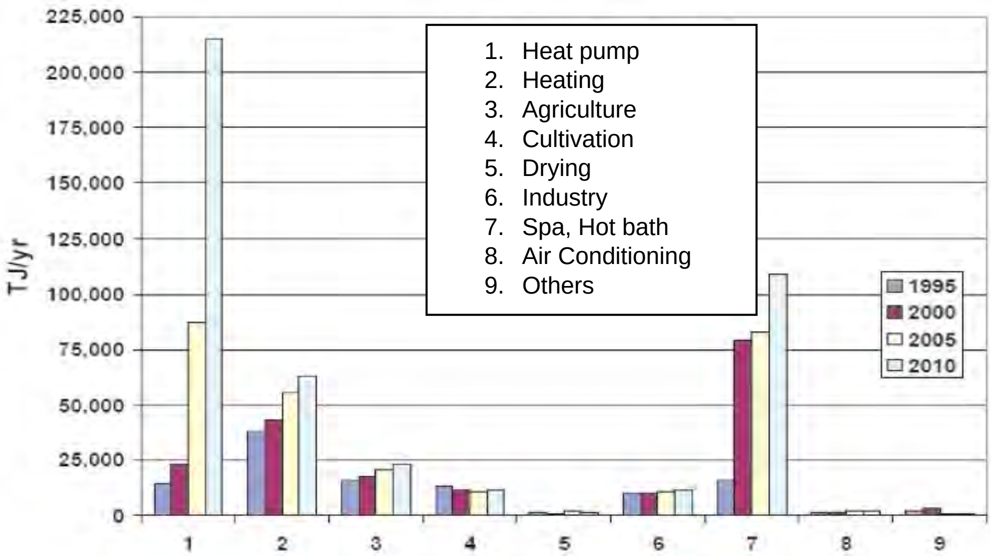

Source: Nikkeiken 2012.11

Fig. 3-4.2 Direct Use of Geothermal Resources

Table 3-4.1 shows cases of the direct use of geothermal resources. The top 10 countries for direct use are the USA, China, Sweden, Norway, Germany, Japan, Turkey, Iceland, the Netherlands and France. Major applications are heat pumps and heating. On the other hand, a high proportion of spas and hot baths is seen in Japan, Turkey and China.

Table 3-4.1 Cases of Direct Use of Geothermal Resources

Capacity (MWt)		Proportion (%)			
		Heat Pump	Heating	Spa, Hot bath	Others
USA	12,612	95	2	1	2 Cultivation Greenhouse
China	8,898	59	15	21	6 Agro-industry
Sweden	4,460	95	3	0	2
Norway	3,300	100	0	0	0
Germany	2,485	90	8	2	0
Japan	2,100	1	4	86	9 Snow melting Greenhouse
Turkey	2,084	2	49	26	23 Greenhouse
Iceland	1,826	0	76	4	20 Snow melting
Netherlands	1,410	99	0	0	1 Greenhouse
France	1,345	74	22	1	2 Cultivation Greenhouse

Source: Nikkeiken 2012.11

3.4.2 Potential for Direct Use of Geothermal Resources in Rwanda

(1) Multipurpose uses of geothermal resources by temperature

Figure. 3-4.3 shows the multipurpose uses of geothermal resources by temperature based on the uses described in 3.4.1. The following are the results of the study of the potential for multipurpose geothermal uses in Rwanda, based upon the characteristics of Rwanda's geothermal resources such as temperature, the current situations of the natural environment and land use around geothermal resources, the conditions of use needed by each facility, etc..

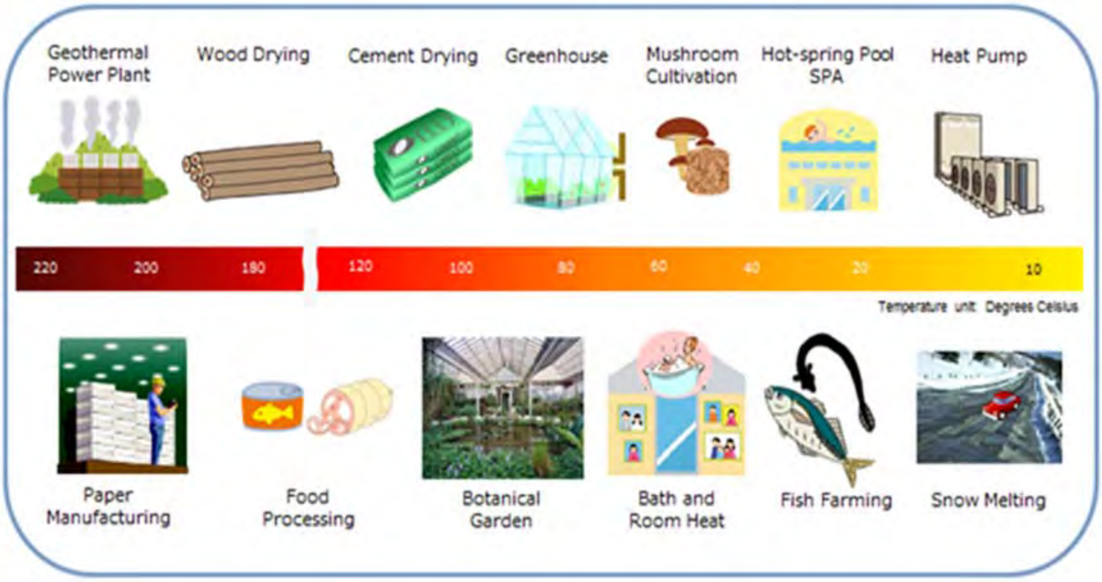

Source: JOGMEC

Fig. 3-4.3 Multipurpose Uses of Geothermal Resources by Temperature

(2) Outline of potential for multipurpose geothermal uses

The potential for multipurpose geothermal uses by area in Rwanda is shown in Table 3-4.2. In Mashyuza in the southern area, there is a hot spring already gushing out hot water of around 47-53 °C which can be used as a spa or hot-spring pool.

In Kinigi in the northwestern area, there is currently no available geothermal resource. However, if hot water or steam is obtained in the future, there is a potential for direct geothermal use as a spa, hot-spring pool, or greenhouse for flower cultivation.

In Karago, hot water at 73°C is currently welling up, but the establishment of facility like a spa or hot-spring pool is difficult, because the acreage is limited. If steam at around 190°C is obtained in the future, then there is a potential for direct geothermal use as the heat source for drying tea leaves at a tea processing factory.

In Gisenyi in the northwestern area, there is also hot water welling up at around 70-73 °C. However, direct use of the geothermal resource cannot be expected, since the establishment of facilities is difficult due to the limited acreage.

There is also a spring welling up at Iriba with a water temperature of 22°C. However, the temperature is too low to be used easily. If hot water of around 80 degrees Celsius can be obtained in the future, then it can be used as a spa and hot-spring pool.

Table 3-4.2 Potential for Multipurpose Geothermal Uses in Rwanda By Area

Fields		Characteristics	Uses
South	Mashyuza /Bugarama	(1)47-53 °C hot water (2) In the event that steam is obtained in the future	(1)Spa, hot-spring pool (2)Rice drying
Northwest	Kinigi	Geothermal resources are not available at present. Uses described on the right may be possible if hot water or steam is obtained in the future.	(1) Spa, hot-spring pool (Collaboration with Gorilla Tours) (2) Cultivation of flowers such as roses in greenhouses (3) Potato conservation (4) Pyrethrum drying
	Karago	(1) 73 °C hot water (2) If steam of about 190 °C is obtained in the future	(1) Facility establishment is difficult due to the limitation of acreage (2) Heat source for drying tea leaves at a tea factory
	Gisenyi	(1) 70-73 °C hot water (2) If steam is obtained in the future	(1)Facility establishment is difficult due to the limitation of acreage (2) Potato conservation
	Iriba	(1) 22 °C water (2) If hot water of higher temperature is obtained in the future	(1) Facility establishment is difficult due to low temperature (2) Spa, hot-spring pool

Source: JICA study team

Table 3-4.3 below shows both the current and future multipurpose uses of geothermal resources by geothermal resource in Rwanda.

Table 3-4.3 Potential for Multipurpose Geothermal Uses in Rwanda
by Geothermal Resource

Category	Resources	Utilization equipment	Purpose	Place
Current Candidates	Hot spring	Spa	Domestic	Mashyuza
		Hot spring pool		
Future Candidates		Spa		Kinigi Iriba
		Hot spring pool		
	Hot spring or Steam	Greenhouses for Flower Cultivation	Export	Kinigi
	Steam	Tea drying		Karago
		Potato conservation		Kinigi, Gisenyi
		Pyrethrum drying	Export Finally	Kinigi
		Rice drying	Domestic	Bugarama
		Fish drying (such as Sambaza)	Export	Gisenyi

Source: JICA study team

3.4.3 Business Model of Multipurpose Geothermal Uses in Mashyuza in the Southern Area

In Mashyuza, located at an altitude of about 1,200m in the southern area, an acreage of about 150m×400m is available (Fig. 3-4.4). There is already a hot-spring gushing out hot water of around 47-53^{o}C that can be used for spas and hot-spring pools (Fig. 3-4.4). Since the land is the property of CIMERWA Ltd, a cement company, if this private company establishes a facility such as a spa and/or hot-spring pool in the future, there is a possibility that the use of the facility will be restricted to CIMERWA employees, or it may be open to the public (Table 3-4.4, Fig. 3-4.5).

With regard to the operation of this facility, service level management including operation and maintenance (O&M), which may include outsourcing, is considered to be key to success. The IRR is approximately 9% for 15 years. The results of the IRR estimation are described below in
Appendix 2-4.

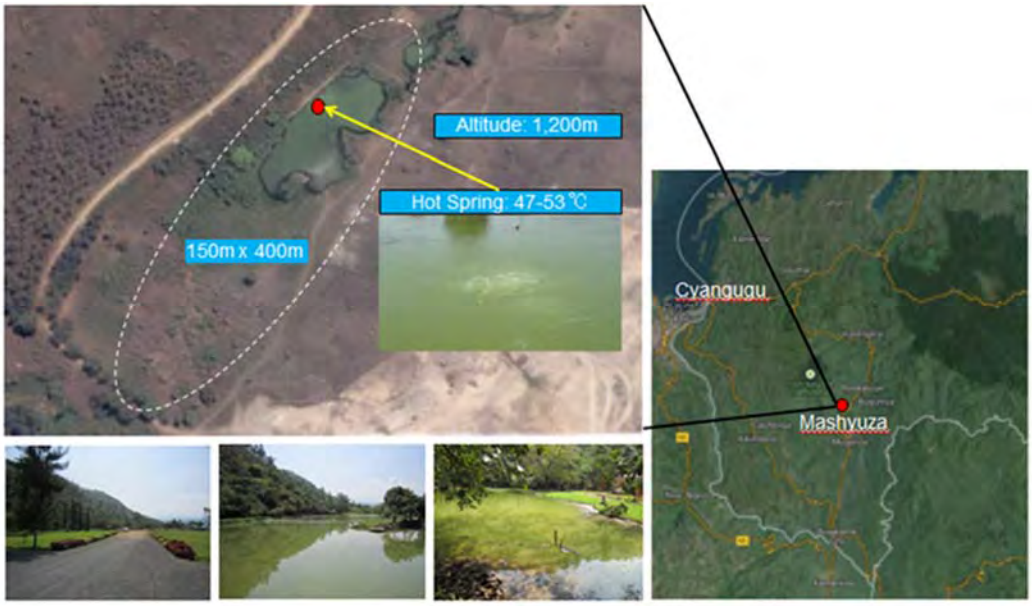

Source: JICA study team

Fig. 3-4.4 Potential for Geothermal Uses in Mashyuza

Table 3-4.4 Business Model for Mashyuza

Category	Outline
Concept	Spa with Hot spring, Private bathing rooms, Massage room, Restaurant and Market
Main targets	Women and Families
Land owner	Private, CIMERWA Ltd
Area	150m x 400m
Implementing body	Private
Approximate initial cost	1 Mil. USD
Payout time	7.4 years
IRR	9%
Conditions of success	Service level management including Operation and Maintenance

Source: JICA study team

Source: JICA study team

Fig. 3-4.5 Images of Spa at Masyuza

The idea of using geothermal resources for a spa and hot-spring pool in Mashyuza can also be applied to the resource in Kinigi in the northwestern area.

3.4.4 Business Model of Multipurpose Geothermal Uses in Kinigi in the Northwestern Area

The altitude of Kinigi in the northwestern area is about 2,600m. The area is farmland where Irish Potatoes and pyrethrum plants are cultivated (Fig. 3-4.6).

Test drilling will be conducted in Kinigi in the future, and, if hot water is obtained in Kinigi in the future, it can be used in spas and hot-spring pools, just as in Mashyuza in the southern area.

Also, if steam or hot water becomes available in Kinigi in the future, there is a potential for geothermal direct use in greenhouses for cultivating flowers, such as roses (Fig. 3-4.7). Cultivated roses and other flowers will be exported to foreign countries like the Netherlands, via Kigali International Airport. Meanwhile, roses and other flowers must be kept appropriately refrigerated during transportation.

The maximum, minimum and average temperatures in Bigogwe near Karisimbi are as shown in Fig. 3-4.8. The average temperature is 14^{o}C, while the maximum is around 20-23^{o}C and the minimum is around 6-9^{o}C. For the cultivation of roses, the temperature must be kept for about 23^{o}C during the day and about 18^{o}C during the night (Fig. 3-4.8). The temperature in the greenhouses will be appropriately controlled by using geothermal resources. Additionally, a supply of freshwater required for the cultivation of flowers must be ensured.

Table 3-4.5 below shows the business model of the greenhouses for flower cultivation. It is assumed that the implementing body will be a private company. Product differentiation and sustainable operation and maintenance (O&M) will be key to success. The IRR is approximately 15% for 15 years. The results of the IRR estimation are described below in Appendix 2-4.

Source: JICA study team

Fig. 3-4.6 Potential for Geothermal Uses in Kinigi

Source: JICA study team

Fig. 3-4.7 Examples of Roses Grown in Greenhouses in Rwanda

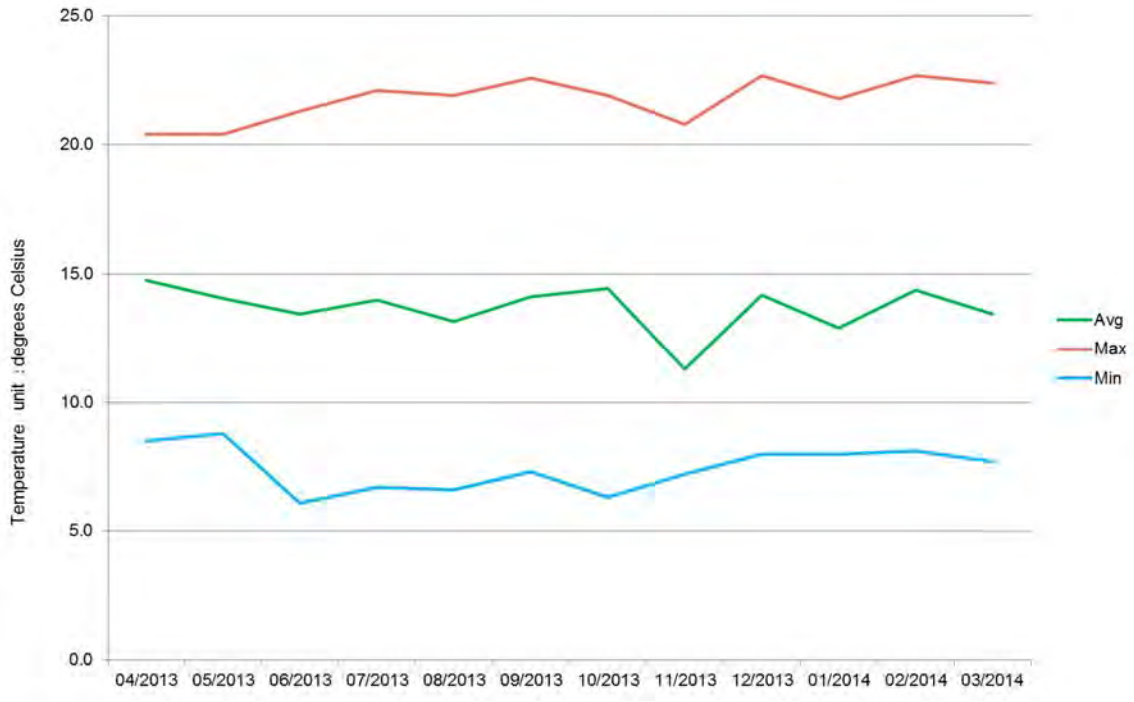

Source: JICA study team

Fig. 3-4.8 Temperatures in Bigogwe

Table 3-4.5 Business Model for Kinigi

Category	Outline
Concept	Greenhouses for Flower Cultivation
Main targets	Roses for export
Land owner	Private
Area	20 ha
Implementing body	Private
Approximate initial cost	8 Mil. USD
Payout time	5 years
IRR	15
Conditions of success	Differential Marketing Operation and Maintenance

Source: JICA study team

3.4.5 Business Model of Multipurpose Geothermal Uses in Karago in the Northwestern Area

In Karago in the northwestern area, which is located at about 2,290m altitude, there is already a hot-spring gushing out hot water of 73^{o}C (Fig. 3-4.9). However, the spring is in the lake, so the source of the hot spring appears at the ground surface during the dry season, but disappears under water during the rainy season. In addition, the source of the hot spring is surrounded by small hills and mountains, so the securing of land required for establishing a spa or hot-spring pool is very difficult.

If steam of approximately 190^{o}C is obtained in the future, then it can be used as the heat source for drying tea leaves at the private tea processing factory (NYABIHU Tea Factory: Kenyan-owned), which is located about 1,900m from the source of the hot spring. The tea factory currently uses woody biomass as its heat source (Fig. 3-4.10), so steam must be supplied at a lower cost.

The following two cases can be considered: either REG establishes a pipeline connecting from the source of the hot spring to the tea factory and supplies or sells steam to the tea factory; or the tea factory itself establishes the pipeline. Pipeline infrastructure management including operation and maintenance will be key to success. If the tea factory establishes the pipeline, the IRR is approximately 8% for 15 years (Table 3.4-6). The results of the IRR estimation are described below in the Appendix 2-4.

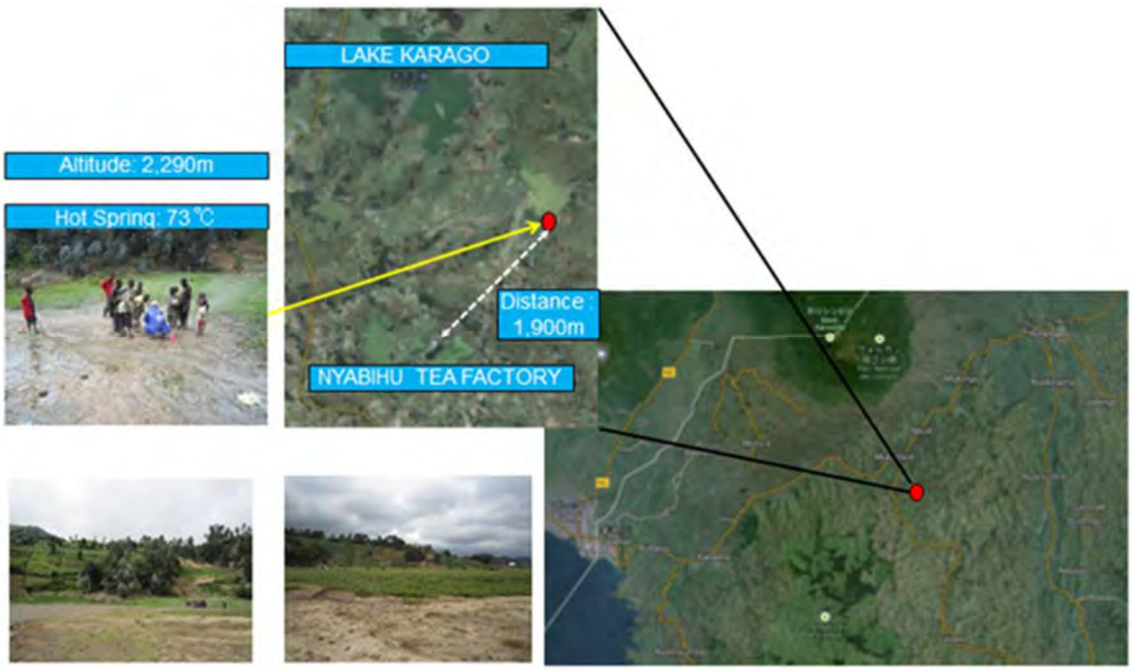

Source: JICA study team

Fig. 3-4.9 Potential for Geothermal Uses in Karago

Source: JICA study team

Fig. 3-4.10 Use of Woody Biomass at Tea Factory

Table 3-4.6 Business Model for Karago

Category	Outline
Concept	Tea Drying
Main targets	Private, NYABIHU Tea Factory
Current energy use	Firewood 6.0 m^3 of firewood for 2 tons of processed tea
Required Steam pressure and temperature	10-11 Bars, 190 degrees Celsius
Implementing body	Private
Approximate initial cost	151,300 USD
Payout time	7.8 years
IRR	7.5%
Conditions of success	Operation and Maintenance

Source: JICA study team

3.4.6 Potential of Geothermal Uses in Gisenyi in the Northwestern Area

The altitude of Gisenyi in the northwestern area is about 1,470m. There, hot water of around 70-73^{o}C is currently welling up (Fig. 3-4.11). However, the establishment of a facility like a spa or hot-spring pool is difficult, because the acreage is limited, and thus the direct use of geothermal resources cannot be expected.

Some of the residents, however, use the hot spring by putting bananas, eggs, etc. close to the gushing point of the hot spring to boil them. Therefore, the hot-spring is directly used at a small level to cook food.

Source: JICA study team

Fig. 3-4.11 Potential for Geothermal Uses in Gisenyi

3.4.7 Potential for Geothermal Uses in Iriba in the Northwestern Area

In Iriba, there is a cold spring welling up with a temperature of 22^{o}C, but that is too cool to be used easily. If hot water of around 80^{o}C can be obtained in the future, then it can be used as a spa or hot-spring pool.